

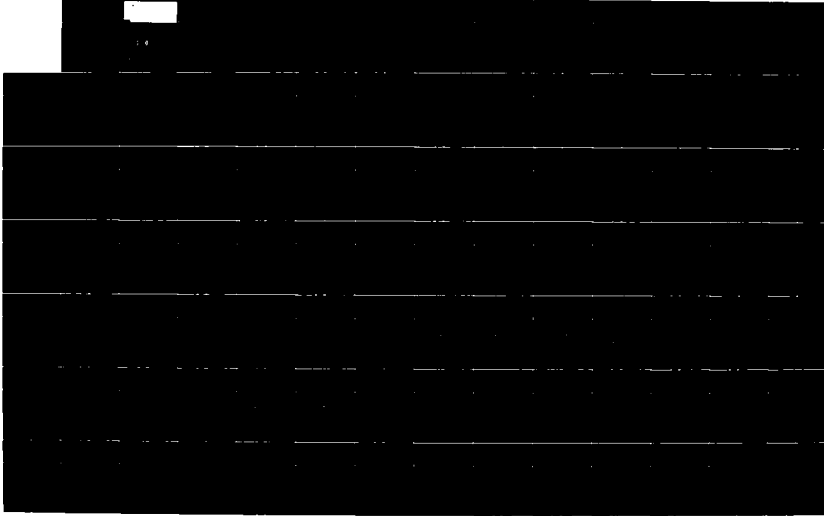
AD-A172 983

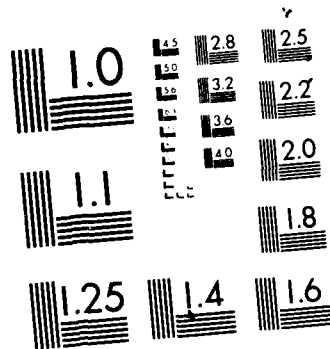
RANDOM-CHOICE-METHOD SOLUTIONS FOR TWO-DIMENSIONAL  
PLANAR AND AXISYMMETRIC. (U) TORONTO UNIV DONGSUIEN  
(ONTARIO) INST FOR AEROSPACE STUDIES 2 C SHI ET AL.  
JAN 86 UTIAS-297 AFOSR-TR-86-0582 F/C 2874

1/2

UNCLASSIFIED

NL





MICROCOPY RESOLUTION TEST CHART  
NATIONAL BUREAU OF STANDARDS 1963-A



INSTITUTE  
FOR  
AEROSPACE STUDIES

UNIVERSITY OF TORONTO

AD-A172 903

2

AFOSR-TR. 86-0902

RANDOM-CHOICE-METHOD SOLUTIONS FOR TWO-DIMENSIONAL  
PLANAR AND AXISYMMETRIC STEADY SUPERSONIC FLOWS

DTIC  
ELECTE  
OCT 08 1986  
S D

by

Z. C. Shi and J. J. Gottlieb

DTIC FILE COPY

AIR FORCE OFFICE OF SCIENTIFIC RESEARCH (AFSC)  
NOTICE OF TRANSMITTAL TO DTIC  
This technical report has been reviewed and is  
approved for public release IAW AFR 190-12.  
Distribution is unlimited.  
MATTHEW J. KETTER  
Chief, Technical Information Division

Approved for public release;  
distribution unlimited.

January 1986

UTIAS Report No. 297  
CN ISSN 0082-5255

86 10 6 071

UNCLASSIFIED

TYPE CLASSIFICATION OF THIS PAGE (When Data Entered)

REPORT DOCUMENTATION PAGE

READ INSTRUCTIONS  
BEFORE COMPLETING FORM

1. REPORT NUMBER <b>AFOSR-TR- 86-0902</b>		2. GOVT ACCESSION NO. <b>ADA172903</b>	3. RECIPIENT'S CATALOG NUMBER
4. TITLE (and Subtitle) RANDOM-CHOICE-METHOD SOLUTIONS FOR TWO-DIMENSIONAL PLANAR AND AXISYMMETRIC STEADY SUPERSONIC FLOWS		5. TYPE OF REPORT & PERIOD COVERED Interim	
7. AUTHOR(s) Z. C. Shi and J. J. Gottlieb		6. PERFORMING ORG. REPORT NUMBER UTIAS Report No. 297	
3. PERFORMING ORGANIZATION NAME AND ADDRESS University of Toronto, Inst. for Aerospace Studies, 4925 Dufferin St., Downsview, Ontario, Canada, M3H 5T6		8. CONTRACT OR GRANT NUMBER(S) AF-AFOSR 82-0096	
11. CONTROLLING OFFICE NAME AND ADDRESS Air Force Office of Scientific Research/NA, Bldg. 410, Bolling Air Force Base, DC 20332, U.S.A.		10. PROGRAM ELEMENT, PROJECT, TASK AREA & WORK UNIT NUMBERS <b>61102F</b> <b>2307/41</b>	
14. MONITORING AGENCY NAME & ADDRESS (if different from Controlling Office) <b>same as 11</b>		12. REPORT DATE January 1986	
		13. NUMBER OF PAGES 57	
		15. SECURITY CLASS. (of this report) Unclassified	
		15a. DECLASSIFICATION/DOWNGRADING SCHEDULE	
16. DISTRIBUTION STATEMENT (of this Report) Approved for public release; distribution unlimited.			
17. DISTRIBUTION STATEMENT (of the abstract entered in Block 20, if different from Report)			
18. SUPPLEMENTARY NOTES			
19. KEY WORDS (Continue on reverse side if necessary and identify by block number) 1. Random choice method. 2. Steady supersonic flows. 3. Supersonic inlet flows. 4. Free-jet flows.			
20. ABSTRACT (Continue on reverse side if necessary and identify by block number) A random choice method (RCM) is developed for obtaining fairly practical and efficient numerical solutions for two-dimensional planar and axisymmetric steady supersonic flows, such as those for sharp-edged planar airfoils, supersonic inlets of aircraft engines, pointed bodies of revolution, supersonic nozzles, and free jets. This method is based on the solution of a Riemann problem, which is the elemental solution of the hyperbolic equations of two-dimensional steady supersonic flows. The Riemann problem consists of two waves separated by a slip stream, and each wave can be either an oblique shock wave or a Prandtl			

UNCLASSIFIED

SECURITY CLASSIFICATION OF THIS PAGE (When Data Entered)

Meyer expansion wave. Advanced techniques are given for solving the Riemann problem iteratively, handling the boundary conditions along body and free-jet surfaces, and computing only certain parts of flow fields of interest. Many interesting and practical numerical solutions are presented for different types of planar and axisymmetric flows, to demonstrate the applicability, capability, and limitations of the RCM. Numerical results are shown to be in excellent agreement with both known analytical solutions and results from the method of characteristics.

UNCLASSIFIED

RANDOM-CHOICE-METHOD SOLUTIONS FOR TWO-DIMENSIONAL  
PLANAR AND AXISYMMETRIC STEADY SUPERSONIC FLOWS

by

Z. C. Shi and J. J. Gottlieb

Submitted April 1985

UTIAS Report No. 297  
CN ISSN 0082-5255

Acknowledgements

The first author would like to express his sincere gratitude and appreciation to the Chinese Aerodynamic Research and Development Center in Mianyang, Sichuan, for providing the opportunity of taking a leave of absence and undertaking a research and study program at the University of Toronto in Canada.

The first author is also very pleased to have had the opportunity of both studying and doing research at the University of Toronto Institute for Aerospace Studies.

The authors would like to express their sincere appreciation to Dr. Tsutomu Saito for some consultations regarding the present work. He introduced the random-choice method at UTIAS, when he solved one-dimensional unsteady flow problems.

Financial support from the Natural Sciences and Engineering Research Council of Canada and the U.S. Air Force Office of Scientific Research (Grant No. AF-AFOSR-82-0096) by means of operating grants to the second author are gratefully acknowledged. This financial support provided a stipend for the first author and covered the computer costs, which was necessary for undertaking and completing this research work.



Accession For	
NTIS CRA&I	<input checked="" type="checkbox"/>
DTIC TAB	<input type="checkbox"/>
Unannounced	<input type="checkbox"/>
Justification .....	
By .....	
Distribution /	
Availability Codes	
Dist	Avail and/or Special
A-1	

### Abstract

A random-choice method (RCM) is developed for obtaining fairly practical and efficient numerical solutions for two-dimensional planar and axisymmetric steady supersonic flows, such as those for sharp-edged planar airfoils, supersonic inlets of aircraft engines, pointed bodies of revolution, supersonic nozzles, and free jets. This method is based on the solution of a Riemann problem, which is the elemental solution of the hyperbolic equations of two-dimensional steady supersonic flows. The Riemann problem consists of two waves separated by a slip stream, and each wave can be either an oblique shock wave or a Prandtl-Meyer expansion wave. Advanced techniques are given for solving the Riemann problem iteratively, handling the boundary conditions along body and free-jet surfaces, and computing only certain parts of flow fields of interest. Many interesting and practical numerical solutions are presented for different types of planar and axisymmetric flows, to demonstrate the applicability, capability, and limitations of the RCM. Numerical results are shown to be in excellent agreement with both known analytical solutions and results from the method of characteristics.

Table of Contents

	Page
Title Page . . . . .	i
Acknowledgements . . . . .	ii
Abstract . . . . .	iii
Table of Contents . . . . .	iv
Notation . . . . .	vi
1.0 INTRODUCTION . . . . .	1
1.1 Literature Review . . . . .	1
1.2 Scope of the Present Study . . . . .	3
2.0 ANALYSIS FOR THE RANDOM-CHOICE METHOD . . . . .	4
2.1 General Equations for Planar and Axisymmetric Flows . . . . .	4
2.2 General Riemann Problem . . . . .	5
2.3 Solution of the Riemann Problem for Steady Supersonic Planar Flows . . . . .	6
2.4 Random -Sampling Procedure . . . . .	10
2.5 Random-Number Algorithm . . . . .	14
2.6 Accuracy of the Flow-Field Computations . . . . .	16
2.7 Boundary Conditions . . . . .	16
2.8 Operator-Splitting Technique to Obtain Axisymmetric-Flow Solutions . . . . .	18
3.0 PRACTICAL METHOD OF REDUCING RANDOM-CHOICE-METHOD COMPUTATIONS . . . . .	21
4.0 LIMITATIONS OF THE RANDOM-CHOICE METHOD . . . . .	22
4.1 Steady Supersonic Planar Flows . . . . .	22
4.2 Steady Supersonic Axisymmetric Flows . . . . .	22

Table of Contents (continued)

	Page
5.0 NUMERICAL RESULTS AND DISCUSSIONS . . . . .	23
5.1 Steady Supersonic Planar Flows . . . . .	24
5.1.1 Flow over a compressive corner . . . . .	24
5.1.2 Flow over an expansive corner . . . . .	24
5.1.3 Gradual compressive corner that gives a focussed compression wave . . . . .	24
5.1.4 Flow over a symmetric double-wedge . . . . .	25
5.1.5 Flows in duct inlets . . . . .	26
5.1.6 Flow over a parabolic shaped airfoil . . . . .	27
5.1.7 Free-jet flows from a slot . . . . .	28
5.2 Steady Supersonic Axisymmetric Flows . . . . .	29
5.2.1 Flow over a cone . . . . .	29
5.2.2 Flow over a cone-cylinder . . . . .	30
5.2.3 Flow over a parabolic-nosed cylinder . . . . .	30
5.2.4 Flow over a symmetric double-cone . . . . .	31
5.2.5 Flow over a parabolic-spindle . . . . .	32
5.2.6 Free-jet flows from a circular orifice . . . . .	32
6.0 CONCLUDING REMARKS . . . . .	33
7.0 REFERENCES . . . . .	34
Figures . . . . .	40
Appendix A: COMPUTER-PROGRAM LISTING FOR SOLVING TWO-DIMENSIONAL STEADY SUPERSONIC FLOW PROBLEMS . . . . .	A1

## Notation

### Alphanumeric symbols

a	gas sound speed
A	constant defined by Eq. 46
B	constant defined by Eq. 46
C	constant defined by Eq. 46
$C_p$	pressure coefficient
e	total energy per unit volume [ $e = \epsilon + \rho(u^2 + v^2)/2$ ]
f(W)	function of W in Eqs. 1 and 2
g(W)	function of W in Eqs. 1 and 2
G	vector defined by Eq. 45
h(W,r)	function of W and radius r in Eqs. 1 and 2
i	integer for numbering mesh points in the axial direction
j	integer for numbering mesh points in the radial direction
M	flow Mach number
p	static pressure
P(x,r)	sampling point for the Riemann problem
r	radial coordinate
$r_b$	radius of an axisymmetric body
R	gas constant
S	a state for the Riemann problem
t	thickness of a planar airfoil
T	static gas temperature
u	axial component of the gas velocity
v	radial component of the gas velocity
W	solution vector [ $\rho, \rho u, \rho v, e$ ] from Eqs. 1 and 2
x	axial coordinate along the free-stream flow
$y_b$	locus of the airfoil surface

### Greek symbols

$\alpha$	coefficient for planar ( $\alpha = 0$ ) and axisymmetric ( $\alpha = 1$ ) flows
$\beta$	angle of a characteristic line or a Mach wave (measured clockwise from the radial axis)
$\gamma$	specific-heat ratio
$\delta$	angle of flow deflection through a shock or rarefaction wave
$\delta_b$	boundary-surface angle measured from the longitudinal axis
$\Delta$	axial and radial increments (e.g., $\Delta x$ and $\Delta r$ )

### Notation (continued)

$\epsilon$	internal energy per unit volume
$\eta$	pressure ratio $p_*/p_l$ and $p_*/p_r$
$\kappa(\eta)$	function of $\eta$ defined by Eq. 16
$\theta$	angle of a radial line from a cone apex
$\theta_c$	semivertex angle of a wedge or cone
$\mu$	Mach angle [ $\mu = \sin^{-1}(1/M)$ ], also a function of $\eta$ and $M_a$ from Eq. 17
$\nu(M)$	Prandtl-Meyer function in Eq. 8
$\xi$	flow angle $\pi/2 - \tan^{-1}(v/u)$ , measured clockwise from the radial axis (also, angle of a slip surface or slip stream)
$\pi$	ratio of circumference and diameter of a circle (3.1415927)
$\rho$	static density
$\sigma_s$	shock angle measured clockwise from the radial axis
$\chi(\eta, M_a)$	function of $\eta$ and $M_a$ from Eq. 18
$\Omega$	value of the random variable equidistributed in the range $-1/2$ to $+1/2$

### Subscripts

a	denotes conditions ahead of an oblique shock or expansion wave
b	denotes conditions behind an oblique shock or expansion wave
h	denotes the value at the rarefaction-wave head
j	index for numbering the radial position of a grid point
l	denotes the initial state of the gas on the left side of the discontinuity in the Riemann problem
min	minimum value
r	denotes the initial state of the gas on the right side of the discontinuity in the Riemann problem
t	denotes the value at the rarefaction-wave tail
*	denotes a common value on either side of the slip surface

### Superscripts

i	index for numbering the axial position of a grid point
-	overhead bar denotes the sampled solution for the planar-flow case
~	overhead tilde denotes the first-order sampled solution in MacCormack's operator-splitting scheme (Eq. 48)

## 1.0 INTRODUCTION

### 1.1 Literature Review

Numerical models and analyses have proven very powerful for the study or simulation of complex fluid-dynamic flows. If properly validated, these models can provide an accurate description of the flow field. Additionally, they can provide a means of validating new physical and mathematical hypotheses, thereby providing fundamental knowledge about flow problems of interest.

Two-dimensional planar and axisymmetric steady supersonic flows of gases can be described, with suitable assumptions, by a hyperbolic system of conservation laws. Numerical solutions of the hyperbolic system should satisfy the following criteria: 1) the computed solution should be sufficiently accurate in smooth parts of the flow, 2) discontinuities in the flow, such as oblique shocks and slip streams (or slip surfaces), should not only remain sharp but also be propagated or transported at the correct speed, and 3) such discontinuities should be computed stably without numerical oscillations.

The method of characteristics has been used most widely up to the 1970s for obtaining numerical solutions of steady supersonic flows over planar and axisymmetric bodies. Isenberg and Lin<sup>1</sup>, Clippinger, Giese and Carter<sup>2</sup>, Ferri<sup>3</sup>, Shapiro<sup>4</sup>, and Liepmann and Roshko<sup>5</sup> found many important applications of this method for supersonic flows around thin sharp-edged airfoils and slender pointed bodies of revolution with attached shock waves, and also for supersonic flows in aircraft-engine inlets and in many types of nozzles. In the application of the method of characteristics, flow properties are constrained by ordinary differential equations that apply along characteristic lines in flow regions without discontinuities, so that solutions can be obtained on a characteristic mesh. Special adaptive procedures are needed to include and track both oblique shocks and slip streams, and this is the primary difficulty in employing this method. Each flow problem normally needs a new computer program, because the computer logic is specific to the problem. As a result, the method of characteristics is not often used to solve flow problems.

The finite-difference method<sup>6-8</sup> is another numerical means of solving flow problems which has been widely used. In order to incorporate shocks and slip streams in the solutions, special schemes like artificial and numerical viscosity have to be employed. For example, von Neuman and Richtmyer<sup>9</sup> were the first to introduce an artificial viscosity term into the Lagrangian form of the gasdynamic equations. This scheme, like those and others that followed, automatically handle shocks and slip streams, but they either introduce undesirable oscillations in the solution near these discontinuities or smear them out over several grid points. Automatically handling discontinuities is so advantageous that the finite-difference method is widely used today for all sorts of flow problems, despite the fact that the undesirable smearing and also incorrect placement of discontinuities affects the quality and accuracy of the solution.

Over the past two decades the finite-element method has been developed for the solution of flow problems<sup>10</sup>. To the present time, this method has been used frequently to solve successfully problems involving incompressible flows and steady compressible subsonic flows, but it has not been sufficiently well developed at present to solve hyperbolic equations with similar success.

The particle-in-cell (PIC) and fluid-in-cell (FLIC) methods, have been applied with success to solve a wide variety of multifluid flow problems that

involve large slippages and distortions,<sup>11-13</sup> like those that take place when a projectile penetrates a liquid or metal. The PIC method is a combined Eulerian and Lagrangian scheme that utilizes Lagrangian fluid particles to transport mass, momentum, and energy through an Eulerian mesh of cells,<sup>11</sup> whereas the FLIC method uses only an Eulerian scheme to transport fluid.<sup>12-13</sup> Although the use of such transported particles or fluid facilitates in obtaining the solution of a problem, these methods are not widely employed because the predictions contain aphysical fluctuations in fluid quantities and excessive smearing of discontinuities, and they also normally demand a large computer memory and computation time.

Taylor and Maccoll<sup>14</sup> and Maccoll<sup>15</sup> in their early studies (1933, 1937) solved the flow around an infinite right-circular cone moving supersonically with an attached, conical, bow shock of constant strength. For this special problem, they were able to obtain a self-similar solution in terms of ordinary differential equations, and extensive tables of flow properties around cones, which is based on these early studies, can be found in Ref. 16.

If a body in a supersonic flow is sufficiently slender and smooth, then flow deflections or perturbations will be small. Shocks will be sufficiently weak such that the flow for practical purposes can be considered to be homentropic (i.e., uniform entropy) and therefore irrotational. For this case the most popular theories introduce a velocity potential to obtain an approximate linear perturbation solution. The perturbation flow solution for disturbance produced by the body is defined such that it is simply superposed on the uniform free-stream velocity. Such perturbation solutions can be found in papers by von Karman and Moore<sup>17</sup>, Lighthill<sup>18-19</sup>, Ward<sup>20</sup>, Whitham<sup>21-22</sup>, and Van Dyke<sup>23</sup>, and they have been used recently by Ritzel and Gottlieb<sup>24</sup> to obtain the overpressure signatures from actual projectiles and by Devan<sup>25</sup> to get surface pressures on axisymmetric bodies. Although perturbation solutions are easy to use, they are both approximate and limited to supersonic flows of low free-stream Mach number.

A relatively new method has been developed and used in recent years for solving hyperbolic equations, provided that the elemental Riemann problem has a known solution. The random-choice or Glimm's method has the highly desirable capability of automatically including and correctly placing discontinuities like shocks and contact surfaces in the numerical solutions, without any artificial or numerical viscosity, or any other special shock capturing techniques. It was originally developed for solving one-dimensional unsteady planar flow problems by Glimm<sup>26</sup>, based to some extent on earlier work of Godunov<sup>27</sup>. Glimm's method was made more practical for solving planar shock-tube and detonation problems by Chorin<sup>28</sup> first and later by Colella<sup>29-30</sup>, and also extended by means of an operator-splitting technique to solve cylindrical and spherical flow problems by Sod<sup>31</sup> and quasi-one-dimensional gas flows by Fok<sup>32</sup>, Greatrix and Gottlieb<sup>33</sup>, and Glimm, Marshall and Plohr<sup>34</sup>. Many different one-dimensional unsteady-flow problems have been solved successfully in recent years at UTIAS.<sup>35-48</sup>

A well-known mathematical analogy exists between two-dimensional supersonic steady flows and one-dimensional unsteady flows. The essence of this analogy is that both problems are described by hyperbolic systems of conservation laws in two independent variables, and each has a well-known elemental Riemann problem and analytical solution. Since the initial success of developing and employing the random-choice method (RCM) to obtain solutions for one-dimensional unsteady flow problems, it was recognized that similar success might also be achievable for solving analogous two-dimensional steady supersonic flow problems, provided an analogous RCM could be developed.

Marshall and Plohr<sup>49</sup> were the first to develop a RCM for solving two-dimensional steady supersonic flow problems having both planar and axisymmetric geometries. At the same time, Honma, Wada and Inomata<sup>50</sup> developed independently a similar method. In both cases, the Riemann problem was posed and its solution given in a very similar manner. However, Marshall and Plohr used a rectangular mesh in their computations, whereas Honma, Wada and Inomata used combined body-fitted and rectangular meshes. Although this combined mesh system might appear as beneficial initially, it actually increases computation time, is difficult to use with a curved body surface, and is also unnecessary.

In the studies by Marshall and Plohr<sup>49</sup>, and Honma, Wada and Inomata<sup>50</sup>, most of the effort was expended on developing the RCM, and only a few simple exemplary problems were solved to illustrate feasibility. In the first study, numerical solutions were given for the supersonic flow over straight and curved wedges, and also a cone and cylinder combination. In the other study, solutions were given for the flow over a double wedge, a cone, and a double cone.

## 1.2 Scope of the Present Study

The impetus for the present study stems originally from the experimental and analytical work of Ritzel and Gottlieb<sup>24,51-54</sup>. An exact numerical solution for the flow field around supersonic projectiles was being sought to complement the existing approximate analytical method,<sup>24</sup> to explain and accurately predict many features of the measured overpressure signatures.<sup>51-54</sup> It appeared that the RCM would be an ideal method, if it could be developed for two-dimensional steady supersonic flows, based on the previous success with the RCM for solving one-dimensional unsteady flow problems at UTIAS.<sup>33,35-48</sup> Our development of a RCM for solving two-dimensional steady supersonic flow problems began just as we became aware of the developments by Marshall and Plohr<sup>49</sup> and also by Honma, Wada and Inomata<sup>50</sup>, and this former work became very helpful to us.

In this report the RCM is presented and explained in detail for both reference and completeness, even though the RCM analysis was given briefly but elegantly in the previous work. A physical description is also presented for the elemental Riemann problem, which consists of two waves separated by a slip stream, and each wave can be either an oblique shock wave or a Prandtl-Meyer expansion wave. This analysis is embodied in a computer program for obtaining both practical and efficient numerical solutions of two-dimensional planar and axisymmetric steady supersonic flows, such as those for sharp-edged planar airfoils, supersonic inlets of aircraft engines, pointed bodies of revolution, supersonic nozzles, and free jets. Numerical results from this computer program are shown to be in excellent agreement with both known analytical solutions and predictions by the method of characteristics. Additionally, many interesting and practical numerical solutions are presented for different types of planar and axisymmetric flows, in order to demonstrate the applicability, capability, and also some severe restrictions of the RCM.

Advanced techniques are presented in this report to make the computer program both practical and efficient for solving two-dimensional planar and axisymmetric steady supersonic flow problems. Firstly, an efficient parabolic-curve iteration method is used in the solution of the Riemann problem, making the number of iterations normally three or less. Secondly, boundary conditions are handled naturally and easily without special coordinate transformations. At a solid body the flow is made tangent to the surface, and at the edge of a free jet the flow pressure is made equal to the ambient pressure outside of the flow.

Thirdly, an efficient operator-splitting technique is used. Finally, a scheme is devised for numerical computations of certain problems, so that only relevant parts of the flow field are computed, in order to significantly reduce computational time. For example, the part of the flow field containing only the wave emanating from a supersonic projectile is computed, and the free-stream flow before the wave and the slightly varying flow far behind the wave is omitted.

The random-choice method cannot solve all planar and axisymmetric steady supersonic flow problems over arbitrary shaped bodies. Limitations of the RCM are therefore documented and discussed in this report. Previous reports do not even mention most of these limitations.

## 2.0 ANALYSIS FOR THE RANDOM-CHOICE METHOD

### 2.1 General Equations for Planar and Axisymmetric Flows

The partial differential equations for two-dimensional steady supersonic inviscid flows of a gas with planar and axisymmetric geometry<sup>5</sup> can be written as

$$\frac{\partial}{\partial x}[f(W)] + \frac{\partial}{\partial r}[g(W)] = h(W,r), \quad (1)$$

where

$$W = \begin{bmatrix} \rho \\ \rho u \\ \rho v \\ e \end{bmatrix}, \quad f(W) = \begin{bmatrix} \rho u \\ \rho u^2 + p \\ \rho u v \\ u(e + p) \end{bmatrix}, \quad (2)$$

$$g(W) = \begin{bmatrix} \rho v \\ \rho u v \\ \rho v^2 + p \\ v(e + p) \end{bmatrix}, \quad h(W,r) = -\frac{\alpha}{r} \begin{bmatrix} \rho v \\ \rho u v \\ \rho v^2 \\ v(e + p) \end{bmatrix}.$$

The symbols  $p$  and  $\rho$  are the static pressure and density of the gas,  $u$  and  $v$  are the axial ( $x$ ) and radial ( $r$ ) components of the flow velocity,  $\rho u$  and  $\rho v$  are the axial and radial components of momentum, and  $\alpha$  is 1 for an axisymmetric flow. In the case of a planar flow, the axial distance  $x$  becomes the longitudinal distance  $x$ , the radial distance  $r$  becomes the lateral distance  $y$ , and  $\alpha = 0$  for this case. Hence, in the case of planar flows the nonhomogeneous term  $h(W,r)$  does not appear and the equations are homogeneous.

The total energy per unit volume  $e$  in Eqs. 1 and 2 is given by

$$e = \varepsilon + \rho(u^2 + v^2)/2 \quad (3)$$

and contains the internal energy per unit volume

$$\varepsilon = p/(\gamma - 1), \quad (4)$$

where  $\gamma$  denotes the specific heat ratio (constant for a perfect gas). Note that implicit in these equations is the equation of state  $p = \rho RT$  and the sound-speed relation  $a^2 = \gamma RT$ .

The four expressions that are embodied in Eqs. 1 and 2 are the continuity equation, Newton's second law of motion of momentum in the axial and radial directions for an axisymmetric flow (or longitudinal and lateral directions for a planar flow), and the conservation of energy. This system of equations, that is Eqs. 1 to 4, can be solved for a particular problem only if the appropriate initial and boundary conditions are specified.

## 2.2 General Riemann Problem

For the solution of the equations presented in the preceding section by means of the random-choice method (RCM), a Riemann problem must be established first and subsequently solved. The general Riemann problem is considered in this section, and the particular solution for planar and axisymmetric supersonic flows is given later. The presentation is similar to that of Chorin<sup>28</sup>.

Consider the flow field shown in Fig. 1, in which the free-stream flow is aligned approximately along the axial coordinate  $x$  and the radial coordinate  $r$  is approximately normal to the stream line. Let the flow field be subdivided by means of a grid of constant  $\Delta x$  spacing in the  $x$  direction and constant  $\Delta r$  in the radial direction. Also let the indices  $i$  and  $j$  be the labels for the grid corners. Note that each cell of width  $\Delta x$  and height  $\Delta r$  is further subdivided into quarters by the dashed lines, resulting in alternating grid points at the cell corners and centers for the computations.

Let the actual flow field, which may be either smoothly varying in terms of its variables or smoothly varying with discontinuous lines or surfaces, be discretized such that the values of the variables of importance are either known initial conditions or computed ones only at the grid corners and grid centers. In first-order Riemann initial-value problems, the states at two adjacent grid nodes are not joined by a smoothly varying line or surface, but instead the 'constant' states are always joined or separated by means of a discontinuity. The exact location of this created discontinuity is unknown, or the location of an actual one is unknown if it existed - being lost in the discretization process. However, a discontinuity is inserted when necessary at an appropriate location by means of an appropriate random-sampling process.

When inserting a discontinuity in the interval  $\Delta r$ , the only information available is that it occurs somewhere in this interval. Therefore, one can only assume that it has an equal probability of occurring at each point or in each fraction of the interval. Hence, a random variable  $\Omega$  that is equidistributed in an interval from  $-1/2$  to  $+1/2$  may be chosen to get an appropriate location for the discontinuity. If  $\Omega = -1/2$ , for example, the discontinuity can be inserted at  $r = j\Delta r$ , if  $\Omega = 0$  it can be inserted at  $(j+1/2)\Delta r$ , and if  $\Omega = 1/2$  it can then be inserted at  $(j+1)\Delta r$ . Note that this random-sampling process for inserting or locating a discontinuity in the Riemann problem gives the random-choice method its name.

In establishing the general Riemann problem, let  $W_j^i$  denote  $W[i\Delta x, j\Delta r]$ , which are the initial values or a past solution at coordinate point  $[i\Delta x, j\Delta r]$ . Also, let  $W_{j+1}^i$  denote  $W[i\Delta x, (j+1)\Delta r]$ , which are also initial values or a past solution at the adjacent coordinate point  $[i\Delta x, (j+1)\Delta r]$ . Now, if these two sets

of initial conditions or two past solutions are taken as the initial conditions, then the solution  $W_{j+1/2}^{i+1/2}$  farther downstream at the center of the cell or at the coordinate point  $[(i+1/2)\Delta x, (j+1/2)\Delta r]$  needs to be determined, to advance the solution in the axial direction. The initial-value problem which will give this solution can now be expressed as

$$W[i\Delta x, r] = \begin{cases} W_{j+1}^i & \text{if } r \geq (j + 1/2 + \Omega)\Delta r, \\ W_j^i & \text{if } r < (j + 1/2 + \Omega)\Delta r. \end{cases} \quad (5)$$

An initial-value problem of this type that yields the solution  $W_{j+1/2}^{i+1/2}$  is called a Riemann problem.

The solution to a Riemann problem is normally self-similar and can then be expressed in terms of  $r/x$ . When such a solution is obtained, it will extend outward from the discontinuity on the initial line  $x = i\Delta x$ , in the radial direction  $r$  and downstream in the direction  $x$ , eventually overlapping the coordinate point  $[(i+1/2)\Delta x, (j+1/2)\Delta r]$ . The set of values from this solution that falls directly on the point  $[(i+1/2)\Delta x, (j+1/2)\Delta r]$  can then be assigned as the solution  $W_{j+1/2}^{i+1/2}$  to this grid node.

Once the solution of one Riemann problem has been obtained, it is not very difficult to see how this process can be repeated for all cells having the common axial distance  $i\Delta x$ , in order to get the solutions at all cell centers at axial distance  $(i+1/2)\Delta x$ . Then, the solution is advanced column by column in the axial direction, in order to obtain the solution for the entire flow field. In this process, however, suitable boundary conditions would have to be applied at the outer edges of the grid.

It is worth mentioning here that the description of the random-sampling process and assignment of a solution of the Riemann problem to the next grid node differ from those in Chorin's paper<sup>28</sup>. He always puts the discontinuity right at the center of the cell, random samples the Riemann solution downstream, and then assigns this set of values to the next grid node. Although the two methods are mathematically equivalent, the present method and description really provides more physical insight and understanding.

### 2.3 Solution of the Riemann Problem for Steady Supersonic Planar Flows

The solution of the Riemann problem cannot always be obtained in simple analytical form for complex sets of partial differential equations. This is, unfortunately, the case for steady supersonic axisymmetric flows, because the inhomogeneous term  $h(W, r)$  unduly complicates the equations. When this term is absent, as in the specific case of steady supersonic planar flows, an analytical solution can then be obtained. These solutions for planar flows are given first in this section, and the operator-splitting technique which can be applied to modify the planar solutions to yield those for axisymmetric flows is introduced later.

The Riemann problem for the hyperbolic system of equations given by Eqs. 1 and 4 is an initial value problem for which the initial data is known at an axial distance  $i\Delta x$  (Fig. 1), as mentioned earlier. The initial data consist of two states,  $S_l$  on the left (at the larger radius), and  $S_r$  on the right (at the

smaller radius). These two states are separated by an initial discontinuity at some radial distance  $r$  (see Eq. 5), and it breaks into left and right running waves that are swept downstream by the oncoming supersonic flow and separated by a slip surface or slip stream, as shown in Fig. 2.

In the Riemann problem for steady supersonic flows, the left and right running waves can be either an elemental oblique shock wave or Prandtl-Meyer rarefaction wave.<sup>5</sup> These two elemental waves result in four different wave patterns and solutions (see Fig. 2). The left and right running waves are separated by a slip stream, across which the pressure and flow angle are continuous but the density, temperature, flow velocity, and flow Mach number are normally discontinuous. For the case of steady supersonic planar flows of a polytropic gas, the partial differential equations for the Riemann problem can be reduced to analytical equations, and these will soon be presented. For the case of a polytropic gas, only four variables are needed to fully describe a particular state, whether this state is ahead of a shock or rarefaction wave ('a' in Fig. 2), behind a shock or rarefaction wave ('b'), or inside a rarefaction wave. As in past studies<sup>49-50</sup>, the four most convenient variables are the static pressure  $p$ , static density  $\rho$ , flow Mach number  $M = (\{u^2 + v^2\}/a^2)^{1/2}$ , and flow angle  $\xi = \pi/2 - \tan^{-1}(v/u)$ .

Consider the case of a rarefaction wave first. In this case the partial differential equations reduce to ordinary differential equations that then apply along characteristic lines, which can be further integrated for planar flows to obtain the Prandtl-Meyer solution.<sup>5</sup> The centered fan of characteristic lines of a rarefaction wave is depicted in Fig. 3, for rarefaction waves on the left and right sides of the stream line. In this diagram three different angles are depicted. The Mach angle  $\mu$  or the angle of a characteristic line with respect to the stream line is given by  $\sin^{-1}(1/M)$ . The angle of the flow  $\xi$  is measured from the radial axis to the stream line. Therefore, the angle of a particular characteristic line, measured from the radial axis, is given by

$$\beta = \xi \mp \sin^{-1}(1/M), \quad (6)$$

where the minus sign is used for the left rarefaction wave and the positive sign is used for the right rarefaction wave. The state of the gas is constant along one particular characteristic line having an angle  $\beta$ . The flow angle  $\xi$  and Mach number  $M$  for this characteristic line within the fan of characteristics can be related to the initial flow properties (with subscript a) by the equation

$$\pm \xi = \pm \xi_a + v(M) - v(M_a), \quad (7)$$

where

$$v(M) = \left[ \frac{\gamma + 1}{\gamma - 1} \right]^{1/2} \tan^{-1} \left[ \left[ \frac{\gamma - 1}{\gamma + 1} \right]^{1/2} [M^2 - 1]^{1/2} \right] - \tan^{-1} [M^2 - 1]^{1/2} \quad (8)$$

is the well-known Prandtl-Meyer function<sup>5</sup>. The static pressure and density for this characteristic line be related to the flow Mach number by means of

$$p/p_a = \left[ (1 + \frac{\gamma - 1}{2} M_a^2) / (1 + \frac{\gamma - 1}{2} M^2) \right]^{\gamma/(\gamma - 1)} \quad (9)$$

and

$$\rho = \rho_a (p/p_a)^{1/\gamma}. \quad (10)$$

Equation 9 can also be rewritten in the following form

$$M = \left[ \frac{2}{\gamma - 1} \left[ \frac{\rho}{\rho_a} \frac{p_a}{p} \left( 1 + \frac{\gamma - 1}{2} M_a^2 \right) - 1 \right] \right]^{1/2}, \quad (11)$$

which will be important for later work. Because the pressure decreases from one characteristic line to the next through a rarefaction wave, from its head to its tail,  $p \leq p_a$ . Also,  $\rho \leq \rho_a$ , and  $M \geq M_a$ .

Now consider the opposite case of an oblique shock wave. In this case the partial differential equations also yield analytical results for the sudden changes in flow properties across the shock.<sup>5</sup> From the diagrams given in Fig. 4 it should be obvious that

$$\pm \xi_b = \pm \xi_a + [\pi/2 - \sigma_s - \delta] - [\pi/2 - \sigma_s], \quad (12)$$

where  $\xi_a$  and  $\xi_b$  are the stream line angles, measured from the radial axis, ahead of and behind the oblique shock wave,  $\sigma_s$  is the oblique shock angle measured from the radial axis, and  $\delta$  is the flow deflection angle. Also, the positive and negative signs go with the shock wave on the left and right of the stream line, respectively. Based on expressions for oblique shock waves, the previous equation can be expressed in a convenient form as

$$\begin{aligned} \pm \xi_b = \pm \xi_a + \sin^{-1} \left[ \frac{1}{M_b} \left[ 1 + \frac{\gamma + 1}{2\gamma} [p_a/p_b - 1] \right]^{1/2} \right] \\ - \sin^{-1} \left[ \frac{1}{M_a} \left[ 1 + \frac{\gamma + 1}{2\gamma} [p_b/p_a - 1] \right]^{1/2} \right] \end{aligned} \quad (13)$$

for later use. Furthermore, the flow Mach number  $M_b$  behind the oblique shock can be related to the flow Mach number  $M_a$  in front of the shock by

$$M_b = \left[ \frac{2}{\gamma - 1} \left[ \frac{\rho_b}{\rho_a} \frac{p_a}{p_b} \left( 1 + \frac{\gamma - 1}{2} M_a^2 \right) - 1 \right] \right]^{1/2}, \quad (14)$$

where the density  $\rho_b$  behind the shock is given in terms of the pressure ratio  $p_b/p_a$  as

$$\rho_b = \rho_a [2\gamma + (\gamma + 1)(p_b/p_a - 1)] / [2\gamma + (\gamma - 1)(p_b/p_a - 1)], \quad (15)$$

where this last equation is a more recognizable Rankine-Hugoniot relation. Note that the pressure increases from the front to the rear of an oblique shock wave and therefore  $p_b \geq p_a$ . Furthermore,  $\rho_b \geq \rho_a$  and  $M_b \leq M_a$ .

The equations above for oblique shock waves contain two solutions - a weak shock and a strong shock solution. Only the weak-shock solution with the smallest entropy increase should be used, because it is the only one observed in actual flow fields.

In the case of slip streams or surfaces that separate different shock and rarefaction waves, as shown in Figs. 2 to 4, the pressure  $p_b$  and flow angle

$\xi_b$  are both continuous across such streams or surfaces. This is indicated in Fig. 5. However, the density  $\rho_b$  and flow Mach number  $M_b$  are both discontinuous.

The two previous analytical solutions for the elemental shock and rarefaction waves, and the conditions that both the flow angle and pressure must be continuous across the slip line, can now be combined or patched together to give four individual solutions for the four different wave patterns shown in Fig. 2. The type of wave pattern and the strengths of the individual waves depend on the initial conditions, that is the initial left state  $S_l$  ( $p_l, \rho_l, M_l$ , and  $\xi_l$ ) and the initial right state  $S_r$  ( $p_r, \rho_r, M_r$ , and  $\xi_r$ ). Regardless of the initial conditions, the four solutions can be combined into one algorithm. In order to do this in an elegant way, the following functions involving the previous expressions are introduced.<sup>49</sup>

$$\kappa(\eta) = \begin{cases} \eta^{1/\gamma} & \text{if } \eta \leq 1 \\ [2\gamma + (\gamma+1)(\eta-1)]/[2\gamma + (\gamma-1)(\eta-1)] & \text{if } \eta > 1 \end{cases} \quad (16)$$

$$\mu(\eta, M_a) = \left[ \frac{2\kappa(\eta)}{(\gamma-1)\eta} \left[ 1 + \frac{\gamma-1}{2} M_a^2 \right] - \frac{2}{\gamma-1} \right]^{1/2} \quad (17)$$

$$\chi(\eta, M_a) = \begin{cases} \nu[\mu(\eta, M_a)] - \nu(M_a) & \text{if } \eta \leq 1 \\ \sin^{-1} \left[ \left[ 1 + \frac{\gamma+1}{2\gamma} [1/\eta - 1] \right] \mu^{-1}(\eta, M_a) \right] \\ \quad - \sin^{-1} \left[ \left[ 1 + \frac{\gamma+1}{2\gamma} [\eta - 1] \right] M_a^{-1} \right] & \text{if } \eta > 1 \end{cases} \quad (18)$$

In these expressions the symbol  $\eta$  is the pressure ratio across either an oblique shock or expansion wave (i.e.,  $p_b/p_a$ ). These three functions can be applied across the left and right waves of the Riemann problem (see Fig. 5), regardless of whether each is a shock or rarefaction wave. If this is done to connect the flow angles ahead and behind the left and right waves,

$$\xi_* = \xi_l + \chi(p_*/p_l, M_l) \quad (19)$$

and

$$-\xi_* = -\xi_r + \chi(p_*/p_r, M_r) \quad (20)$$

are obtained in terms of the common flow angle  $\xi_*$  and pressure  $p_*$  on each side of the slip stream. These two equations can now be added to eliminate  $\xi_*$  and thereby obtain the implicit equation

$$\xi_r - \xi_l = \chi(p_*/p_l, M_l) + \chi(p_*/p_r, M_r) \quad (21)$$

for the common pressure  $p_*$ . This is the basic equation required to determine the common pressure for each of the four different wave patterns. Then the flow

angle  $\xi_*$  can be obtained from either Eq. 19 or 20, and the flow Mach numbers  $M$  on either side of the slip stream can then be obtained from of Eq. 17, because  $\mu(\eta, M_a)$  is actually the Mach number behind either shock or rarefaction wave. Finally, the densities  $\rho$  follow directly from Eq. 16, because  $\kappa(\eta)$  is actually the density ratio for a shock or rarefaction wave. This completes the basic solution procedure of the Riemann problem.

The iterative procedure of solving Eq. 21 for  $p_*$  that is used in this report is the parabolic-curve method<sup>55</sup>, which is a common numerical technique in China. In this method, a function  $G = \xi_r - \xi_l - \chi(p_*/p_l, M_l) - \chi(p_*/p_r, M_r)$  is defined and initially calculated three times for three different initial values or guesses of  $p_*$ , giving  $(G_1, p_{*1})$ ,  $(G_2, p_{*2})$ , and  $(G_3, p_{*3})$ . A parabolic curve is then fitted to these three sets of values of  $G$  and  $p_*$ , and the value of  $p_*$  when  $G$  equals zero is obtained. Then, this new value  $p_{*4}$  and its associated value  $G_4$ , and the two previous sets of values of  $G$  and  $p_*$ , that is  $(G_2, p_{*2})$  and  $(G_3, p_{*3})$ , can be used to produce a new parabolic curve and estimate of  $p_*$ . This procedure can then be repeated until the solution of  $p_*$  is obtained to the desired degree of accuracy (e.g., error less than  $10^{-3}$  percent).

The first guess of  $p_*$  for the computer code which was used in this study was given by  $(p_l + p_r)/2$ . For the parabolic-curve method, which requires three initial guesses, the second one was frequently  $0.98p_*$  and the third was  $1.02p_*$ .

In the parabolic-curve method, there are always two roots for  $p_*$ . By using the smallest root for  $p_*$ , the weak shock solution is chosen automatically over the strong shock solution. This is one notable advantage of this method. Another advantage is that convergence to the root is accelerated by the use of a parabola instead of a straight line, and it would be virtually just as fast as Newton's method. (In Newton's method additional equations would be needed to find the derivative of  $G$ .) Also, the secant method would likely be slightly slower in convergence than either the parabolic-curve or Newton's method.

#### 2.4 Random-Sampling Procedure

The solution of the initial-value or Riemann problem, given the left and right states  $S_l$  and  $S_r$ , has been determined in the previous section. This solution includes both the type of wave pattern and the strengths of the particular waves. The task now is to use this solution to obtain the particular solution at the next grid node, spaced downstream by a distance  $(1/2)\Delta x$  and midway between the original two grid nodes with states  $S_l$  and  $S_r$ . This is accomplished with a random-sampling procedure that will now be described.

In describing the general Riemann problem in section 2.2, it was briefly mentioned that the initial discontinuity separating constant states  $S_l$  and  $S_r$  was specified by means of selecting a random number from a uniform distribution over  $-1/2$  to  $+1/2$ . Hence, the particular wave pattern from the Riemann solution would have its original discontinuity located at some randomly specified point between the original nodes (circles in Fig. 5) and then branch outward in the downstream direction, as shown in Fig. 5. Then, depending on which part of the flow pattern overlaps the next grid node downstream (the cross in Fig. 5), the solution at this point in the flow field would be assigned to this grid node. For example, if this downstream grid node was between the slip stream and the right wave (see the figure), then the solution of this recently computed state would be assigned to this node. If this downstream node was to the right or ahead of the right wave, then state  $S_r$  would be assigned to this grid node.

The procedure outlined above could be programmed easily for a computer. However, it is easier and customary to program an alternate but fully equivalent procedure. In this procedure the initial discontinuity of the wave pattern is always fixed at the midpoint between the initial two grid nodes, which are shown as circles and having states  $S_l$  and  $S_r$  in Fig. 6. Then the wave pattern is sampled randomly downstream, along a line at a fixed distance  $x+(1/2)\Delta x$  that passes through the downstream grid node (the cross). This sampling point is labelled P in the figure. If the random number  $\Omega$  was equal to  $-1/2$ , then point P would be located at the corner labelled a. If  $\Omega$  was equal to 0, then the point P would be coincident with the downstream grid point, and if  $\Omega$  was equal to  $+1/2$ , then point P would be at the top corner labelled b. The solution for point P from the Riemann problem, denoted as state  $\bar{S}$  or in terms of variables as  $\bar{p}$ ,  $\bar{\rho}$ ,  $\bar{M}$ , and  $\bar{\xi}$ , is then assigned to the downstream grid point.

In the random-sampling procedure there are four basic cases that must be considered. These cases are summarized below and then dealt with in detail.

1. The sampling point  $P[x+(1/2)\Delta x, r+\Omega\Delta r]$  lies to the left of the slip stream, which has a slope  $dr/dx = \cot(\xi_*)$  in the  $(x,r)$ -plane, and the left wave is a shock wave, that is,

$$\Omega\Delta r \geq (1/2)(\Delta x)\cot(\xi_*) \quad \text{and} \quad p_* > p_l.$$

2. The sampling point  $P[x+(1/2)\Delta x, r+\Omega\Delta r]$  lies to the left of the slip stream, which has a slope  $\cot(\xi_*)$  in the  $(x,r)$ -plane, and the left wave is a rarefaction wave, that is,

$$\Omega\Delta r \geq (1/2)(\Delta x)\cot(\xi_*) \quad \text{and} \quad p_* \leq p_l.$$

3. The sampling point  $P[x+(1/2)\Delta x, r+\Omega\Delta r]$  lies to the right of the slip stream, which has a slope  $\cot(\xi_*)$  in the  $(x,r)$ -plane, and the right wave is a shock wave, that is,

$$\Omega\Delta r < (1/2)(\Delta x)\cot(\xi_*) \quad \text{and} \quad p_* > p_r.$$

4. The sampling point  $P[x+(1/2)\Delta x, r+\Omega\Delta r]$  lies to the right of the slip stream, which has a slope  $\cot(\xi_*)$  in the  $(x,r)$ -plane, and the right wave is a rarefaction wave, that is,

$$\Omega\Delta r < (1/2)(\Delta x)\cot(\xi_*) \quad \text{and} \quad p_* \leq p_r.$$

Case 1:  $\Omega\Delta r \geq (1/2)(\Delta x)\cot(\xi_*)$  and  $p_* > p_l$

In this case the shock-wave angle  $\sigma_s$ , measured from the radial axis to the shock wave (see Fig. 4), is given by

$$\sigma_s = \xi_l - \sin^{-1} \left[ \frac{1}{M_l} \left[ 1 + \frac{\gamma+1}{2\gamma} [p_*/p_l - 1] \right]^{1/2} \right]. \quad (22)$$

If the sampling point P lies to the left or in front of the shock wave, that is, if  $\Omega\Delta r > (1/2)(\Delta x)\cot(\sigma_s)$ , then the values for the sampling point P are those of the left state  $S_l$ , or  $\bar{p} = p_l$ ,  $\bar{\rho} = \rho_l$ ,  $\bar{M} = M_l$ , and  $\bar{\xi} = \xi_l$ . In this subcase these

values are then assigned to the downstream grid point (shown as a cross). If the sampling point P lies to the right of or behind the shock wave, that is,  $\Omega\Delta r \leq (1/2)(\Delta x)\cot(\sigma_s)$ , then the sampling-point values for point P are  $\bar{p} = p_*$ ,  $\bar{\rho} = \rho_1 \kappa(p_*/p_1)$ ,  $\bar{M} = \mu(p_*/p_1, M_1)$ , and  $\bar{\xi} = \xi_*$ . In this subcase these values are then assigned to the downstream grid point.

Case 2:  $\Omega\Delta r \geq (1/2)(\Delta x)\cot(\xi_*)$  and  $p_* \leq p_1$

The rarefaction wave is bounded on the left by its head and on the right by its tail, and the equations for these characteristics are given by

$$\beta_h = \xi_1 - \sin^{-1}(1/M_1), \quad (23)$$

$$\beta_t = \xi_* - \sin^{-1}[\mu^{-1}(p_*/p_1, M_1)], \quad (24)$$

where  $\beta_h$  and  $\beta_t$  are the angles of the head and tail characteristics, measured from the radial axis (see Fig. 3). If the sampling point P lies to the left of or in front of the rarefaction-wave head, that is,  $\Omega\Delta r \geq (1/2)(\Delta x)\cot(\beta_h)$ , then the sampling point values for P are simply those of the left state  $S_1$  or  $\bar{p} = p_1$ ,  $\bar{\rho} = \rho_1$ ,  $\bar{M} = M_1$ , and  $\bar{\xi} = \xi_1$ . If the sampling point lies to right of or behind the rarefaction-wave tail, that is,  $\Omega\Delta r \leq (1/2)(\Delta x)\cot(\beta_t)$ , then the values for sampling point P are  $\bar{p} = p_*$ ,  $\bar{\rho} = \rho_1 \kappa(p_*/p_1)$ ,  $\bar{M} = \mu(p_*/p_1, M_1)$ , and  $\bar{\xi} = \xi_*$ .

Finally, if the sampling point lies inside the characteristic fan of the rarefaction wave, then the values for the sampling point are more difficult to obtain, because the solution is iterative. From the angle of the characteristic line passing through the sampling point P, the equation

$$\bar{\xi} - \sin^{-1}(1/\bar{M}) = \pi/2 - \tan^{-1}(2\Omega\Delta r/\Delta x) \quad (25)$$

relates the two unknowns  $\bar{\xi}$  and  $\bar{M}$ . The Prandtl-Meyer equation,

$$\bar{\xi} = \xi_1 + \nu(\bar{M}) - \nu(M_1), \quad (26)$$

with the same two unknowns can be used to eliminate  $\bar{\xi}$ , yielding the implicit equation in  $\bar{M}$

$$\nu(\bar{M}) - \sin^{-1}(1/\bar{M}) = -\xi_1 + \nu(M_1) + \pi/2 - \tan^{-1}(2\Omega\Delta r/\Delta x). \quad (27)$$

This equation is solved for  $\bar{M}$  by employing the parabolic-curve method that was described earlier. Newton's method could also be used, and it would probably give a faster convergence. Finally,  $\bar{\xi}$  is obtained from either of Eqs. 25 or 26, and the expressions

$$\bar{p} = p_1 \left[ \frac{2 + (\gamma - 1)M_1^2}{2 + (\gamma - 1)\bar{M}^2} \right]^{\gamma/(\gamma-1)}, \quad (28)$$

$$\bar{\rho} = \rho_1 \kappa(\bar{p}/p_1), \quad (29)$$

give the final values for  $\bar{p}$  and  $\bar{\rho}$ .

Case 3:  $\Omega\Delta r < (1/2)(\Delta x)\cot(\xi_*)$  and  $p_* > p_r$

Case 3 is a mirror image of case 1. The same logic applies but there are some changes that occur in the equations, and these are mainly subscripts and mathematical symbols.

In this case the shock-wave angle  $\sigma_s$ , measured from the radial axis to the shock wave (see Fig. 4), is given by

$$\sigma_s = \xi_r + \sin^{-1}\left[\frac{1}{M_r} \left[1 + \frac{\gamma+1}{2\gamma}(p_*/p_r - 1)\right]^{1/2}\right]. \quad (30)$$

If the sampling point P lies to the right (in front of the shock wave), that is, if  $\Omega\Delta r < (1/2)(\Delta x)\cot(\sigma_s)$ , then the values for the sampling point P are those of the right state  $S_r$ , or  $\bar{p} = p_r$ ,  $\bar{\rho} = \rho_r$ ,  $\bar{M} = M_r$ , and  $\bar{\xi} = \xi_r$ . In this subcase these values are then assigned to the downstream grid point (shown as a cross). If the sampling point P lies to the left of or behind the shock wave, that is,  $\Omega\Delta r \geq (1/2)(\Delta x)\cot(\sigma_s)$ , then the sampling-point values for point P are  $\bar{p} = p_*$ ,  $\bar{\rho} = \rho_r \kappa(p_*/p_r)$ ,  $\bar{M} = \mu(p_*/p_r, M_r)$ , and  $\bar{\xi} = \xi_*$ . In this subcase these values are then assigned to the downstream grid point.

Case 4:  $\Omega\Delta r < (1/2)(\Delta x)\cot(\xi_*)$  and  $p_* \leq p_r$

Case 4 is a mirror image of case 2. The same logic applies but some changes occur in the equations, such as subscripts and mathematics symbols.

The rarefaction wave is bounded on the right by its head and on the left by its tail, and the equations for these characteristics are given by

$$\beta_h = \xi_r + \sin^{-1}(1/M_r) \quad (31)$$

and

$$\beta_t = \xi_* + \sin^{-1}[\mu^{-1}(p_*/p_r, M_r)]. \quad (32)$$

where  $\beta_h$  and  $\beta_t$  are the angles of the head and tail characteristics, measured from the radial axis (see Fig. 3). If the sampling point P lies to the right of or in front of the rarefaction-wave head, that is,  $\Omega\Delta r \leq (1/2)(\Delta x)\cot(\beta_h)$ , then the sampling point values for P are those of the right state  $S_r$ , or  $p = \bar{p}_r$ ,  $\bar{\rho} = \rho_r$ ,  $\bar{M} = M_r$ , and  $\bar{\xi} = \xi_r$ . If the sampling point lies to left of or behind the rarefaction-wave tail, that is,  $\Omega\Delta r \geq (1/2)(\Delta x)\cot(\beta_t)$ , then the values for sampling point P are  $\bar{p} = p_*$ ,  $\bar{\rho} = \rho_r \kappa(p_*/p_r)$ ,  $\bar{M} = \mu(p_*/p_r, M_r)$ , and  $\bar{\xi} = \xi_*$ .

Finally, if the sampling point lies inside the characteristic fan of the rarefaction wave, then the values for the sampling point are more difficult to obtain, because the solution is iterative. From the angle of the characteristic line passing through the sampling point P, the equation

$$\bar{\xi} + \sin^{-1}(1/\bar{M}) = \pi/2 - \tan^{-1}(2\Omega\Delta r/\Delta x) \quad (33)$$

relates the two unknowns  $\bar{\xi}$  and  $\bar{M}$ . The Prandtl-Meyer equation expressed in the

following form,

$$\bar{\xi} = \xi_r - v(\bar{M}) + v(M_r), \quad (34)$$

with the same two unknowns, can be used to eliminate  $\bar{\xi}$ , yielding the implicit equation in  $\bar{M}$ ,

$$v(\bar{M}) - \sin^{-1}(1/\bar{M}) = \xi_r + v(M_r) - \pi/2 + \tan^{-1}(2\Omega\Delta r/\Delta x). \quad (35)$$

This equation is solved for  $\bar{M}$  by employing the parabolic-curve method that was described earlier. Finally,  $\bar{\xi}$  is obtained from either of Eqs. 33 or 34, and the expressions

$$\bar{p} = p_r \left[ \frac{2 + (\gamma - 1)M_r^2}{2 + (\gamma - 1)\bar{M}^2} \right]^{\gamma/(\gamma-1)}, \quad (36)$$

$$\bar{\rho} = \rho_r \kappa(\bar{p}/p_r), \quad (37)$$

give the final values for  $\bar{p}$  and  $\bar{\rho}$ .

In the random-choice method, it is natural to think of using a new value of the random number  $\Omega$  for each cell, that is for each combination of  $i$  and  $j$ . However, the practical effect of such a choice with finite spacings of  $\Delta x$  and  $\Delta r$  is disastrous, except for flow-field data that is nearly constant, as originally pointed out by Chorin.<sup>28</sup> If this is in fact done there is a finite probability that a given state will propagate to both the left and right, thereby creating a spurious constant state. The numerical results will become less accurate and more jagged (as if the results contain numerical noise). In the random-choice method used here, a new random number  $\Omega$  is chosen only once per new level in the axial direction, that is once for each new step  $\Delta x$ . This random number is then used for all cells of this column. This is now a common practice for the random-choice method.

## 2.5 Random-Number Algorithm

The type of random-number algorithm plays a significant role in both the behavior of the solution and the quality of numerical results from the random-choice method. Better random numbers produce numerical results that are more accurate (e.g., more accurate placement of the position of shocks in the flow field), and these results also have less jaggedness or numerical noise.<sup>28-30,47</sup> It is now known that the best random numbers for the random-choice method are ones that are actually nonrandom but equidistributed, or ones that become equidistributed relatively quickly or alternatively tend as fast as possible to approximate equipartition in the range from  $-1/2$  to  $+1/2$ .<sup>28</sup> In this regard it appears at the present time that the best random-number algorithm for use with the random-choice method is that due to Van der Corput.<sup>29-30,47</sup> This random-number algorithm appears in Van der Corput's original work<sup>56</sup>, is given in the book by Hammersley and Handscomb<sup>57</sup>, and is also discussed by Colella<sup>29-30</sup>. This algorithm is also presented here because it is rather short and also for the sake of completeness.

For the Van der Corput algorithm, suppose that the natural numbers are expressed in the scale of notation with a radix equal to 2, so that

$$n = \sum_{k=0}^m i_k 2^k. \quad (38)$$

This is also the binary expansion of the number sequence  $n = 1, 2, 3, \dots$ , etc., where  $i$  is a binary number that equals only 0 and 1. Then, a set of random numbers  $\Omega_n$  can be obtained by simply writing the digits of these numbers in their reverse order, preceded by a decimal point. This gives the following series

$$\Omega_n = \sum_{k=0}^m i_k 2^{-(k+1)}. \quad (39)$$

The method of getting the sequence of random numbers from the above equations might seem to be a little unclear. In order to clearly illustrate the manner in which this sequence is constructed, the first few elements of the various sequences involved are written down for convenience in the table given below.

n (decimal)	$i_k$ (binary)	$\Omega_n$ (binary)	$\Omega_n$ (decimal)
1	1	0.1	0.5000
2	10	0.01	0.2500
3	11	0.11	0.7500
4	100	0.001	0.1250
5	101	0.101	0.6250
6	110	0.011	0.3750
7	111	0.111	0.8750
8	1000	0.0001	0.0625
9	1001	0.1001	0.5625
10	1010	0.0101	0.3125

The decimal numbers  $n$  are first changed into the binary numbers  $i_k$ . Then these binary numbers are reversed and a point or decimal is put in the front to get  $\Omega_n$  as binary numbers. Finally, these binary numbers are simply converted back into decimal numbers, yielding  $\Omega_n$  in decimal notation, and covering the entire range from 0 to 1.

It can be noted that  $\Omega_n$  is less than 1/2 if  $n$  is even, and  $\Omega_n$  is greater than 1/2 if  $n$  is odd, but  $\Omega_n$  always covers the range from 0 to 1. Furthermore, we have  $(k/4) \leq \Omega_n < ((k+1)/4)$  if  $n = j_k \pmod{4}$ , with  $k = 1, 2$ , and  $4$ , where  $j_0 = 0$ ,  $j_1 = 2$ ,  $j_2 = 1$ , and  $j_3 = 3$ . Finally, note that this Van der Corput random-number algorithm, like all of the others with radix different than 2, is equidistributed.

## 2.6 Accuracy of the Flow-Field Computations

The accuracy of computations of the flow field depends mainly on the size of the grid. The constant grid spacing  $\Delta r$  in the radial direction is specified, independent of the problem. This spacing depends on the particular problem being solved, the quality of numerical results desired, and the time and cost of the computations. A suitably small grid spacing in the radial direction will ensure almost any accuracy desired, provided that computer roundoff errors are not encountered.

The grid spacing  $\Delta x$  in the axial direction should not be specified independently or arbitrarily, because this spacing can affect the numerical accuracy of the results. If  $\Delta x$  is very small, numerical accuracy is maintained but the number of computations and resulting computational cost are high. Hence, given the spacing  $\Delta r$ , the other spacing  $\Delta x$  should be made as large as possible, without making the numerical solution unstable or inaccurate. In the random-choice method, which is an explicit method, there is no essential criterion for numerical stability. In other words, the solution for any length  $\Delta x$  is stable. However, if  $\Delta x$  is too large the numerical results will be inaccurate, because the effects of overlapping of adjacent wave patterns is ignored. Experience shows that numerical accuracy can be maintained in the solution of nonstationary one-dimensional flows if the time step is limited by or specified according to the Courant-Friedrichs-Lewy criterion.<sup>28,48</sup> This same criterion is used here for two-dimensional steady supersonic flows.

The Courant-Friedrichs-Lewy criterion is a limitation on the size of  $\Delta x$ . For this condition to be satisfied, the wave pattern cannot spread out radially by more than a distance of  $\Delta r$  over the distance  $\Delta x$ . This means that adjacent wave patterns should not interfere or overlap, otherwise the numerical accuracy will decrease. This criterion is expressed as

$$\Delta x \leq \Delta r |\tan(\xi \mp \mu)|_{\min}, \quad (40)$$

where  $\xi$  is the angle of a stream line measured from the radial axis and  $\mu$  is the Mach angle measured between the stream line and a Mach wave. The negative sign is employed for the case of a left Mach wave and the positive sign is used with a right Mach wave. In this study, the largest  $\Delta x$  is normally used, that is,

$$\Delta x = \Delta r |\tan(\xi \mp \mu)|_{\min}. \quad (41)$$

However, whenever  $\Delta x$  is larger than  $\Delta r$ , which occurs for highly supersonic flows because the wedge-shaped pattern is not widely spread,  $\Delta x$  is further restricted by being set equal to  $\Delta r$ . This helps produce more smoothly varying numerical results or profiles in the axial direction.

## 2.7 Boundary Conditions

Boundary conditions must normally be specified at the outer extremities of the flow field. These are normally needed for the outermost grid points in the radial direction and sometimes near or at the origin. One or both of these boundaries can be the direct result of a solid body or a rigid surface in the flow, which are normally approximated as local straight-line segments if the surface is curved. One of these boundaries can also be an arbitrary edge of the flow field, across which waves can move freely without reflection as they

leave the flow field. Finally, the boundary may also be that of a jet of gas or free jet passing through another gas that is essentially stationary and has a basically uniform pressure. All of these boundary conditions are considered herein.

Firstly, consider the continuous boundary condition. In this simple case the flow field is ended at a radial distance that is specified for convenience. Any compression, shock, or expansion wave which impinges on this boundary must be allowed to pass out of the flow field without any significant reflection or influence on the flow field, just as if the flow field continued indefinitely in the radial direction. Let the flow field end (at radius  $r$  for example), and let the flow properties be calculated at a grid node at this radial distance  $r$  and axial distance  $x+(1/2)\Delta x$  (e.g., cross in Fig. 6). The previous right state  $S_r$  ( $p_r, \rho_r, M_r, \xi_r$ ) at the coordinate point  $[x, r-(1/2)\Delta r]$  is already known. Now, by creating a pseudo or an artificial left state  $S_l$  outside the flow field at the coordinate point  $[x, r+(1/2)\Delta r]$ , which has identical flow conditions as that of the right state (i.e.,  $p_l = p_r, \rho_l = \rho_r, M_l = M_r$ , and  $\xi_l = \xi_r$ ), the Riemann problem can then be solved in the usual manner to obtain the required flow conditions downstream at the desired coordinate point  $[x+(1/2)\Delta x, r]$  on the boundary. Finally, note that the previous specification of this boundary condition is only approximate, and minor wave reflections can sometimes occur, especially if the gradients of the actual flow properties across the boundary are relatively large.

Now consider the case of a rigid surface that compresses or expands the flow. For the purpose of illustration, let the flow be above the surface of a body. In this case the left state  $S_l$  ( $p_l, \rho_l, M_l, \xi_l$ ) is known at the coordinate point  $[x, r+(1/2)\Delta r]$  within the flow (see Fig. 6), and the flow properties for the downstream state at coordinate point  $[x+(1/2)\Delta x, r]$  need to be computed. Although this grid node may be located inside or outside of the flow, its state is still computed for either case, and furthermore employed in the computations in subsequent steps. In order to obtain the flow properties at this downstream grid node, an artificial state  $S_r$  is first created for the coordinate point  $[x, r-(1/2)\Delta r]$  that is located inside the body.

The properties  $p_r, \rho_r, M_r$ , and  $\xi_r$  of this artificial right state are obtained by applying a symmetric boundary condition. An artificial flow with a right wave is created inside the body to simply counteract the flow outside such that the flow deflection of the resulting slip stream is tangent to the surface of the body. From the point of view of symmetry, therefore,  $p_r = p_l, \rho_r = \rho_l, M_r = M_l$ , and  $\xi_r = \xi_l - 2\delta$ , where  $\delta$  is the flow deflection angle. This symmetry gives left and right waves of the same type and with the same strength, and the angle  $\delta$  is positive for a left shock wave and negative for a left rarefaction wave. The deflection angle  $\delta$  can be related to the angle of the body surface by  $\delta = \xi_l - \pi/2 + \tan^{-1}(dr_b/dx)$  or  $\delta = -\xi_r + \pi/2 - \tan^{-1}(dr_b/dx)$ , where  $dr_b/dx$  is the local slope  $\tan(\delta_b)$  of the surface. Hence,  $\xi_r = \pi - \xi_l - 2\tan^{-1}(dr_b/dx)$  is the final result for the flow properties at the artificial state  $S_r$ . Now that both left and right states are known, the Riemann problem can be solved and random sampling applied in the usual manner to determine the new flow properties at the downstream grid node.

Finally, consider the case of a free-jet boundary. For illustration purposes again, let the free-jet flow be above or to the left of the boundary. As in the previous case, the left state  $S_l$  ( $p_l, \rho_l, M_l, \xi_l$ ) is known, the flow properties at the downstream grid point need to be computed, and an artificial right state  $S_r$  needs to be established. A symmetric boundary condition is again

applied, with a slight difference in the last step. Firstly,  $p_r = p_1$ ,  $\rho_r = \rho_1$ ,  $M_r = M_1$ , and  $\xi_r = \xi_1 - 2\delta$ , where  $\delta$  is the again flow deflection angle. This symmetry also gives left and right waves of the same type and with the same strength, and the angle  $\delta$  is positive for a left shock wave and negative for a left rarefaction wave. The flow deflection angle can again be expressed in the form  $\delta = \xi_1 - \pi/2 + \delta_b$  or  $\delta = -\xi_r + \pi/2 - \delta_b$ , where  $\delta_b$  is the angle of the free-jet surface. However, the free-jet-surface angle  $\delta_b$  is unknown and the flow deflection angle  $\delta$  cannot be calculated from  $\delta_b$ . This angle has to be obtained from known boundary information.

The information required is that the pressure at the free-jet surface is equal to the pressure of the fluid or gas surrounding the free jet. Hence, the strengths  $p_*/p_1$  and  $p_*/p_r$  of the left and right waves are known, and the type of waves are also known. Based on the known strength of the left running wave the flow deflection angle can readily be calculated for a left shock wave ( $p_*/p_1 \geq 1$ ) or a left rarefaction wave ( $p_*/p_1 < 1$ ), by using the appropriate equations for oblique shock or rarefaction waves. In the present case this is particularly simple, by making use of previously introduced equations. The flow deflection angle  $\delta$  is the negative of the previously defined function  $\chi(\eta, M)$ , that is,  $\delta = -\chi(p_*/p_1, M_1)$  in our case. This then gives the flow angle at the right state as  $\xi_r = \xi_1 + 2\chi(p_*/p_1, M_1)$ . This completes the specification of the right artificial state, so that the normal Riemann problem can be solved and random sampling applied to get all the flow properties at the downstream state.

## 2.8 Operator-Splitting Technique to Obtain Axisymmetric-Flow Solutions

The previous analysis is complete for the random-choice method to solve two-dimensional, planar, steady, supersonic flow problems, that is problems for which the inhomogeneous term  $h(W, r)$  in Eqs. 1 and 2 is nonexistent or just zero (because  $\alpha = 0$ ). For axisymmetric flows, however, this is not true because the inhomogeneous term is nonzero ( $\alpha = 1$ ). Some additional analysis is required to correct the planar-flow solution, which is determined first for the case of axisymmetric-flow problems, such that the axisymmetric-flow solution of interest is then obtained. The operator-splitting technique, originally introduced to the random-choice method by Sod<sup>31</sup> to include the inhomogeneous term as a correction to solve one-dimensional unsteady flow problems with an area change, is also used in this study.

In the case of the operator-splitting technique, the first step is to solve the homogeneous set of equations in conservation form,

$$\frac{\partial}{\partial x}[f(\bar{W})] + \frac{\partial}{\partial r}[g(\bar{W})] = 0, \quad (42)$$

for  $\bar{W} = [\bar{p}, \bar{p}\bar{u}, \bar{p}\bar{v}, \bar{e}]$  by means of the past analysis for the Riemann problem. Once this Riemann solution  $\bar{W}$  for a planar flow is known, the second step is to use the set of equations given by

$$\frac{\partial}{\partial x}[f(W)] = h(\bar{W}, r) \quad (43)$$

to correct this planar solution  $\bar{W}$  to obtain the axisymmetric-flow solution  $W$ . Because the right hand side of this equation is known, it becomes an ordinary

differential equation, and the correction at the node on the  $i^{\text{th}}$  column and  $j^{\text{th}}$  row is obtained by means of a Cauchy-Euler finite-difference scheme in the form

$$f(W_j^i) = f(\bar{W}_j^i) + h(\bar{W}_j^i, r_j) \Delta x, \quad (44)$$

where  $\Delta x$  is the incremental distance from the previous left and right states to this downstream grid node. The solution  $W$  can then be written in the form

$$\begin{bmatrix} \rho u \\ \rho u^2 + p \\ \rho u v \\ u(e + p) \end{bmatrix} = \begin{bmatrix} \bar{\rho} \bar{u} \\ \bar{\rho} \bar{u}^2 + \bar{p} \\ \bar{\rho} \bar{u} \bar{v} \\ \bar{u}(\bar{e} + \bar{p}) \end{bmatrix} - \frac{\Delta x}{r} \begin{bmatrix} \bar{\rho} \bar{v} \\ \bar{\rho} \bar{u} \bar{v} \\ \bar{\rho} \bar{v}^2 \\ \bar{v}(\bar{e} + \bar{p}) \end{bmatrix} = \begin{bmatrix} G_1 \\ G_2 \\ G_3 \\ G_4 \end{bmatrix}, \quad (45)$$

or much more simply as  $\rho u = \lambda \bar{\rho} \bar{u} = G_1$ ,  $p + \rho u^2 = \bar{p} + \lambda \bar{\rho} \bar{u}^2 = G_2$ ,  $\rho u v = \lambda \bar{\rho} \bar{u} \bar{v} = G_3$ , and  $u(e + p) = \lambda \bar{u}(\bar{e} + \bar{p}) = G_4$ , where  $\lambda = 1 - (\Delta x/r)\bar{v}/\bar{u}$  is a correction factor. If  $\lambda$  is equal to unity there is no correction required, and as  $\lambda$  deviates from unity the correction becomes less accurate. From the first and third of the last four of these equations it can be clearly seen that the radial velocity  $v$  will always be invariant during the correction procedure.

The values of  $G_1$ ,  $G_2$ ,  $G_3$ , and  $G_4$  and can be manipulated to yield values of  $p$ ,  $\rho$ ,  $u$ ,  $v$ ,  $e$ ,  $M$ , and  $\xi$ . The quadratic equation

$$A \rho^2 - 2B \rho - C = 0, \quad (46)$$

with

$$A = [G_3^2/G_1 - 2G_4]/G_1 = \bar{v}^2 - 2(\bar{e} + \bar{p})/\bar{p},$$

$$B = -[\gamma/(\gamma-1)]G_2 = -[\gamma/(\gamma-1)](\lambda \bar{\rho} \bar{u}^2 + \bar{p}),$$

and

$$C = [(\gamma+1)/(\gamma-1)]G_1^2 = [(\gamma+1)/(\gamma-1)](\lambda \bar{\rho} \bar{u})^2,$$

is first established in terms of the density  $\rho$ , and then the solution for the density is given by

$$\rho = [B + (B^2 + AC)^{1/2}]/A. \quad (47)$$

The other primitive variables then follow from  $u = G_1/\rho = \lambda \bar{\rho} \bar{u}/\rho$ ,  $v = G_3/G_1 = \bar{v}$ ,  $p = G_2 - G_1/\rho = \bar{p} + \lambda \bar{\rho} \bar{u}^2(1 - \bar{\rho}/\rho)$ , and  $e = \rho G_4/G_1 - p = (\bar{e} + \bar{p})\bar{\rho}/\rho - p$ . Finally,  $M = [(u^2 + v^2)/(\gamma p/\rho)]^{1/2}$  and  $\xi = \pi/2 - \tan^{-1}(v/u)$ , completing the corrected axisymmetric-flow solution for this grid node  $(i, j)$ .

The procedure of correcting the initial planar-flow solution to obtain the axisymmetric-flow solution by means of the operator-splitting technique is explicit, and this keeps the entire random-choice method explicit. Note also that the boundary conditions are not used in the operator-splitting technique, because they enter only during the procedure of obtaining the initial Riemann solution for the planar flow. The correction scheme by means of the operator-splitting technique is applied in the random-choice method at each grid point within the flow field, except for nodes on the origin ( $r = 0$ ). At the origin no correction is needed, because the correction factor  $\lambda = 1 - (\Delta x/r)\bar{v}/\bar{u}$  equals unity by virtue of the fact that  $\bar{v}/r$  equals zero at the origin. A correction is normally done just after the initial Riemann problem for the planar flow is

computed, or just after an entire column is computed. Therefore, each initial Riemann solution for the planar flow is obtained from both the left and right states that have been previously corrected to give the axisymmetric-flow solution. Making the correction at every half-step is important for improving the resolution and accuracy of the numerical results, without much additional effort. This type of correction scheme is first order and can be called an 'asymmetric' operating-splitting technique<sup>29,58</sup>, and it is used most often in the computations in this report.

There is also another first-order equivalent correction scheme called a 'symmetric' operator-splitting technique<sup>29,58</sup>. For this scheme the equations are the same as those already given in this section. However, in this scheme the correction is applied twice in succession for each grid point in each alternate column (in the radial direction) and not at those columns in between. This scheme is seldom used in the present study, although it gives equivalent results with the same computational effort.

There is also a second-order correction technique due to MacCormack<sup>8,58</sup>. The two equations for this predictor-corrector technique are

$$f(\tilde{W}_j^i) = f(\bar{W}_j^i) + h(\bar{W}_j^i, r_j) \Delta x, \quad (48)$$

$$f(W_j^i) = \frac{1}{2} \left[ f(\bar{W}_j^i) + f(\tilde{W}_j^i) + h(\tilde{W}_j^i, r_j) \Delta x \right],$$

where  $\tilde{W}$  is the first-order intermediate result of the first step by forward differencing and  $W$  is the final second-order solution from the second step by backward differencing. This scheme is infrequently used in this study, because it requires more computations per step without increasing the accuracy.

A second-order correction scheme would not normally be used with a first-order random-choice method, because there is no increase in accuracy to be expected. However, in some cases numerical noise can be reduced, and this can be advantageous and justify its use. This is not the case in the present investigation.

It is worthwhile mentioning here that the introduction of an operator-splitting technique in the solution of axisymmetric-flow problems contributes numerical error. The technique gives accurate results only when the correction for the inhomogeneous term is relatively small. In axisymmetric flows for which the radius  $r$  includes zero, the correction, because of the  $1/r$  factor in  $h(W, r)$ , becomes unduly large and is therefore inaccurate. Hence, numerical results for some parts of axisymmetric flow fields which include small values of radial distance should not be expected to be computed accurately. Furthermore, and very importantly, parts of axisymmetric flow fields away from the center of symmetry but which originate or depend on parts of the flow field that include the center of symmetry may not be as accurate as expected.

Sod<sup>59</sup> has suggested recently that more accurate numerical results can be obtained with the operator-splitting technique if the value of the radius  $r$  in the inhomogeneous term  $h(W, r)$  is computed at the sampling point, rather than at the location of the downstream grid node. Although the computational effort of adding this improvement is virtually negligible, most RCM codes do not include this improvement. At large radii or numerous grid points from the origin the improvement is, of course, inconsequential. For small radii or less than a few

grid nodes from the origin the operator-splitting correction can then change. However, these changes were discovered to be insignificant in the solution as a whole, and have not been included in most of the numerical results to be given in later chapters.

### 3.0 PRACTICAL METHOD OF REDUCING RANDOM-CHOICE-METHOD COMPUTATIONS

In numerical computations of planar and axisymmetric steady supersonic flows, large portions of the flow field can be entirely free of wave motion or have insignificant wave motion. These portions of the flow field need not be computed in most cases, which can result in a marked reduction in computational time with a significant saving in computational cost.

Consider the free-stream flow ahead of a planar or axisymmetric body, as shown in Fig. 7. Because the wave emanating from the body is swept downstream as it moves outward in the supersonic flow, free-stream conditions ahead of the wave exist over a large portion of the flow field (labelled A in the figure). This is particularly true when the free-stream Mach number is large. In any case, it is rather easy and often highly beneficial in reducing computational costs to write the computer program in such a way that computer computations are skipped at all of these grid points for which the flow properties are simply constant.

Now consider the flow in region C of Fig. 7, downstream of the main wave of interest in region B. The variation in the flow properties throughout region C is small and of little interest. If an appropriate boundary condition is used along the dashed line shown, the flow properties in region C can be eliminated. This termination line must be sufficiently far behind the body such that all the important or interesting parts of the flow field are included in the numerical computations. For planar and axisymmetric bodies one can start this line at a radial distance equal to zero and an axial distance of approximately one-half to one body length behind the end of the body, depending on the flow field. Then, across this boundary during the computations the flow angle can be taken to have a linear variation (constant gradient). Hence, the flow angle at the artificial state to the right of this boundary  $\xi_r$  is given by

$$\xi_{j-1} = 2\xi_j - \xi_{j+1} \quad \text{or} \quad \xi_r = 2\xi_1 - \xi_{j+1}, \quad (49)$$

if the flow is above the boundary and the flow angle  $\xi_{j+1}$  is for the second grid point inside the terminal line. This specification of  $\xi_{j-1}$  or  $\xi_r$  for the right artificial state is actually equivalent to the specification of a solid boundary with a surface slope  $\pi/2 - 2\xi_j + \xi_{j+1}$  or  $\pi/2 - \xi_{j-1}$  somewhere between the left and right states that straddle this terminal line. Therefore, the handling of flow computations at this terminal line reduces to the simple case of applying the previous solid-body or rigid-wall boundary condition with a body slope given by  $\pi/2 - 2\xi_j + \xi_{j+1}$ .

As the flow field is being computed from the terminal boundary line to the leading shock wave, this terminal line can be inserted in the computations by making it run approximately parallel to the leading shock wave. This is easily accomplished by selecting a convenient number of grid nodes between the leading shock wave and the terminal line. Therefore, the numerical computations for the main outward moving wave are done in the form of a band with a constant width, which is labelled B in Fig. 7.

## 4.0 LIMITATIONS OF THE RANDOM-CHOICE METHOD

### 4.1 Steady Supersonic Planar Flows

The random-choice method can be applied to obtain solutions to numerous different types of planar-flow problems (see the numerical solutions presented in chapter 5). The only limitation is that the steady flow has to be supersonic everywhere in the computed flow field. Hence, for flows over bodies, oblique shock waves must normally be attached either to the leading edge of the body or one of its protuberances. Supersonic flows around bodies with a blunt leading edge or supersonic flows that contain 'pockets' of subsonic flow cannot, therefore, be computed.

It is worthwhile to note that the random-choice method cannot calculate all supersonic flows over wedges for which the oblique shock is attached to the leading edge, because an attached shock can still have a subsonic flow behind it if the wedge angle is sufficiently large<sup>60-61</sup>. Consequently, the limitation in the application of the random-choice method for solving steady planar flows is most properly that the flow must always be supersonic and not the criterion of shock attachment or detachment.

### 4.2 Steady Supersonic Axisymmetric Flows

The random-choice method can also be used to solve many different types of axisymmetric-flow problems. However, its application is more limited in the case of axisymmetric flows than planar flows. Besides the obvious limitation that the steady flow has to be supersonic everywhere within the computed flow field, there is one additional limitation that restricts the application of the random-choice method, and also one additional difficulty that can make the grid spacing undesirably small.

The one additional limitation stems directly from using a first-order random-choice method for which the planar solution is computed first and then corrected by means of the operator-splitting technique to obtain the desired axisymmetric-flow solution. For certain axisymmetric flow conditions which involve relatively large flow-deflection or turning angles through shock waves, the corresponding planar solution does not always exist. Hence, there is no planar solution in such cases to correct to obtain the desired axisymmetric-flow solution. As a result of this unfortunate limitation, axisymmetric flows with such large flow deflections cannot be computed, or flow fields cannot be fully computed.

This limitation is well illustrated by a plot of the maximum possible deflection angle through an oblique shock that produces a sonic flow behind it and is attached to a wedge and a cone. Such a plot as shown in Fig. 8 can be generated from the tables and charts in the NASA Ames handbook<sup>61</sup>. The maximum deflection angle for the case of the cone is substantially larger than that for the wedge. Consequently, the random-choice method cannot solve a planar Riemann problem for which the maximum deflection angle lies between the results for the cone and wedge, because the oblique shock wave for the case of the wedge would produce a subsonic flow downstream of the shock. For these conditions the shock would normally be detached from the wedge, but it could be also attached with a subsonic flow, as mentioned previously.

The previously documented limitation can be rather restrictive for the

computations of certain types of axisymmetric-flow problems. For example, most military projectiles that are designed for flight Mach numbers between 1 and 3 have noses with semivertex angles  $\theta$  which are between the maximum deflection angles of the cone and wedge. Furthermore, they generally have small but abrupt protuberances in their body shape which produce large flow deflections. Hence, the flow fields around such bodies cannot be computed practically by the present first-order random-choice method. This is rather unfortunate because a lot good experimental data exists for military projectiles<sup>24,51-54</sup>, which would have been extremely useful in verifying the capability of the present random-choice method for computing axisymmetric-flow fields.

The additional difficulty with sometimes having to use an undesirably fine grid mesh when computing axisymmetric-flow fields (as compared to planar ones) is now described. This difficulty arises only when the flow field is computed at the origin (i.e.,  $r = 0$  or  $r \cong 0$ ), and is connected directly with the use of a first-order random-choice method for which the planar solution is computed first and then corrected by means of the operator-splitting technique to obtain the axisymmetric-flow solution. In this case the correction by the operator-splitting technique for a small radius is large and inaccurate, as mentioned at the end of the previous section.

In order to limit this type of inaccuracy to a smaller portion of the flow field near the origin, a finer mesh is required, because this type of error typically diminishes from cell to cell farther from the origin (and not just on increasing the radial distance). The inaccuracy will generally become negligible after a certain number of cells away from the origin (e.g., twenty). This is the main reason why a finer mesh will help limit the spatial extent of the error. However, a finer mesh results in an increase in computational time and cost.

The discussion of a particular example can be helpful. Consider the steady supersonic flow over the axisymmetric body shown in Fig. 7. The correction by the operator-splitting technique will give inaccurate flow properties over the entire body and also away from it if too few cells are used (e.g., 10 cells per body radius). If more cells are used the flow properties will be inaccurate in only the vicinity of the nose and tail of the body. Because of the inaccurately computed flow field in these two regions, the formation of both the front and rear shocks and their subsequent placement in the flow field will be affected. If this type of error extends outward for about 20 cells, then 100 cells per body radius, say, would be needed to try limit this inaccurate region to only a small part of the flow field. The use of 100 cells per body radius is generally undesirably large for solving such problems, as compared to as few as 20 cells per body radius for a wedge flow for example. This example helps highlight the unfortunate problem of being forced to resort to an undesirably fine mesh to retain computational accuracy when employing the present random-choice method for solving certain axisymmetric-flow problems that include the origin in the flow-field solution.

## 5.0 NUMERICAL RESULTS AND DISCUSSION

Numerical results from the random-choice method (RCM) are presented and discussed for many different planar and axisymmetric flow problems, in order to illustrate the capability and flexibility of the RCM. Results are given first for planar flows and then for axisymmetric flows. In each case the solution to the simplest problem is presented first, followed by problems with increasing

complexity. In some cases theoretical results are also presented to verify the numerical or RCM results. Furthermore, for each problem the flow is taken to be that a perfect diatomic gas or perfect air having a specific-heat ratio of 7/5 or 1.40.

## 5.1 Steady Supersonic Planar Flows

### 5.1.1 Flow over a compressive corner

The first problem involves a uniform flow at a flow Mach number  $M_1$  equal to 3 that encounters a compressive wedge of 30 degrees. This wedge deflects the flow by means of a single oblique shock wave attached to its leading edge. The numerical results for this relatively simple problem are shown in Fig. 9, where the theoretical oblique-shock-wave location is also depicted. The RCM and exact solutions for the shock-wave location are in excellent agreement, although the RCM predicts a slightly different shock angle. On the average the random position of the shock location from the RCM is correct, within numerical error. The RCM and exact solutions for the uniform flow properties behind or downstream of the oblique shock are in perfect agreement, as should be expected of the RCM for this simple problem. The location of the wedge surface in the RCM computations is also shown (for interest). Note that the RCM results were calculated with a grid of 100 nodes in the lateral (y) direction and 100 in the longitudinal (x) direction. However, only every eighth grid node in the longitudinal direction is shown, and this number is indicated in the inset as RCM (8).

### 5.1.2 Flow over an expansive corner

The second problem also involves an initially uniform flow, but at a flow Mach number  $M_1$  equal to 2 over an expansive corner with an angle of 30.53 degrees. The flow is turned by a centered or Prandtl-Meyer rarefaction wave that emanates from the sharp corner, as depicted in Fig. 10a. The numerical (RCM) and exact results for the locations of the head and tail of the expansion fan are shown in the figure to be in excellent agreement. Again, the RCM and exact results for the flow behind the rarefaction wave are in perfect agreement, as should be expected for this simple problem. Note that the numerical results have been computed with a grid with 100 nodes in the y direction and 100 nodes in the x direction, but results are given for only every eighth node in the figure.

RCM and exact results for spatial distributions of the flow properties through the rarefaction-wave fan are shown in Figs. 10b and 10c. Profiles in the longitudinal direction x (along the dashed horizontal line in Fig. 10a) are given first in Fig. 10b and profiles in the lateral direction y (dashed vertical line in Fig. 10a) appear last. In each case the agreement between the RCM and exact results is excellent, mainly because a sufficient number of nodes was used to guarantee good agreement.

### 5.1.3 Gradual compressive corner that gives a focussed compression wave

The problem in this case is the turning of an initially uniform steady supersonic flow by a contoured compressive corner that produces a focussed compression wave which results in an oblique shock wave (see Figs. 11a to 11d). This type of problem has recently been studied with an approximate analysis by

Emanuel<sup>62-63</sup>. The focal point of the compression wave is the origin of the primary oblique shock wave, a slip stream (dashed line) that separates the flow through the shock wave from the isentropic flow through the oblique compression wave, and a weak secondary disturbance that can be either an oblique shock or a Prandtl-Meyer rarefaction wave, depending on the initial flow conditions and final wall angle. The secondary wave moves outward from the focal point and subsequently reflects first from the wedge surface, then interacts with the slip stream and eventually overtakes the primary shock wave. The free-stream flow Mach numbers  $M_1$  for the four sets of numerical results presented in Figs. 11a to 11d are 1.3, 1.64, 2.0, to 4.0, respectively, as indicated in the figures. These initial conditions correspond exactly to some of those used in Emanuel's investigations. Note that the flow Mach number  $M$  and pressure ratio  $P = p/p_1$  are indicated for various flow regions in the four figures.  $M_1$  and  $p_1$  are the initial or free-stream conditions.

The contoured boundary surface to produce the focussed compression wave is not a known function, but has to be determined for the computations<sup>62</sup>. In the present study it was generated numerically with the RCM. The flow is first reversed so that it goes through a centered Prandtl-Meyer expansion wave (e.g., from  $M = 1.178$  to  $M_1 = 1.64$  in Fig. 11b). This expansion flow is computed and these computations include tracing a stream line at some reasonable distance away from the corner. This line then becomes the contoured boundary surface for the computations of the reverse flow through the focussed compression wave.

The graphical results shown in Figs. 11a to 11d were constructed from the numerical or RCM results, which used a rather fine grid of 200 nodes in the  $y$  direction. The number of nodes in the  $x$  direction varied, being 574, 539, 496 and 260 for Figs. 11a to 11d, respectively. None of the results in the figures are theoretical, although exact results could have been obtained by employing the method of characteristics and Rankine-Hugoniot equations, and approximate predictions are available also from the work of Emanuel<sup>62-63</sup>. Note that the fan of characteristics for the focussed compression wave has been constructed as straight lines, as would occur for the theoretical solution of a focussed compression wave. The flow properties inside the fan (such as the pressure, density, flow Mach number, and flow angle) were then checked to see if they were constant along these straight lines. They were indeed very close to being constant along these lines, showing that the lines are indeed characteristic lines. It was also found that the focal point was well defined in a very small region of space (shown as a solid dot), corresponding to an area about the size of  $4\Delta x\Delta y$ . The numerical error in the constancy of flow properties along the characteristic lines and in defining the focal point is small because of the fine grid used in the computations.

Some of the numerical results, such as the oblique shock angle, were compared to those from the analyses of Emanuel<sup>62-63</sup>, and the agreement was very good, provided that his weak shock solutions were used. Such comparisons are not presented here, mainly because his analysis is not exact and any small differences in the comparisons are therefore not known to result from the RCM or his approximate solution.

#### 5.1.4 Flow over a symmetric double-wedge

Numerical computations of a supersonic flow ( $M_1 = 2$ ) over a double wedge are presented in Fig. 12a and 12b. This symmetric double wedge is 1 unit long, has a thickness of 0.0525 units, and its semivertex angle is 6 degrees. The

number of grid points was 100 in the y direction and 220 in the x direction.

The wave diagram appears first in Fig. 12a. It shows the trajectories of both the front and rear shocks from the leading and trailing edges of double wedge, as well as showing clearly the spreading of the expansion fan emanating from the double-wedge corner formed by the junction of the bases of the wedges. This fan eventually expands such that its head overtakes the front shock and the tail falls into the rear shock, after which the interaction of the shocks and expansion wave continually causes the strengths of both shocks and the expansion wave to diminish. The flow Mach number  $M$  and pressure ratio  $P$  ( $p/p_1$ ) in regions having a constant states are also indicated.

The exact solution for the trajectories of the front and rear shocks and the head and tail of the expansion wave, prior to their interaction, are shown for comparison. The agreement in general is very good, although the front shock trajectory from the RCM lies slightly out front of that from the exact solution. The agreement can be improved, of course, by using more grid points.

Pressure distributions through the entire wave produced by the double wedge are shown in Fig. 12b at different lateral distances away from the double wedge. These profiles show clearly how the wave from the double wedge evolves into a decaying N-shaped wave at larger lateral distances.

#### 5.1.5 Flows in duct inlets

Supersonic flows into ducts of changing cross-section always involve oblique shock and rarefaction waves. Numerical solutions for seven duct inlet problems are now given and discussed (see Figs. 13 to 19). For these solutions the number of grid points in the y direction was 100 for the first three cases and 150 for the remainder, whereas the number of grid nodes in the x direction was 350, 300, 500, 360, 290, 350, and 350 for the seven cases. In all cases the wave diagrams are presented, along with numerical results for the flow Mach number and pressure in regions of constant state. Further, exact solutions are given for the trajectories of oblique shock waves, rarefaction-wave heads and tails, and slip streams. In the seven cases the RCM and exact solutions are in good agreement, and this agreement can be improved by using more grid nodes.

The first case is for a uniform free-stream flow ( $M_1 = 2.0$ ) entering a duct inlet for which the bottom duct surface is a compressive wedge of 6 degrees and the upper duct surface is a flat plate parallel to the free-stream flow (see Fig. 13). The oblique shock wave emanating from the lower wedge crisscrosses the duct four times as it reflects alternately from the upper and lower duct walls. Its last reflection from the bottom surface is a Mach wave, because at this last reflection point the wedge surface is simply terminated by a corner to make the duct area constant thereafter.

The second case is similar to the first one but has two distinct differences in the inlet-duct geometry. The bottom wedge surface with an angle of 6 degrees is no longer terminated by a corner, and the upper surface no longer is a flat plate but instead is a compressive wedge of 2 degrees (see Fig. 14). Computations of this flow field has been terminated just ahead of the second oblique shock-wave reflection at the upper surface, because the next reflected shock has subsonic flow behind it. Hence, any additional flow field cannot be solved by means of the random-choice method, illustrating one of its primary limitations that was mentioned previously.

For the third case of an inlet-duct flow the upper duct surface is a flat plate aligned with the free-stream flow ( $M_1 = 2.0$ ) and the lower duct surface is also a flat plate but with an expansive corner at the leading edge (see Fig. 15). In this case a Prandtl-Meyer expansion wave emanates from this sharp corner and continues to spread as it crisscrosses the duct through reflections from the upper and lower surfaces. Note that in this case the flow is expanded to a lower pressure and higher Mach number by the crisscrossing rarefaction wave such that it adjusts to the larger flow area in the duct. In the first two cases the flow was compressed to a higher pressure and lower Mach number by the crisscrossing shock wave in the process of adjusting the flow to the smaller duct area.

In the fourth case the upper and lower surfaces of the inlet duct are both compressive wedges (Fig. 16). The upper wedge has an angle of 6 degrees and the lower one has an angle of only 3 degrees. In this case oblique shock waves originate from the leading edges of the wedges and crisscross the duct. Their interactions produce slip streams, and the subsequent interaction of the oblique shock waves and slip streams produce additional weak reflected waves. In all cases the flow properties in various regions of constant states can be determined accurately to machine precision, although the boundaries of these regions are less accurate, within numerical error.

The fifth case is similar to the last one with two compressive wedges. In this case, however, the compressive wedges are both 6 degrees and the two oblique shock waves that originate at their leading edges therefore have the same strength (Fig. 17). Consequently, their subsequent interactions before and after reflecting at the side walls produce slip streams with identical flow properties on each side. Hence, slip streams do not appear in the figure.

In the sixth case the upper surface of the inlet duct is an expansive wedge of 2 degrees and the lower surface is a compressive wedge of 6 degrees (see Fig. 18). The main features of this flow are the interaction of the two oblique shock and rarefaction waves which produce a slip stream of finite width, that is a slip region. Such regions are routinely handled by the RCM.

The seventh and final case is for the supersonic flow in a duct inlet consisting of two expansive wedges, one of 1 degree for the upper surface and the other of 2 degrees for the lower surface (Fig. 19). In this case the main features are two Prandtl-Meyer expansion waves that emanate from the two sharp expansive corners and crisscross the duct. A slip stream or region from the interaction of the two rarefaction waves does not appear because it does not exist for such an isentropic flow.

#### 5.1.6 Flow over a parabolic shaped airfoil

Numerical computations were done for a supersonic flow ( $M_1 = 2.0$ ) over a parabolic shaped airfoil with an arbitrary length  $L$  and maximum thickness to length ratio  $t/L$  of 0.10. The symmetric airfoil shape is given by the equation  $y_b/L = 2(t/L)[x/L - (x/L)^2]$ . For this particular case the trajectories of the front and rear shock waves look like those sketched in Fig. 7, and overpressure signatures as a function of longitudinal distance ( $x$ ) are presented in Fig. 20. The first signature is for the overpressure  $(p-p_1)/p_1$  along the airfoil surface, and the second, third, and fourth overpressure signatures are at lateral distances ( $y$ ) from the airfoil of one, ten, and one hundred body thicknesses. (These distances are indicated in the figure by  $y = 1t, 10t, \text{ and } 100t.$ )

The evolution of the wave with lateral distance into an N shape is readily apparent. One can also observe that the wave is decreasing nonlinearly in amplitude and simultaneously stretching. The peak overpressure decays almost as  $y^{-1/2}$  at larger lateral distances, in direct agreement with nonlinear acoustic or aerodynamic theory for weak but finite-amplitude waves (with nonlinear wave steepening effects).<sup>64</sup> Note that linear aerodynamic theory would predict that the wave amplitude and length would simply be constant with increasing lateral distance.

The computations for the parabolic shaped airfoil were done initially for the flow around the airfoil ( $0 < y < 1.9$ ) with 190 grid nodes. Then the computations were continued with a coarser mesh containing only every second point, leaving only about one hundred grid nodes in the vertical direction through the outward moving wave, as described in chapter 3. The first three overpressure signatures were computed in this manner, and the number of nodes was sufficient to ensure that these signatures are of high quality. For the fourth one, the computations were redone with a much coarser mesh, that is, 175 grid nodes in the range  $0 < y < 3.5$ . Then the computations were continued with an even coarser mesh containing only every fifth point, thereby leaving only about forty grid nodes in the vertical direction. This is why the quality of the last signature is not quite as good as the previous three.

#### 5.1.7 Free-jet flows from a slot

Two sets of RCM computations have been completed for supersonic streams that issue from a slot into a surrounding quiescent fluid of constant pressure (see Figs. 21 and 22). In both cases the flow prior to emerging from the slot with parallel walls was uniform. The resulting free-jet flows differ markedly in structure mainly because the first free jet (Fig. 21) has an initially higher pressure than that of the surrounding fluid and the other free jet (Fig. 22) has a lower pressure. In both cases only the lower half of the free jet has been computed by the RCM; the upper symmetric half has been added as dashed lines for completeness. The flow Mach number  $M$  and pressure ratio  $P$  ( $p/p_1$ ) are also shown for various regions of constant state.

In the first case of a free-jet flow from the slot the initial Mach number  $M_1$  is 1.40 and the ratio of the quiescent fluid pressure to that initially in the flow in the slot is 0.749 (Fig. 21). In these numerical results it can be readily seen that symmetric rarefaction waves emanate from the slot corners and expand the flow before they eventually reflect at the jet boundaries and form compression waves. These compression waves then compress the free jet as they come to a focus, eventually back to the original flow conditions and cross-sectional area at the slot (within numerical error). In the case of perfectly accurate numerical computations (no numerical error), this process would be repeated indefinitely for subsequent free-jet lobes.

One measure of the accuracy of the RCM for this first free-jet computation is the degree of focussing of the compression waves at the end of the first lobe. Although the RCM does not produce a perfect focal point, the focus was found to be within an area equal to  $4\Delta x\Delta y$ , which is highly commendable of the RCM method. Another measure of the accuracy is the straightness of the head and tails of the computed rarefaction and compression waves. These are indeed quite straight because sufficient grid points were used in the computations to ensure this. For example, the number of grid points was 70 for half of the free jet in the  $y$  direction and 350 in the  $x$  direction.

For the second case of a free-jet flow the initial Mach number  $M_1$  is 1.60 and the ratio of the quiescent fluid pressure to that initially in the flow in the slot is 1.344 (Fig. 22). In these numerical results it can be seen readily that symmetric oblique shock waves emanate from the slot corners and compress the jet flow before they eventually reflect at the jet boundaries as Prandtl-Meyer expansion fans. From this reflection point onward, the free jet is of the same structure as for the previous case. Successive lobes containing alternate expansion and compression waves are simply repeated, as if a slot was located at the end of the shock-wave portion with this contracted jet area and initial jet flow properties of  $M = 1.166$  and  $P = 1.822$ . As for the last case, the RCM is very successful in obtaining these numerical results. Note that the number of grid points in the  $y$  direction is 50 for the one-half of the free jet and 425 in the  $x$  direction.

## 5.2 Steady Supersonic Axisymmetric Flows

### 5.2.1 Flow over a cone

The first problem involves a uniform flow at a flow Mach number  $M_1$  equal to 2.5787 that encounters an infinitely long cone with a semivertex angle  $\theta_c$  of 15 degrees. The cone axis and flow are aligned (Fig. 23). The flow is partly turned suddenly through an oblique shock and then turned gradually thereafter, such that the flow eventually becomes tangent to the cone surface. Furthermore, from theoretical considerations it is well known that the shock angle  $\sigma_s$  is constant and the flow properties along radial lines with angle  $\theta$  between the shock and cone surface are also constant.<sup>5,14-16,60-61</sup>

The flow field was computed with a square mesh ( $\Delta r = \Delta x$ ) and 200 grid nodes in the radial ( $r$ ) direction. RCM computed flow properties for the density ratio  $\rho/\rho_1$ , pressure ratio  $p/p_1$ , flow Mach number  $M$ , and flow angle  $\zeta$  are shown in Figs. 24a, 24b, and 24c, where they are compared to exact tabular solutions<sup>16</sup> (actually very accurate numerical solutions of ordinary differential equations). These results are plotted as a function of the angle  $\theta$  from the axis of the cone to a radial line in the flow field, at three different distances of 80, 160, and 320 grid nodes from the cone apex. Note that the cone surface lies at an angle of 15 degrees and the exact shock location is 27.85 degrees.

The agreement between the RCM and exact results is very good in general. The agreement becomes better for results farther downstream, that is after more grid nodes in the axial direction. One reason for this is that the number of nodes in the radial direction through the RCM computed flow field increases with distance from the cone apex. The data in Fig. 24b has twice as many grid nodes as those given in Fig. 24a, and the data in Fig. 24c has twice as many as those in given Fig. 24b. A second reason is that the flow-field data computed farther away from the cone axis is more accurate by the RCM, because the correction of the planar-flow solution to obtain the axisymmetric-flow solution becomes smaller and therefore more accurate.

The axisymmetric-flow solution in the vicinity of the cone apex can be highly inaccurate, because the operator-splitting correction near the cone axis is large and incorrect. The pressure ratio across the shock can be in error by as much as 70%. However, such perturbations were found to decay with radial distance to almost negligible size by about 25 grid zones away from the axis of the cone. This gives a good indication of the size of the flow field affected, and also how many grid points are required in this and other axisymmetric-flow

problems involving cone-tipped and pointed bodies, to make sure that this inaccurate region is of negligible size compared to the entire flow field.

A close inspection of the RCM and exact results in Figs. 24a to 24c will show that the oblique shock location from the RCM is out front (larger  $\theta$ ) of the exact location. The difference is largest for the data given in Fig. 24a, or nearer the cone apex, and becomes smaller for data given in Figs. 24b and 24c, or as the distance or number of grid nodes from the cone axis increases. The reasons for this difference in shock location are two-fold. Firstly, because the operator-splitting correction can result in flow-field pressures and oblique shock-wave strengths that are too high in the vicinity of the cone apex, the RCM predicted propagation velocity of the oblique shock wave is too high near the cone axis. Secondly, the propagation of the shock depends to a large extent on the random-sampling procedure. This procedure, which assigns some state to the next grid point downstream, is always completed on the intermediate planar solution, and then this downstream state is corrected to give the final solution for axisymmetric flow. Because the oblique shock is always stronger for a planar flow than an axisymmetric one, the sampling procedure on the intermediate planar flow solution therefore propagates the oblique shock wave outwards too quickly, especially in the vicinity of the cone apex. This effect decays with increasing radial distance, but, unfortunately, it usually takes 40 to 50 grid nodes in the radial direction before this effect disappears.

The computation of an oblique shock flow fields over a cone is an excellent test of the capability of the RCM for predicting axisymmetric-flow fields, and also for testing out an initial computer program.

### 5.2.2 Flow over a cone-cylinder

Numerical computations were done for the classical case of the flow over an axisymmetric body with a conical nose on an infinite-length cylinder. The semivertex angle of the conical nose was 11.5 degrees. From these computations the pressure coefficient  $C_p = 2(p - p_1)/\rho_1 u_1^2$  on the surface of the body was obtained, where  $p$  is the static pressure on the body surface. These RCM results are compared to an exact calculation<sup>65</sup> (method of characteristics) in Fig. 25.

The RCM and exact results are in good agreement, with some scatter in the RCM results near the cone apex. This scatter or inaccuracy is due mainly to the inaccuracy of the operator-splitting correction near the cone axis, both of which were just discussed for the previous example. Note that if fewer grid points than 1100 in the  $x$  direction were utilized in the RCM solution, the RCM results would then become worse near the cone apex.

### 5.2.3 Flow over a parabolic-nosed cylinder

Numerical results were obtained for the flow over a cylindrical body with a parabolic nose, for three different free-stream Mach numbers of 2.0, 3.0, and 3.92. The radius  $R$  of the infinite length cylinder is 0.5 arbitrary units, and the equation for its parabolic nose having a length  $L$  of 3.8 units is given by  $r_b/L = 2(R/L)[(x/L) - (x/L)^2]$ . Once again, the pressure coefficient from the RCM data is compared to the exact results (see Figs. 26a, 26b, and 26c), and the exact results are from the method of characteristics<sup>65</sup>. For the three different free-stream Mach numbers the agreement between the RCM and exact results is, in general, good, just as in the previous example. As in the previous case, the

RCM results are less accurate nearer to the apex of the parabolic nose, for the same reasons given previously. In each case the number of grid nodes in the x direction was 840, and the mesh used was square (i.e.,  $\Delta x = \Delta r$ ).

#### 5.2.4 Flow over a symmetric double-cone

The RCM was used to compute the flow field for the supersonic flow over a symmetric double-cone. The cones which were joined at their common bases had a semivertex angle of 10 degrees, and the free-stream Mach number  $M_1$  was 2.075. For the computations a square mesh was employed, having 100 grid nodes per unit length of the double-cone.

The RCM solution in terms of axial distributions of pressure ( $P = p/p_1$ ) at different radial distances from the body are shown in Fig. 27. These results show clearly how the double-cone produces an outwards moving wave that changes in shape and eventually evolves into an N-shaped wave. Furthermore, the numerical results also illustrate the capability of the RCM for obtaining solutions to such problems.

A few comments are worth making regarding the numerical solution. In the first few pressure distributions near the double-cone one can see clearly the initial pressure ramp just behind the front shock (which originates from the conical solution). It is continually being eroded by the rarefaction wave that emanates from expansive corner, as it overtakes the front shock, after which the rarefaction wave interacts with the front shock wave and continually reduces its strength with increasing radial distance.

The flow right next to the surface of the double-cone must follow the surface. When this flow turns suddenly at the nose and tail of the body the front and rear shocks are formed. A little farther away from the body and just after the front shock, the flow on turning suddenly through the front shock still needs to be turned gradually but further to align itself with the body surface. This is the reason for the pressure ramp following the front shock. The rarefaction wave signals the presence of the corner and turns the flow in an attempt to realign it with the surface of the second cone. In the process it overturns the flow toward the surface, and the flow then has to gradually turn away from the surface. This produces the compression wave that is clearly seen in the first pressure profile just ahead of the rear shock. With increasing radial distance from the body, this compression wave steepens and is overtaken by the rear shock. This combining of the two waves is the reason why the rear shock wave is temporarily stronger than the front shock. Farther away from the body the two shock waves become equal in strength and the change in pressure between them becomes linear.

In the computations for the results given in Fig. 27, the free-stream flow field ahead of the front shock was not computed (see chapter 3). This reduces the computational time and cost by about 10%. However, the entire flow field behind the rear shock was computed, in spite of the fact that it is of little interest. Most of it does not need to be computed and can be eliminated as described in chapter 3 to reduce computational time and cost. The results of additional computations for which this lower right part of the flow field was not included are presented in Fig. 28. The computed results are, of course, in perfect agreement with those in Fig. 27, and the extra saving in computational time and cost is about 60%. This illustrates clearly the benefit to be gained by eliminating unnecessary computations of certain parts of the flow field.

The first pressure profile nearest the double-cone in Figs. 27 and 28 contain some jaggedness. This is due to inaccuracies in the operator-splitting correction near the double-cone axis for axisymmetric-flow computations. These errors can be reduced, of course, by increasing the number of grid nodes in the RCM computations, especially for the initial flow field near the double-cone. To illustrate this improvement, the initial flow field in the region contained by the lines  $r = 1.3$  and  $x = 2.0$  was computed first with twice as many grid nodes (200 nodes per unit body length). Then the flow field containing just the outward moving wave was continued outward with only half this number (100 nodes per unit body length), because more grid nodes are not needed farther away from the body. The new results are shown in Fig. 29. The improvement in these RCM results over the previous ones in Fig. 28 is quite obvious, but the extra computational time and cost were 40%.

#### 5.2.5 Flow over a parabolic-spindle shaped body

Numerical computations were done for a supersonic flow ( $M_1 = 2.0$ ) over a parabolic-spindle shaped body with an arbitrary length  $L$  and maximum diameter to length ratio  $D/L$  of 0.10. The shape of the axisymmetric body is given by the equation  $r_b/L = 2(D/L)[x/L - (x/L)^2]$ . For this example the trajectories of the front and rear shock waves look like those sketched in Fig. 7, and overpressure signatures as a function of axial distance ( $x$ ) are presented in Fig. 30. The three signatures are for the overpressure  $(p-p_1)/p_1$  at radial distances ( $r$ ) from the body of one, ten, and one hundred body diameters.

These numerical results show how the wave evolves with radial distance and decays into an N shape. The first two signatures are in good agreement with the prediction of approximate but accurate theory by Lighthill and Whitham (see Ref. 24). The amplitude of the third signature is too high by a factor of about two and the negative overpressure phase is too large. These are simply due to round-off errors from multiple single-precision computations. For example, the radial flow velocity  $v$  at large radii is very small such that the flow angle  $\xi$  measured from the radial axis loses significant digits and becomes virtually  $\pi/2$ . This particular problem could be removed easily by simply redefining the flow angle to be measured more physically from the axial direction. However, this problem does illustrate the important point that numerical results can become saturated with roundoff errors in the case of weak waves.

Note that the computations for the parabolic-spindle body were done initially for the flow around the body ( $0 < r < 0.92$  and  $0 < x < 1.5$ ) with 920 grid nodes in the radial direction and 1500 in the axial direction. Then the computations were continued with a coarser mesh containing only every fifth point, leaving only 185 grid nodes in the radial direction through the outward moving wave, as described in chapter 3.

#### 5.2.6 Free-jet flows from a circular orifice

The first numerical computations of an axisymmetric free-jet flow are for the case of an exit flow Mach number  $M_1$  of 1.2 and a pressure ratio  $P$  ( $p/p_1$ ) of unity. Because the pressure of the fluid outside the free jet is only one tenth of that in the jet at the exit, the free jet expands on emerging from the orifice. Numerical results showing this expansion by tracing the jet boundary are presented in Fig. 31. Also shown is the trajectory of the oblique shock wave, commonly called the barrel shock, which starts as a coalescence of Mach

wave just downstream of the orifice and grows in strength up to the Mach disc. The Mach disc, and the Mach reflection near the periphery of the Mach disc, are sketched in the diagram, because they cannot be computed by the RCM because the flows behind them are subsonic.

The properties of the flow inside the free jet can be studied easily with the RCM. In order to illustrate some of the features, pressure and Mach number distributions with radial distance are included as insets, one in the top diagram and the other in the bottom one. The changes in pressure and flow Mach number from inside the barrel shock to outside the free-jet boundary are, for example, rather pronounced.

The second numerical computations of an axisymmetric free-jet flow are for the case of an exit flow Mach number  $M_1$  of 3.0 and a pressure ratio  $P$  ( $p/p_1$ ) of unity. Because the pressure of the fluid outside the free jet is now twice as high as that in the jet at the exit, the free jet contracts on emerging from the orifice, as shown in Fig. 32. Besides the contracting free-jet boundary the trajectory of the inward moving oblique shock wave is presented. Inside this oblique shock the flow properties are simply the exit conditions. Across this shock the flow properties change drastically, as shown by the insets of pressure and flow Mach number, and then more slowly to the jet boundary.

The inward moving oblique shock eventually nears the axis of symmetry, where it is reflected. Depending on the flow conditions the reflection can be either a regular or Mach reflection. In the present case it appears to be a regular reflection, although the Mach stem could exist and be rather small. The reflected wave is simply sketched in the diagram, because the flow becomes subsonic and the computations could not be continued.

Note that in solving the two free-jet flows, only 51 grid points were used in the radial direction to cover the radius of the orifice in the first problem and 101 were used for the second example.

## 6.0 CONCLUDING REMARKS

A random-choice method has been presented in detail for obtaining fairly practical and efficient numerical solutions for both two-dimensional planar and axisymmetric steady supersonic flows. Innovative techniques were introduced for solving the Riemann problem iteratively, naturally handling boundary conditions at body and free-jet surfaces, and computing only certain parts of flow fields of interest. Many interesting and practical numerical solutions were also given for a variety of different planar- and axisymmetric-flow problems, and compared, in most cases, with known analytical and numerical solutions, in order to demonstrate the applicability, capability, and limitations of this new random-choice method.

For solving planar-flow problems the random-choice method is limited only in that the flow must be everywhere supersonic (see section 4.1). Outside of this single but restrictive limitation the method is highly successful in predicting planar supersonic flow fields both efficiently and accurately. For the solution of axisymmetric-flow problems the random-choice method is further limited in that the flow must be supersonic when solving the intermediate planar Riemann problem (section 4.2), before the operator-splitting correction gives the final axisymmetric results. This can be a severe limitation in that flows over most military projectiles cannot be solved by the present random-choice

method. It is precisely these limitations that make the random-choice method for solving two-dimensional steady planar and axisymmetric supersonic flows less extensive and therefore less useful in applications than its sequel for solving one-dimensional nonstationary flows (for which the latter has no such similar limitations).

The problem of having to resort to an undesirably fine grid mesh in order to maintain numerical accuracy when solving axisymmetric-flow problems that include the axis of symmetry is the direct result of inaccuracies stemming from the application of the operator-splitting technique, as mentioned earlier in section 4.2, and which also became obvious from numerical results presented in section 5.2.

However, the time to solve planar and axisymmetric flow problems with the random-choice method is not unreasonable. Typical times to solve a single Riemann problem are 13 ms for the planar case and 15 ms for the axisymmetric case. The additional 15% is due to additional calculations to include the operator-splitting correction. These times are calculated by taking the total time to execute a job divided by the total number of Riemann problems. Further, these times are given for the UTIAS computer, which is Perkin-Elmer 32-bit mini-computer with a 3250 central processor. Such computation times would be lower by a factor of about four or five for a IBM-3033 or CDC-6600 machine.

Future work might involve the development of a second-order random-choice method for solving axisymmetric-flow problems, one that does not require the operator-splitting technique. In other words, the Riemann problem for an axisymmetric flow would be solved directly, instead of the present first-order indirect method of first solving the planar Riemann problem and then utilizing the operator-splitting technique to correct this intermediate result to get the axisymmetric-flow solution. The advantages of this second-order method would be two-fold. Firstly, the operator-splitting technique would be eliminated along with its inaccurate correction if the radius is small or near zero. This means that a coarser mesh could be used in the computations, although each cell would require more computation time. Secondly, and more importantly, axisymmetric-flow problems that are unsolvable by the present first-order method, because a solution to the planar Riemann problem did not exist, will be able to be solved. The only limitation would be that the flow must be everywhere supersonic. Then the second-order method would be able to provide axisymmetric supersonic flow solutions for most military projectiles, for example, but still not over blunt bodies.

## 7.0 REFERENCES

1. J. S. Isenberg and C. C. Lin, 'The Method of Characteristics in Compressible Flow, part I (Steady Supersonic Flow)', USAF AMC Technical Report No. F-TR-1137A-ND, 1947.
2. R. F. Clippinger, J. H. Giese, and W. C. Carter, 'Tables of Supersonic Flows About Cone Cylinders, part I: Surface Data', BRL Report No. 729, United States Army Ballistic Research Laboratories, Aberdeen Proving Ground, Maryland, 1950.
3. A. Ferri, 'General Theory of High-Speed Aerodynamics', W. R. Sears (Ed.), 'Section G: The Method of Characteristics', Princeton University Press, Princeton, New Jersey, 1954.

4. A. H. Shapiro, 'The Dynamics and Thermodynamics of Compressible Fluid Flow', Vol. II, pp. 676-696, The Ronald Press Company, New York, 1954.
5. H. W. Liepmann and A. Roshko, 'Elements of Gasdynamics', Galcit Aeronautical Series, John Wiley and Sons, New York, 1957.
6. P. Kutler and H. Lomax, 'A Systematic Development of the Supersonic Flow Fields Over and Behind Wings and Wing-Body Configurations Using a Shock-Capturing Finite-Difference Approach', AIAA Paper No. 71-99, 1971.
7. G. A. Sod, 'A Survey of Several Finite Difference Methods for Systems of Nonlinear Hyperbolic Conservation Laws', J. Comp. Phys., Vol. 27, p. 1, 1978.
8. D. A. Anderson, J. C. Tannehill, and R. H. Pletcher, 'Computational Fluid Mechanics and Heat Transfer', McGraw-Hill Book Company, New York, 1984.
9. J. von Neumann and R. D. Richtmyer, 'A Method for the Numerical Calculation of Hydrodynamic Shocks', J. Appl. Phys. Vol. 21, p. 232, 1950.
10. A. J. Baker, 'Finite Element Computational Fluid Mechanics', Hemisphere Publishing Corporation, Washington, D. C., 1983.
11. F. H. Harlow, 'The Particle-in-Cell Computing Method for Fluid Dynamics', Methods in Computational Physics, B. Alder, S. Fernbach, and M. Rotenberg (Eds.), Vol. 3, pp. 319-343, Academic Press, New York, 1964.
12. M. Rich, 'A Method for Eulerian Fluid Dynamics', Report No. LAMS-2826, Los Alamos Scientific Laboratory, Los Alamos, New Mexico, 1963.
13. R. A. Gentry, R. E. Martin, and B. J. Daly, 'An Eulerian Differencing Method for Unsteady Compressible Flow Problems', Journal of Computational Physics, Vol. 1, pp. 87-118, 1966.
14. G. I. Taylor and J. W. Maccoll, 'The Air Pressure on a cone Moving at High Speed - I', Proceedings of the Royal Society of London, series A, Vol. 139, pp. 278-311, 1933.
15. J. W. Maccoll, 'The Conical Shock Wave Formed by a Cone Moving at High Speed', Proceedings of the Royal Society of London, series A, Vol. 159, pp. 459-472, 1937.
16. Z. Kopal (Ed.), 'Tables of Supersonic Flow Around Cones', Massachusetts Institute of Technology, MIT Technical Report No. 1, Murray Printing Company, Cambridge, Massachusetts, 1947.
17. Th. von Karman and N. B. Moore, 'The Resistance of Slender Bodies Moving with Supersonic Velocities with Special Reference to Projectiles', Transactions of the American Society of Mechanical Engineers, Vol. 54, pp. 303-310, 1932.
18. M. J. Lighthill, 'Supersonic Flow Past Bodies of Revolution', Research and Memorandum No. 2003, Aeronautical Research Council, United Kingdom, 1945.
19. M. J. Lighthill, 'Supersonic Flow Past Slender Bodies of Revolution the Slope of Whose Meridian Section is Discontinuous', Quarterly Journal of Mechanics and Applied Mathematics, Vol. 1, part 1, pp. 90-102, 1948.

20. G. N. Ward, 'Supersonic Flow Past Slender Points Bodies', Quarterly Journal of Mechanics and Applied Mathematics, Vol. 2, PP. 75-97, 1949.
21. G. B. Whitham, 'The Behaviour of Supersonic Flow Past a Body of Revolution, Far From the Axis', Proceedings of the Royal Society of London, series A, Vol. 201, No. 1064, pp. 89-109, 1950.
22. G. B. Whitham, 'The Flow Pattern of a Supersonic Projectile', Communications on Pure and Applied Mathematics, Vol. 5, pp. 301-348, 1952.
23. M. D. Van Dyke, 'First and Second-Order Theory of Supersonic Flow Past Bodies of Revolution', Journal of Aeronautical Sciences Vol. 18, pp. 161-178, March 1951.
24. D. V. Ritzel and J. J. Gottlieb, 'The Overpressure Signature from a Supersonic Projectile', UTIAS Report No. 298, to be printed.
25. L. Devan, 'An Improved Second-Order Theory of Inviscid Supersonic Flow Past Bodies of Revolution', AIAA Paper No. 80-0030, AIAA 18th Aerospace Sciences Meeting, 14-16 January 1980, Pasadena, California.
26. J. Glimm, 'Solution in the Large for Nonlinear Hyperbolic Systems of Equations', Communications in Pure and Applied Mathematics, Vol. 18, pp. 697-715, 1965.
27. S. K. Godunov, 'A Difference Method for Numerical Calculation Discontinuous Solutions of Equations of Fluid Dynamics' (in Russian), Mat. Sb. 47, pp. 271-306, Moscow, 1959.
28. A. J. Chorin, 'Random Choice Solution of Hyperbolic System', Journal of Computational Physics, Vol. 22, pp. 517-533, 1976.
29. P. Colella, 'Glimm's Method for Gas Dynamics,' Society for Industrial and Applied Mathematics, Journal of Scientific and Statistical Computing, Vol. 3, No. 1, March 1982.
30. P. Colella, 'An Analysis of the Effect of Operator Splitting and the Sampling Procedure on the Accuracy of Glimm's Method,' Report No. LBL-8874, Lawrence Berkeley Laboratory, Physics, Computer Science and Mathematics Division, University of California, Berkeley, California, December 1978.
31. G. A. Sod, 'A Numerical Study of a Converging Cylindrical Shock', Journal of Fluid Mechanics, Vol. 83, pp. 785-794, 1977.
32. S. K. Fok, 'Extension of Glimm's Method to the Problem of Gas Flow in a Duct of variable Cross-Section', Report No. LBL-12322, Lawrence Berkeley Laboratory, Physics, Computer Science and Mathematics Division, University of California, Berkeley, California, December 1980.
33. D. R. Crocetta and J. J. Gottlieb, 'An Analytical and Numerical Study of a Shock Wave Interaction with an Area Change,' University of Toronto Institute for Aerospace Studies, UTIAS Report No. 268, November 1982.
34. J. Glimm, G. Marshall, and B. Plohr, 'A Generalized Riemann Problem for Quasi-One-Dimensional Gas Flows', Advances in Applied Mathematics, Vol. 5, No. 1, pp. 1-30, 1984.

35. T. Saito and I. I. Glass, 'Application of Random Choice Method to Problems in Gasdynamics', Progress in Aerospace Science, Vol. 21, pp. 201-247, 1984. Also, 'Application of Random Choice Method to Problems in Shock and Detonation Dynamics', UTIAS Report No. 240, University of Toronto Institute for Aerospace Studies, Downsview, Ontario, October 1979.
36. H. Miura and I. I. Glass, 'On a Dusty Gas Shock Tube', Proceedings of the Royal Society of London, Series A, Vol. 382, pp. 373-388, 1982. Also, UTIAS Report No. 250, University of Toronto Institute for Aerospace Studies, Downsview, Ontario, May 1981. Furthermore, presented at the New York Academy of Sciences Conference on Physio-Chemical Hydrodynamics, 13-17 June 1982, New York, U.S.A.
37. H. Miura and I. I. Glass, 'On the Passage of a Shock Wave Through a Dusty-Gas Layer', Proceedings of the Royal Society of London, Series A, Vol. 385, pp. 85-105, 1983. Also, UTIAS Report No. 252, University of Toronto Institute for Aerospace Studies, Downsview, Ontario, January 1982.
38. T. Saito and I. I. Glass, 'Temperature Measurements at an Implosion Focus', Proceedings of the Royal Society of London, Vol. 384(A), pp. 217-231, 1982. (Also UTIAS Report No. 260, December 1982.)
39. J. J. Gottlieb, O. Igra, and T. Saito, 'Simulation of a Blast Wave With a Constant-Area Shock Tube Containing Perforated Plates in the Driver', Proceedings of the Eighth International Symposium on Military Applications of Blast Simulation, Vol. 2, pp. 7-1 to 7-21, sponsored by the Gruppe for Rüstangsdienste, AC-Laboratorium Spiez, Spiez, Switzerland, symposium held on the 20-24 June 1983 in Spiez, Switzerland.
40. J. J. Gottlieb and T. Saito, 'An Analytical and Numerical Study of the Interaction of Rarefaction Waves with Area Changes in Ducts - Part 1: Area Reductions', UTIAS Report No. 272, University of Toronto Institute for Aerospace Studies, Downsview, Ontario, November 1983.
41. J. J. Gottlieb and O. Igra, 'Interaction of Rarefaction Waves with Area Reductions in Ducts', Journal of Fluid Mechanics, Vol. 137, pp. 287-307, December 1983.
42. H. Honma and I. I. Glass, 'Weak Spherical Shock-Wave Transitions of N-Waves in Air with Vibrational Excitation', Proceedings of the Royal Society of London, Series A, Vol. 391, pp. 55-83, 1984. Also, UTIAS Report No. 253, University of Toronto Institute for Aerospace Studies, Downsview, Ontario, 1983.
43. H. Miura and I. I. Glass, 'Formation of a Shock Wave in a Dusty Gas by a Moving Piston', UTIAS Report No. 275, University of Toronto Institute for Aerospace Studies, Downsview, Ontario, March 1984.
44. H. Miura, T. Saito and I. I. Glass, 'Normal Reflection of a Shock Wave at a Rigid Wall in a Dusty Gas', UTIAS Report No. 274, University of Toronto Institute for Aerospace Studies, Downsview, Ontario, March 1984.
45. H. S. Murty and J. J. Gottlieb, 'Analytical and Numerical Study of the Flow in a Shock Tube with an Area Change at the Diaphragm Section', UTIAS Technical Note No. 255, University of Toronto Institute for Aerospace Studies, Downsview, Ontario, May 1984.

46. S. C. M. Lau and J. J. Gottlieb, 'Numerical Reconstruction of Part of an Actual Blast-Wave Flow Field to Agree with Available Experimental Data', UTIAS Technical Report No. 251, August 1984.
47. O. Igra, J. J. Gottlieb, and T. Saito, 'An Analytical and Numerical Study of the Interaction of Rarefaction Waves with Area Changes in Ducts - Part 2: Area Enlargements', UTIAS Report No. 273, December 1984.
48. J. J. Gottlieb, T. Saito, and K. Y. Zhang, 'Numerical Prediction of Blast-Wave Flows Inside and Outside the Darlington Generating Station Power House in the Event of an Explosion at the Nearby Railroad Tracks', UTIAS Technical Note 239, University of Toronto Institute for Aerospace Studies, Downsview, Ontario, to be printed.
49. G. Marshall and B. Plohr, 'A Random Choice Method for Two-Dimensional Steady Supersonic Shock Wave Diffraction Problems', Journal of Computational Physics, Vol. 56, part 3, pp. 410-427, December 1984.
50. H. Honma, M. Wada, and K. Inomata, 'Random-Choice Solutions for Two-Dimensional and Axisymmetric Supersonic Flow', ISAS Report S. P. No. 2, Institute of Space and Astronautical Science, Proceedings of the Symposium on Mechanics for Space Flight, Tokyo, Japan, March 1984.
51. D. V. Ritzel and J. J. Gottlieb, 'Measurements of Overpressure Signatures from Supersonic Projectiles - Part I: The 106-mm HEAT Round (U)', DRES Suffield Memorandum No. 1034, Defence Research Establishment Suffield, Ralston, Alberta, July 1982.
52. D. V. Ritzel and J. J. Gottlieb, 'Measurements of Overpressure Signatures from Supersonic Projectiles - Part II: The 3-inch/70 MK34 Projectile (U)', DRES Suffield Memorandum No. 1041, Defence Research Establishment Suffield, Ralston, Alberta, June 1982.
53. D. V. Ritzel and J. J. Gottlieb, 'Measurements of Overpressure Signatures from Supersonic Projectiles - Part III: The 5-inch/54 MK41 Projectile (U)', DRES Suffield Memorandum No. 1042, Defence Research Establishment Suffield, Ralston, Alberta, June 1982.
54. D. V. Ritzel and J. J. Gottlieb, 'Measurements of Overpressure Signatures from Supersonic Projectiles - Part IV: The 3-inch/50 MK33 Projectile (U)', DRES Suffield Memorandum No. 1043, Defence Research Establishment Suffield, Ralston, Alberta, June 1982.
55. De-gui Liu, Jing-gao Fei, Yong-jiang Yu, and Guang-yaung Li, 'A Compendium of FORTRAN Algorithms', The Publishing House of the National Defence Industry, Beijing, China, Vol. 1, pp. 354-358, 1980.
56. Van der Corput, 'Verteilungsfunktionen', Proc. Kon. Adad. Wet., Vol. 38, pp. 813-821 and pp. 1058-1066, Amsterdam, 1935.
57. J. M. Hammersley and D. C. Handscomb, 'Monte Carlo Methods', Methuen and Company Limited, London, 1975.
58. R. W. MacCormack and A. J. Paullay, 'Computational Efficiency Achieved by Time Splitting of Finite Difference Operators', AIAA Paper No. 72-154, AIAA Tenth Aerospace Sciences Meeting, San Diego, California, 17-19 January 1972.

59. G. A. Sod, 'Lecture Notes in Physics', Vol. 90, pp. 492-514, Springer-Verlag, Berlin, 1979.
60. M. J. Zucrow and J. D. Hoffman, 'Gas Dynamics', Vol. 1, John Wiley and Sons, 1976.
61. NASA Ames Research Staff, 'Equations, Tables, and Charts for Compressible Flow', Report No. 1135 (Supercedes NACA TN 1428), NASA Ames Research Center, Moffett Field, California.
62. G. Emanuel, 'Near-Field Analysis of Compressive Supersonic Ramp', Physics of Fluids, Vol. 25, No. 4, pp. 1127, 1982.
63. G. Emanuel, 'Numerical Method and Results for Inviscid Supersonic Flow over a Compressive Ramp', Computers and Fluids, Vol. 11, No. 4, pp. 367-377, 1983.
64. K. O. Friedrichs, 'Formation and Decay of Shock Waves', Communications on Applied Mathematics, Vol. 1, pp. 211-245, 1948.
65. N. F. Krasnov, 'Aerodynamics of Bodies of Revolution', Edited and annotated by D. N. Morris, American Elsevier Publishing Company, New York, 1970.

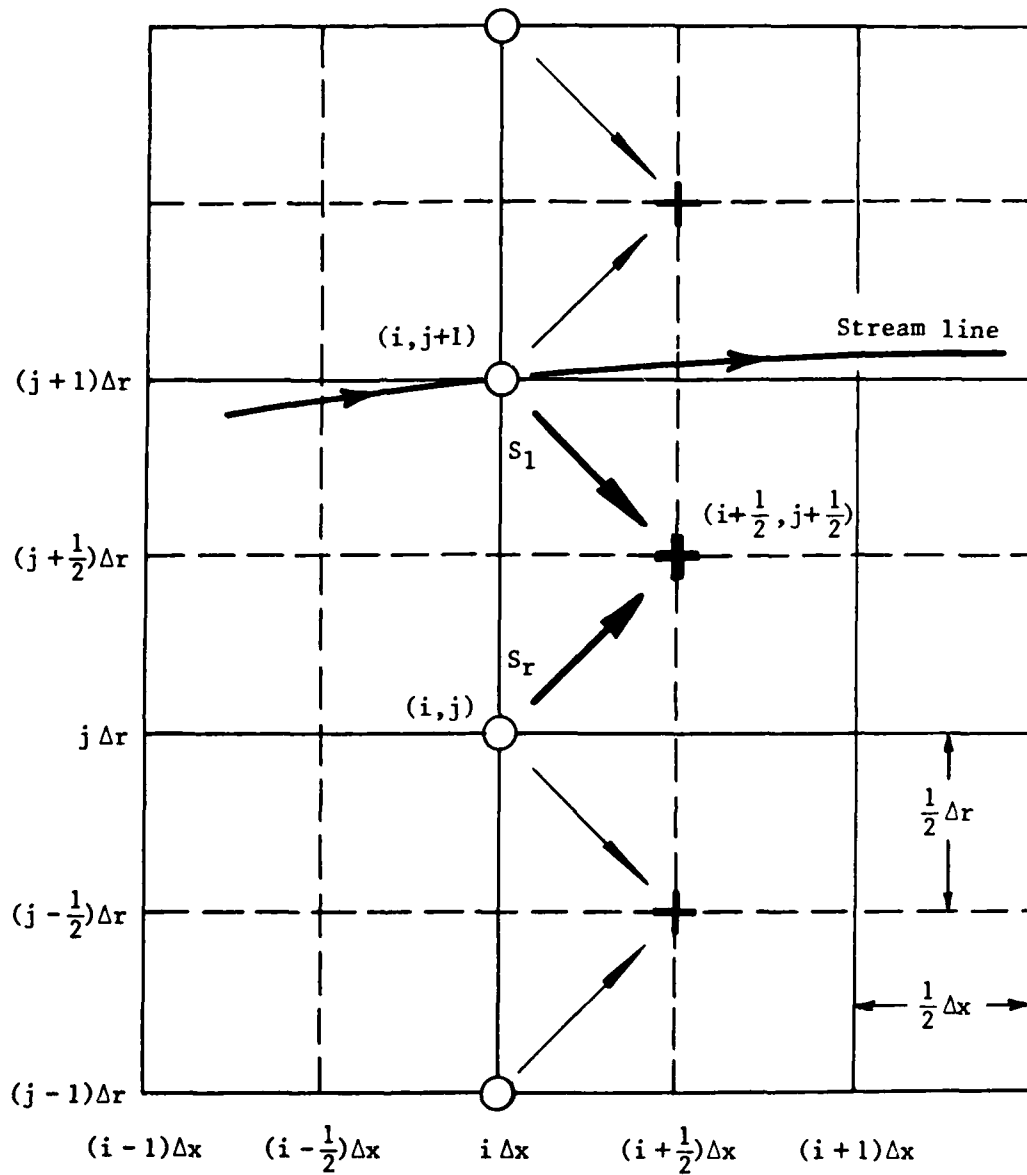


Fig. 1. Grid for the random-choice method.

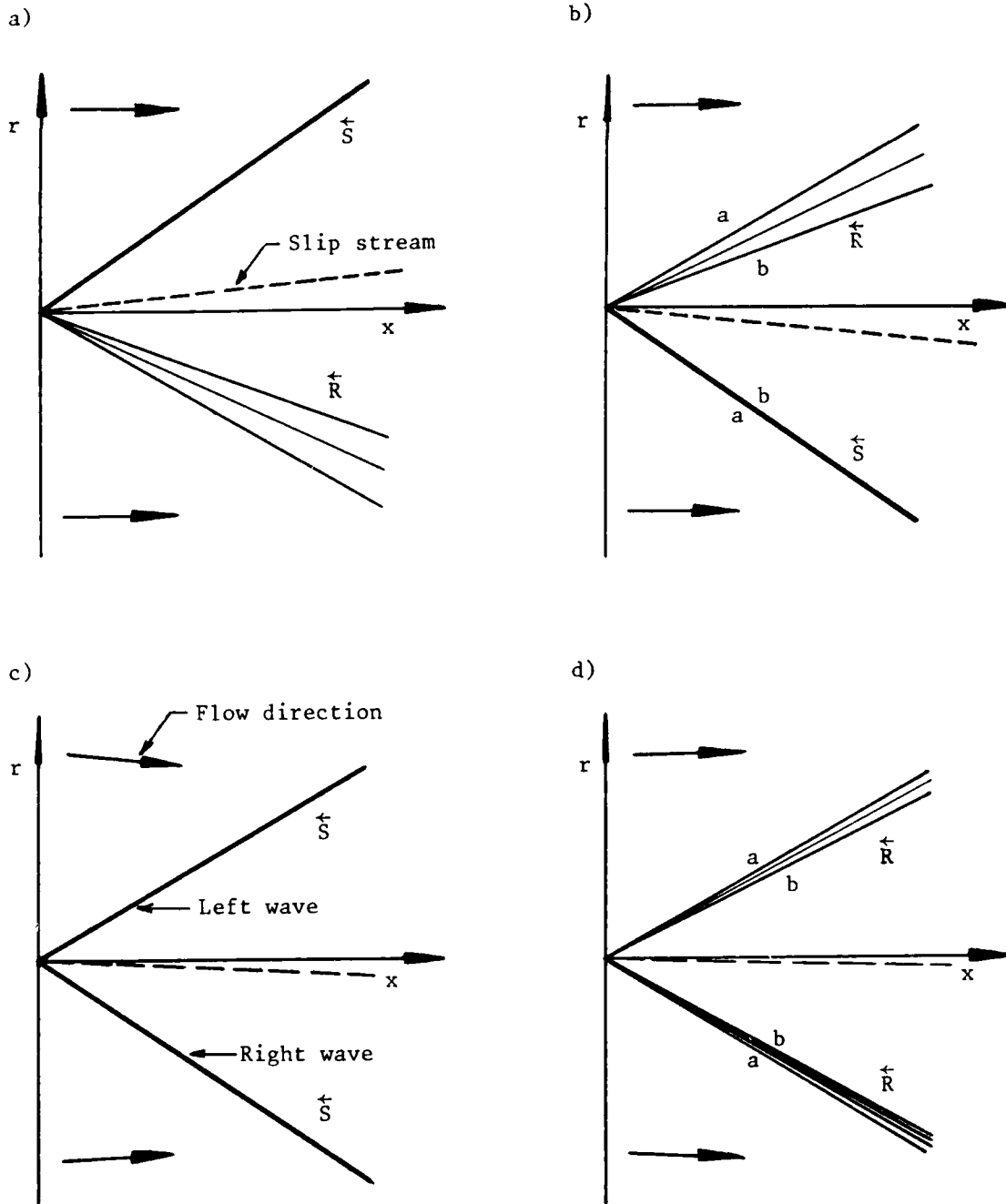


Fig. 2. Four different wave patterns for the Riemann problem, composed of elemental oblique shock waves ( $\vec{S}$ ) and Prandtl-Meyer rarefaction waves ( $\vec{R}$ ), and separated by a slip stream.

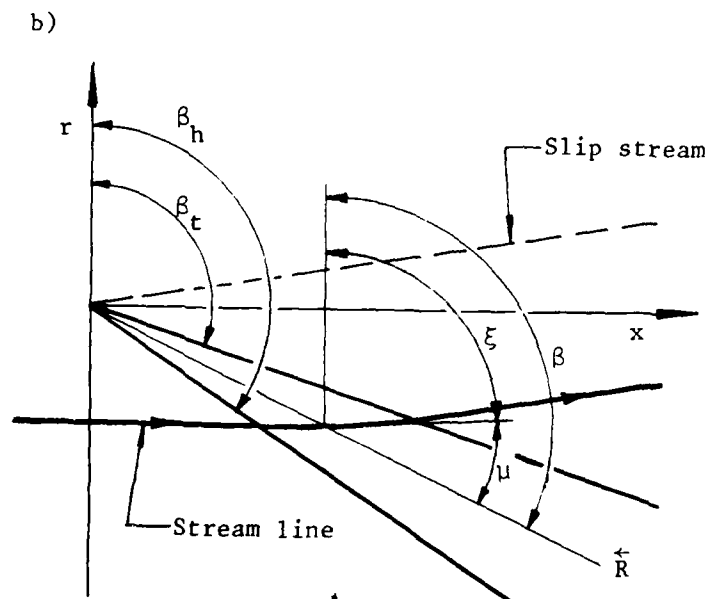
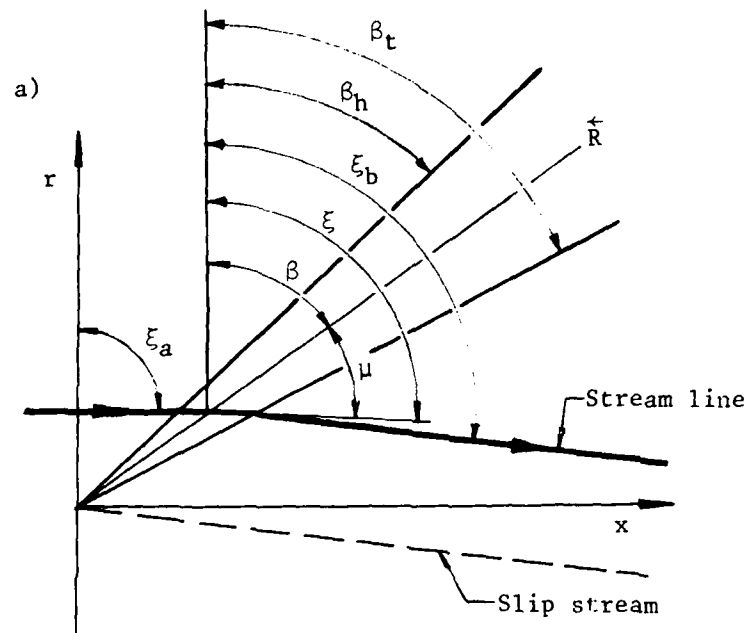


Fig. 3. Diagram of leftward (a) and rightward (b) rarefaction waves and the definition of various flow and wave angles.

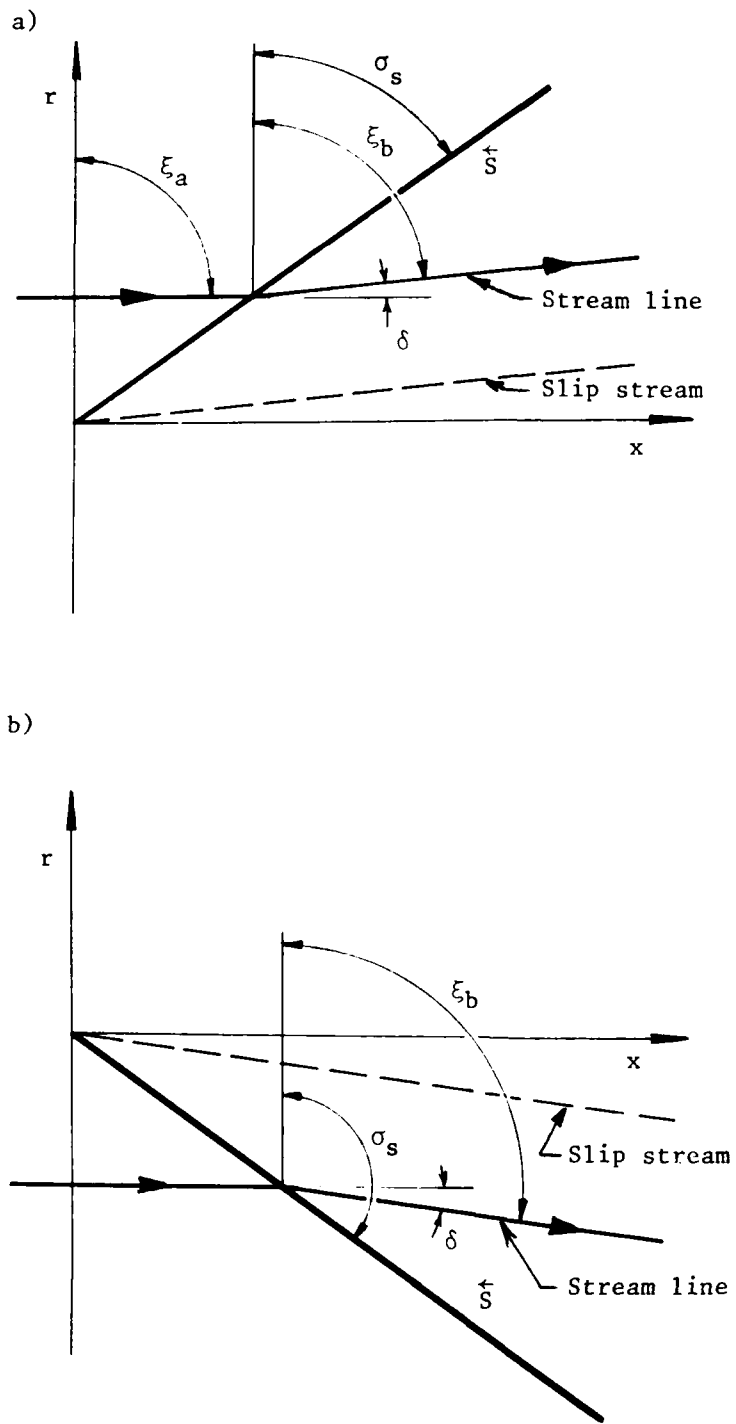


Fig. 4. Diagram of leftward (a) and rightward (b) shock waves and the definition of various flow angles.

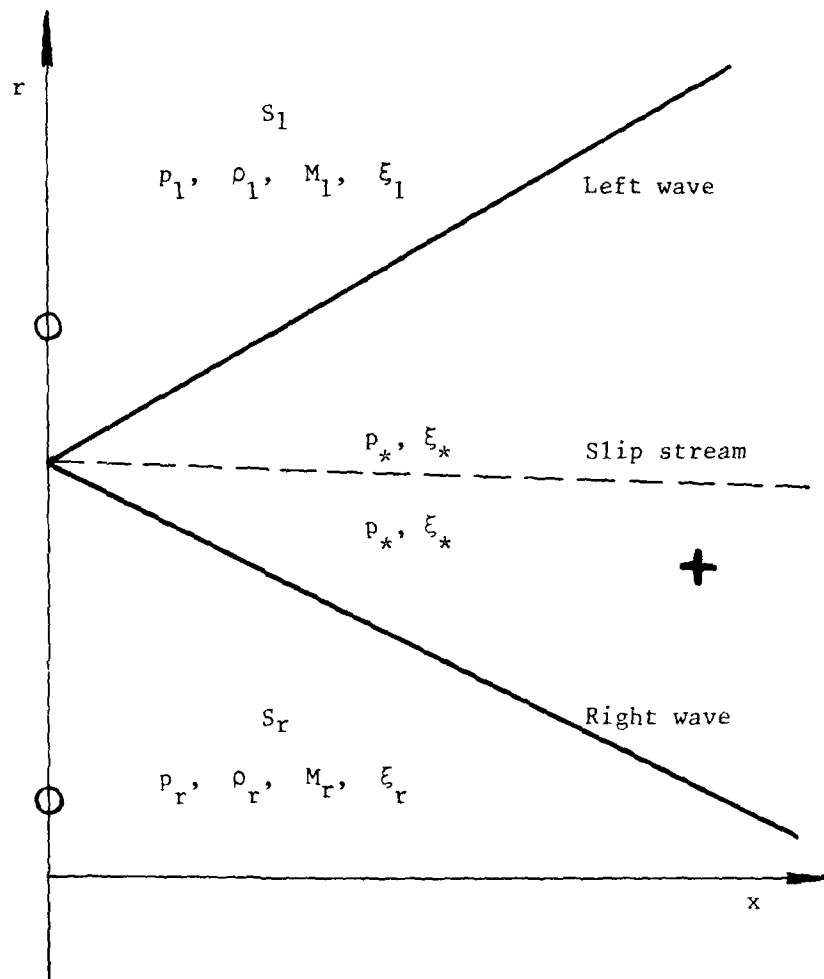


Fig. 5. Riemann problem showing the left state  $S_1$ , right state  $S_r$ , and the continuity of pressure  $p_*$  and flow angle  $\xi_*$  across the slip stream.

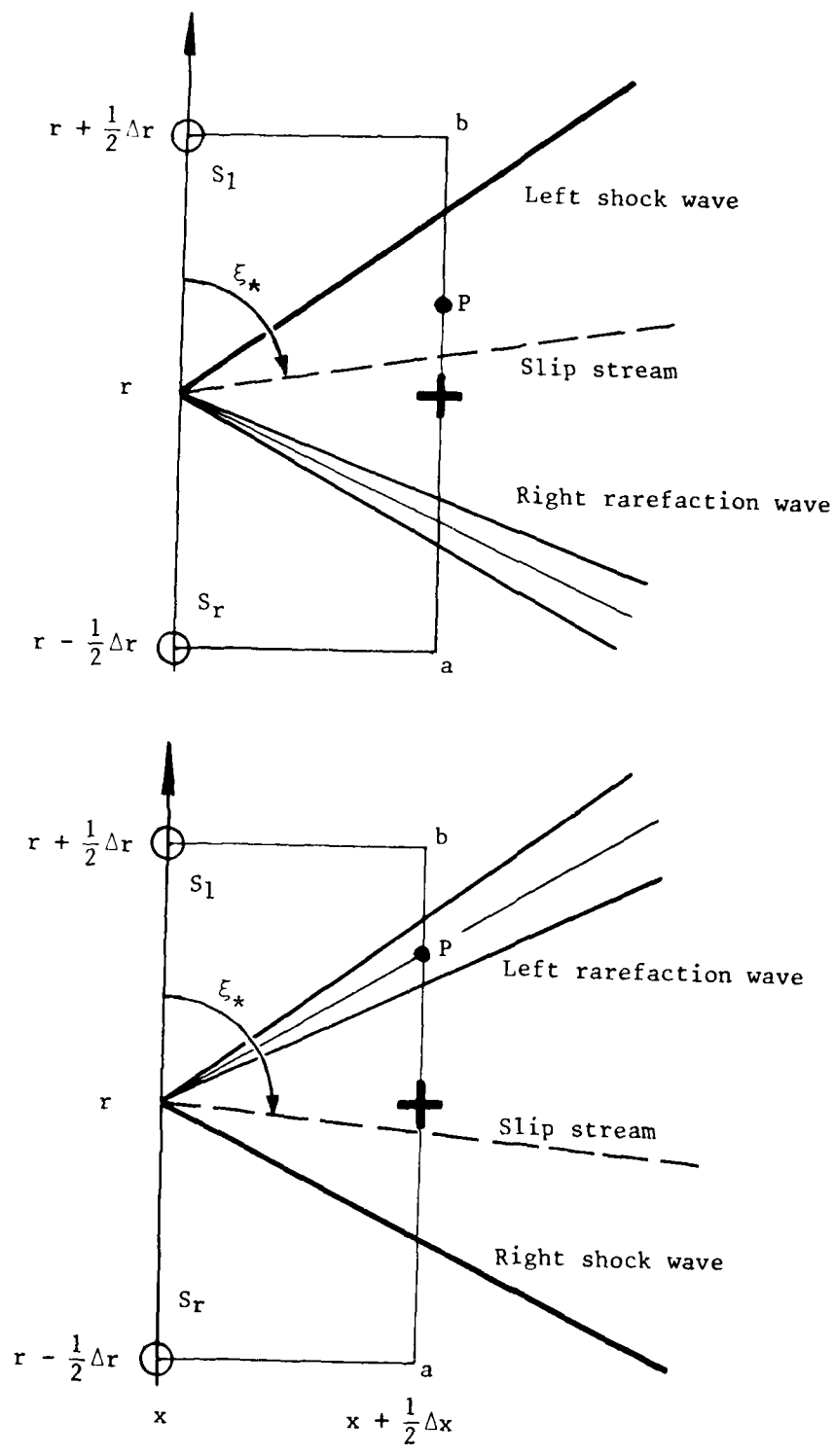


Fig. 6. Diagram showing the random sampling point P.

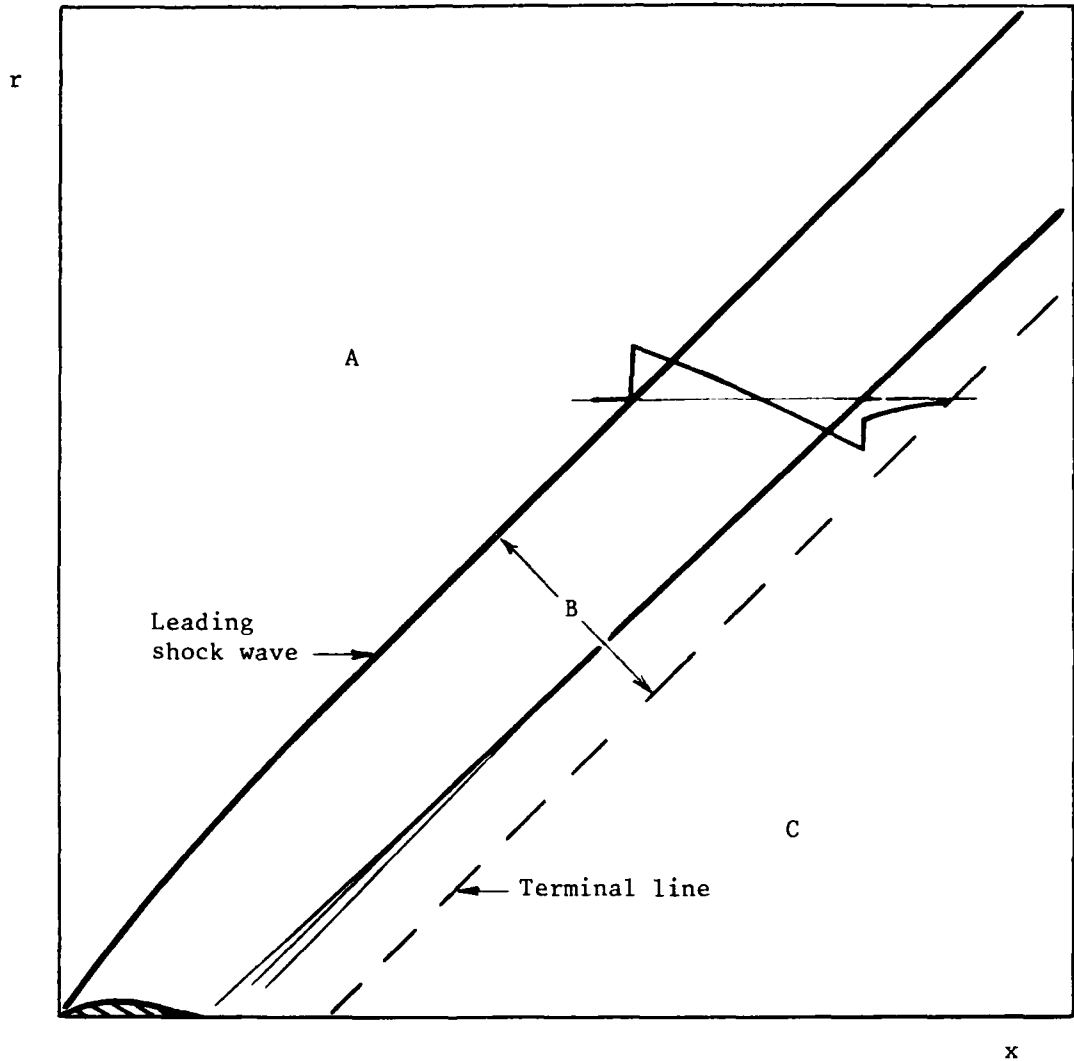


Fig. 7. Illustration of the planar or axisymmetric flow field from a body in a supersonic flow, showing regions of free-stream conditions (A), computed flow conditions (B), and uncomputed flow conditions (C).

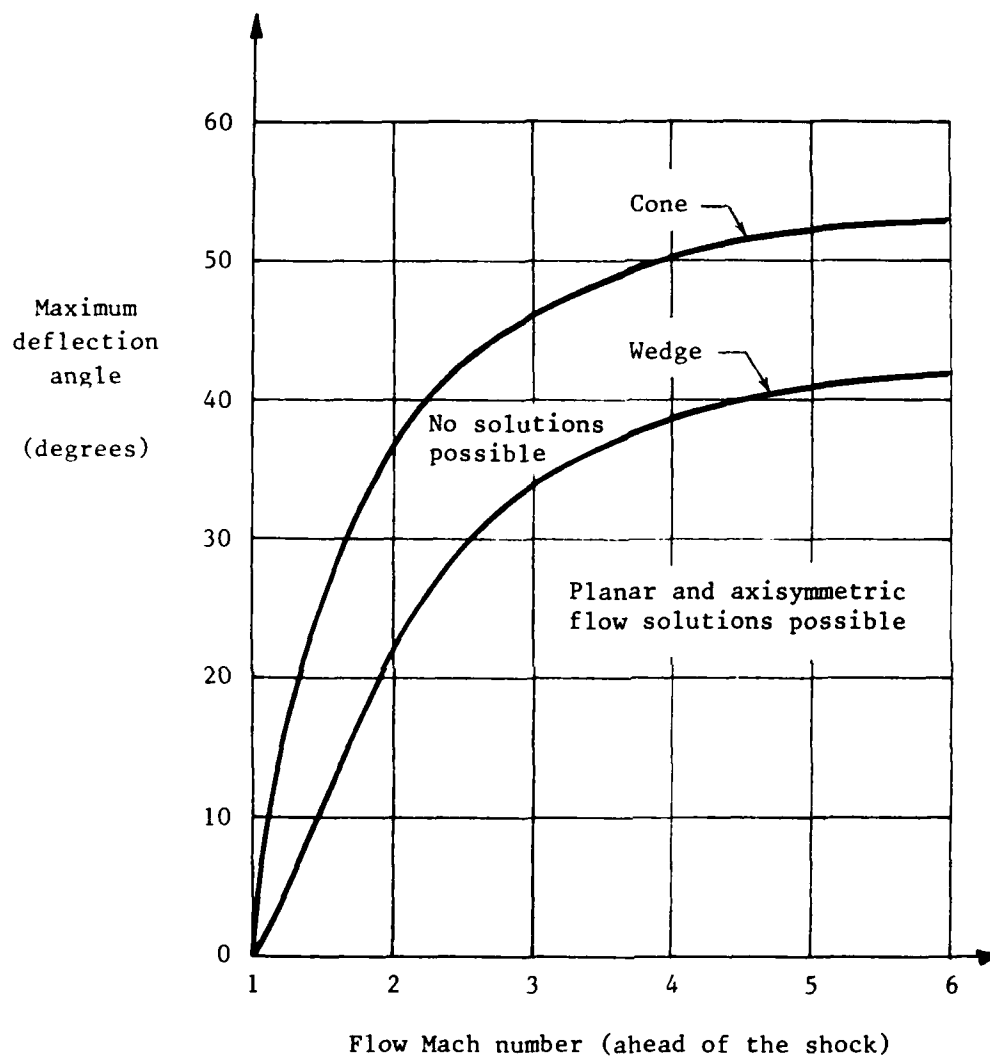


Fig. 8. Maximum deflection angle of the flow through an oblique shock wave that produces a sonic flow behind it ( $\gamma = 7/5$ ).

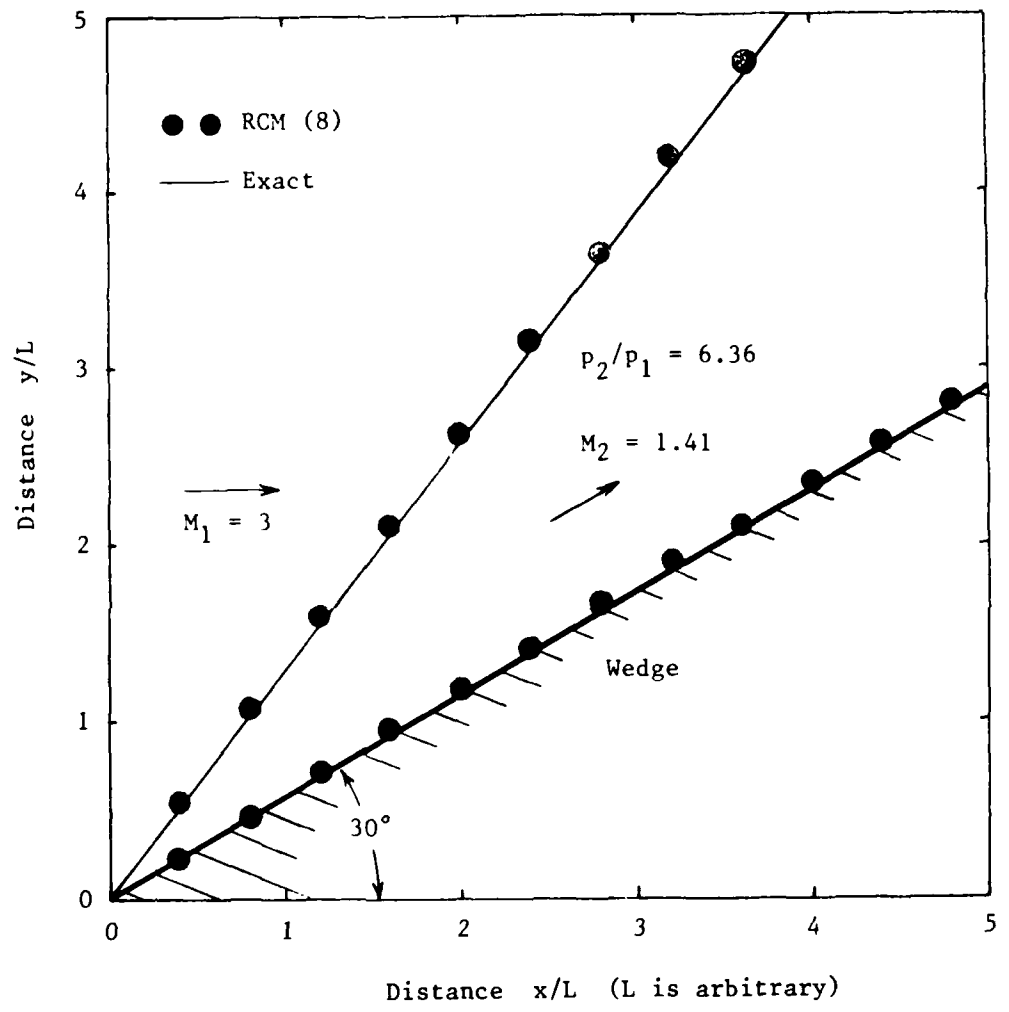


Fig. 9. Planar flow over a compressive corner.

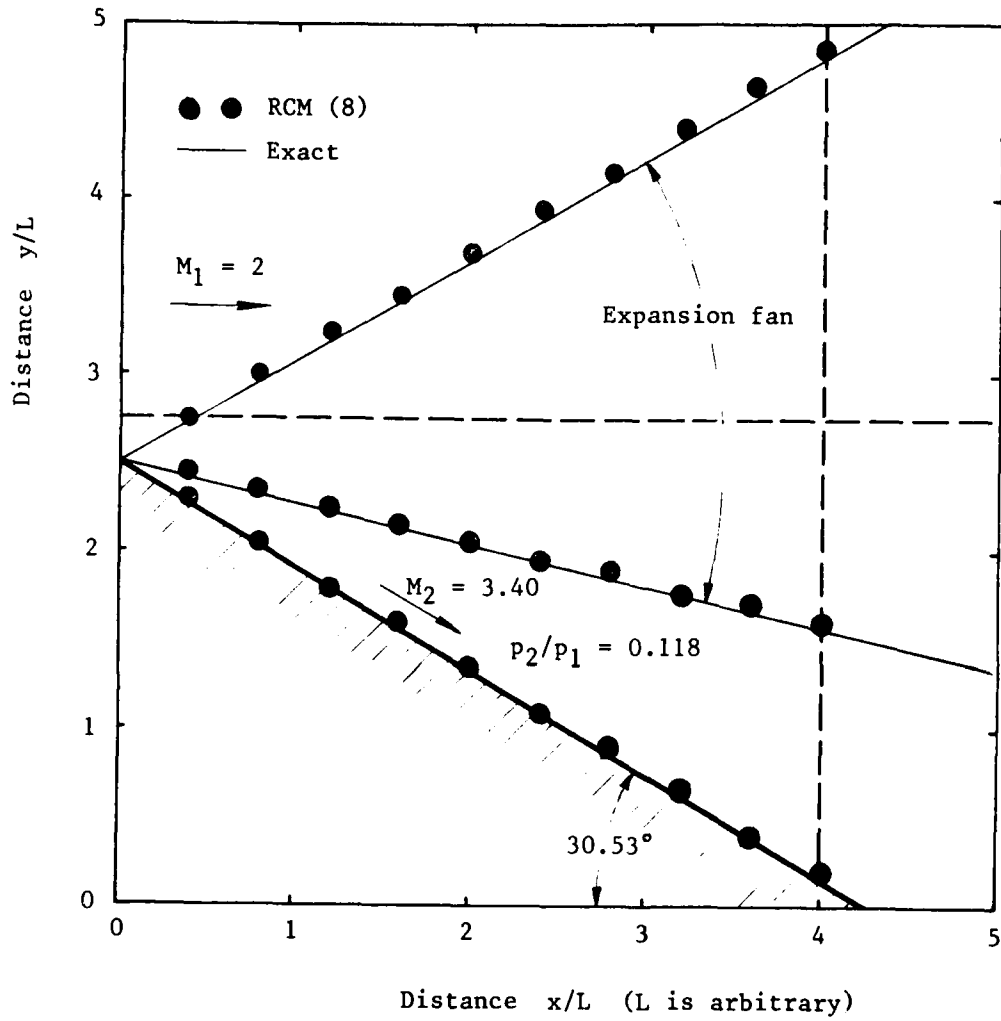


Fig. 10a. Flow over an expansive corner.

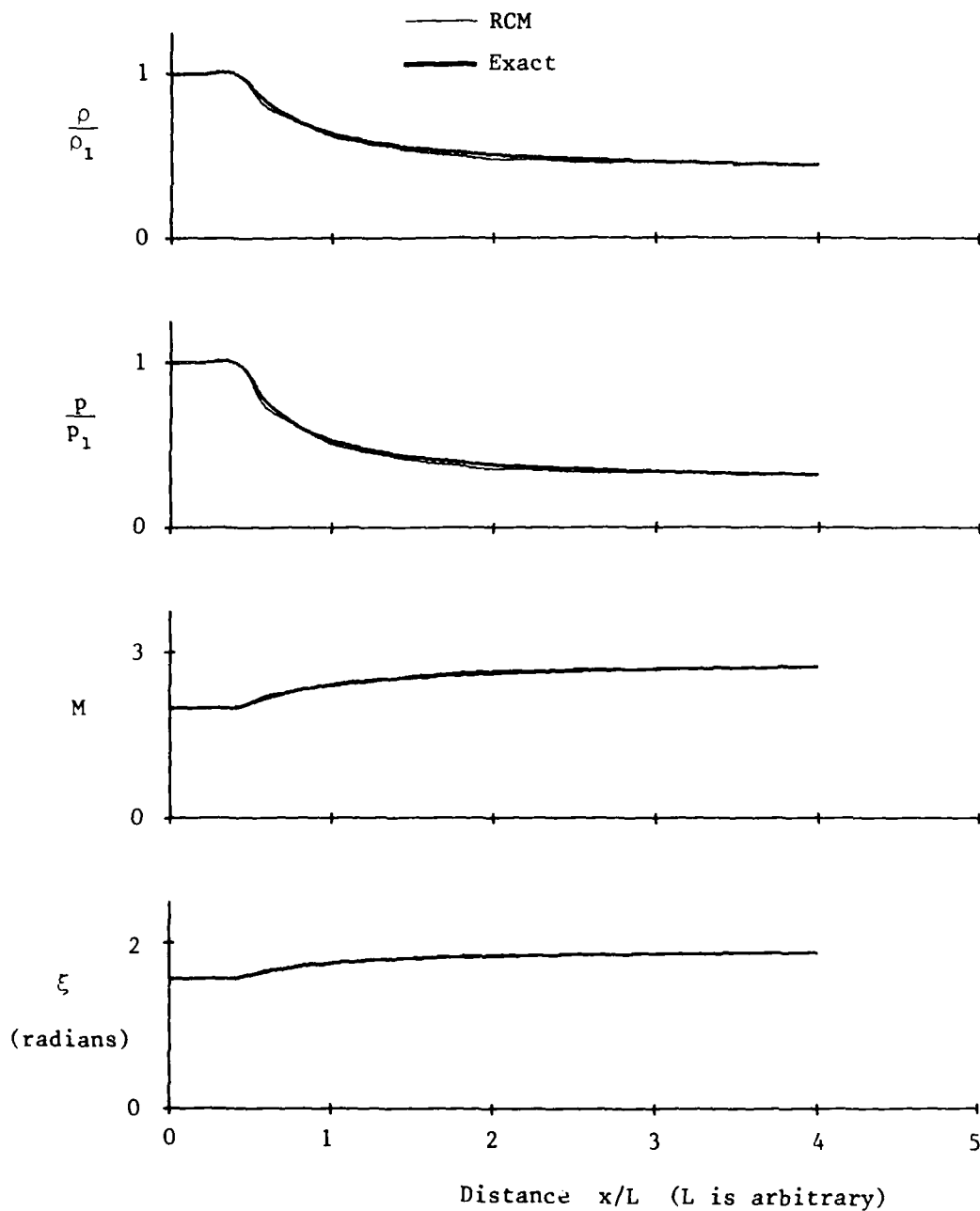


Fig. 10b. Comparison of RCM and exact solutions for the flow over an expansive corner ( $y = 2.75$  units).

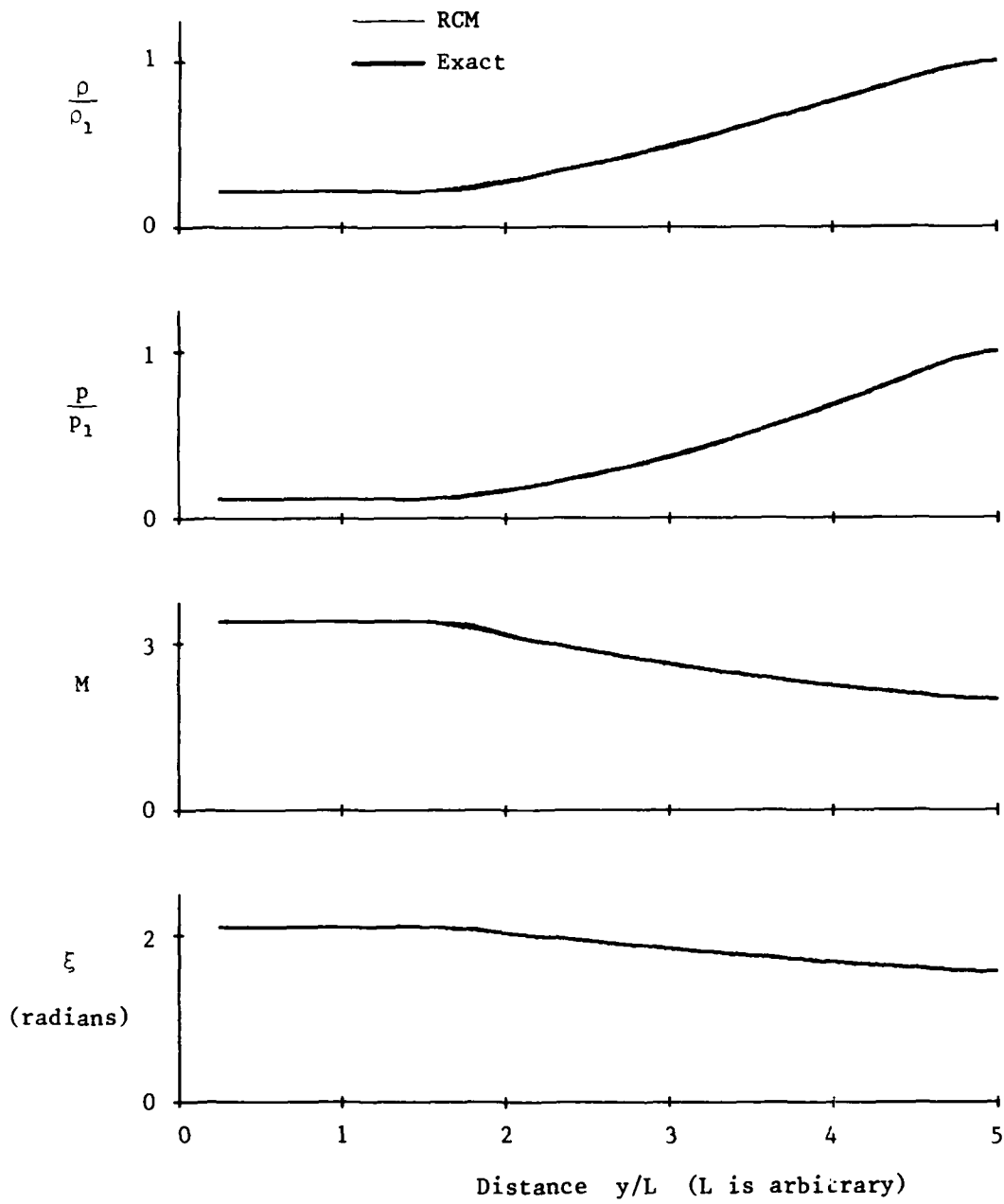


Fig. 10c. Comparison of RCM and exact solutions for the flow over an expansive corner ( $x = 4.0$  units).

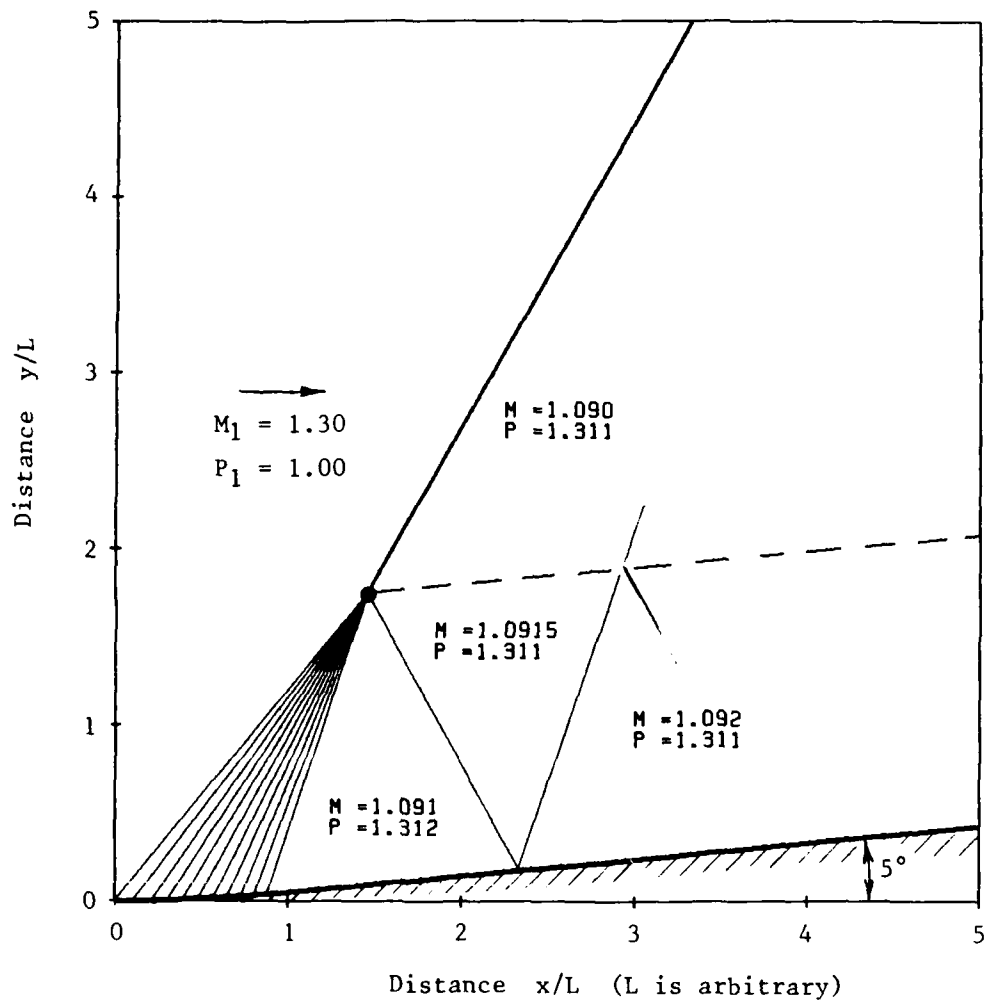


Fig. 11a. Flow over a contoured compressive corner ( $M_1 = 1.30$ ).

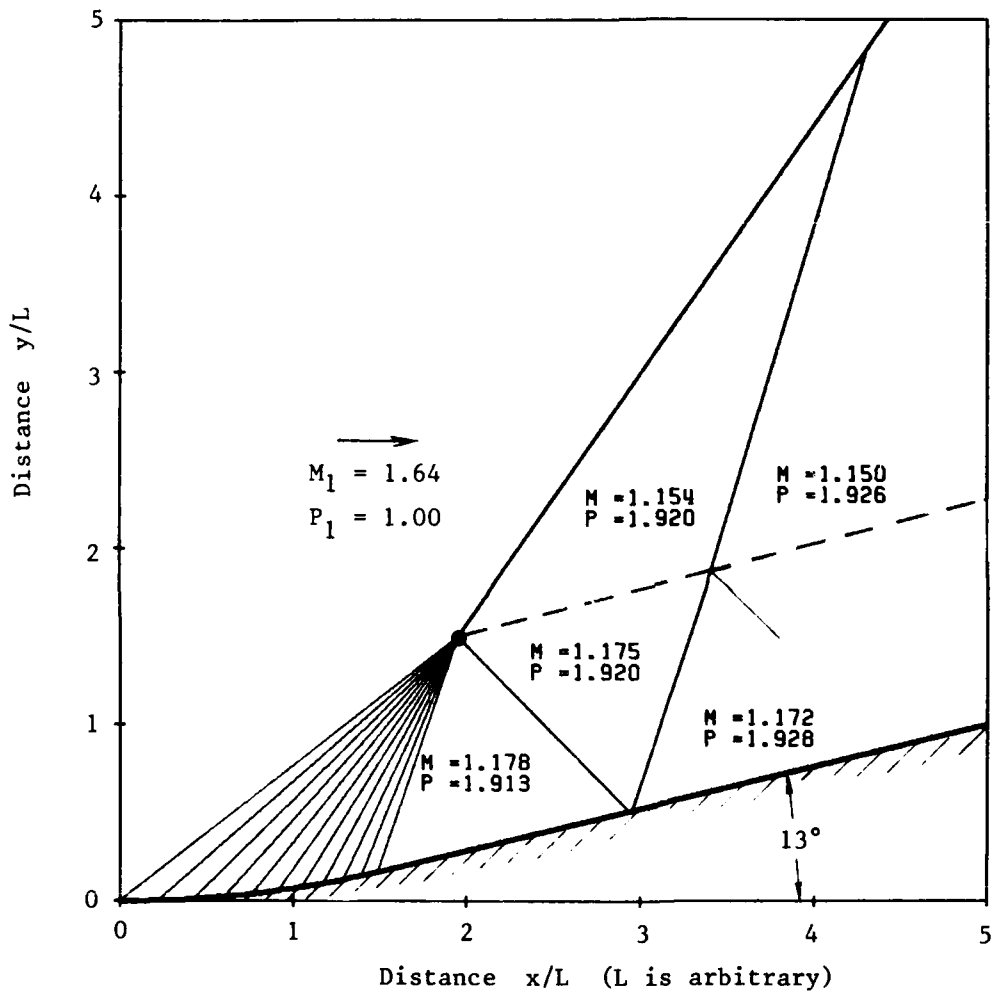


Fig. 11b. Flow over a contoured compressive corner ( $M_1 = 1.64$ ).

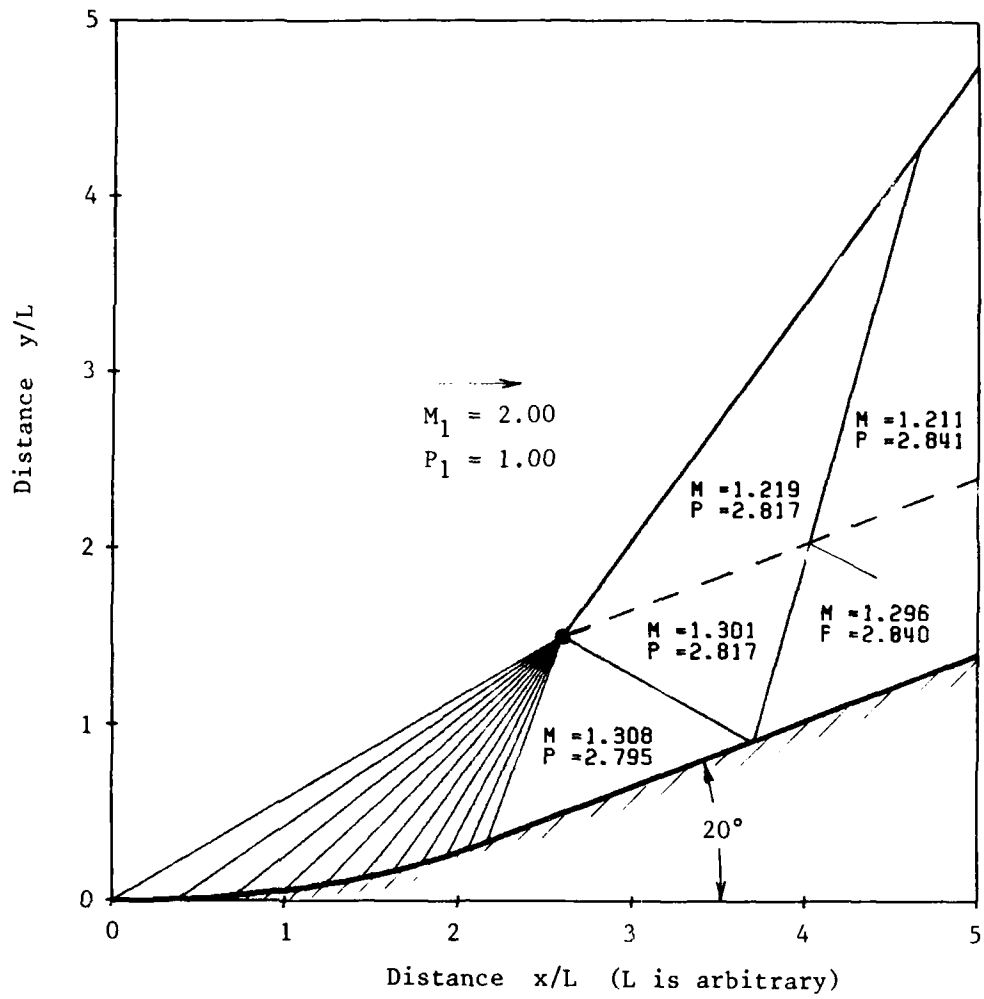


Fig. 11c. Flow over a contoured compressive corner ( $M_1 = 2.00$ ).

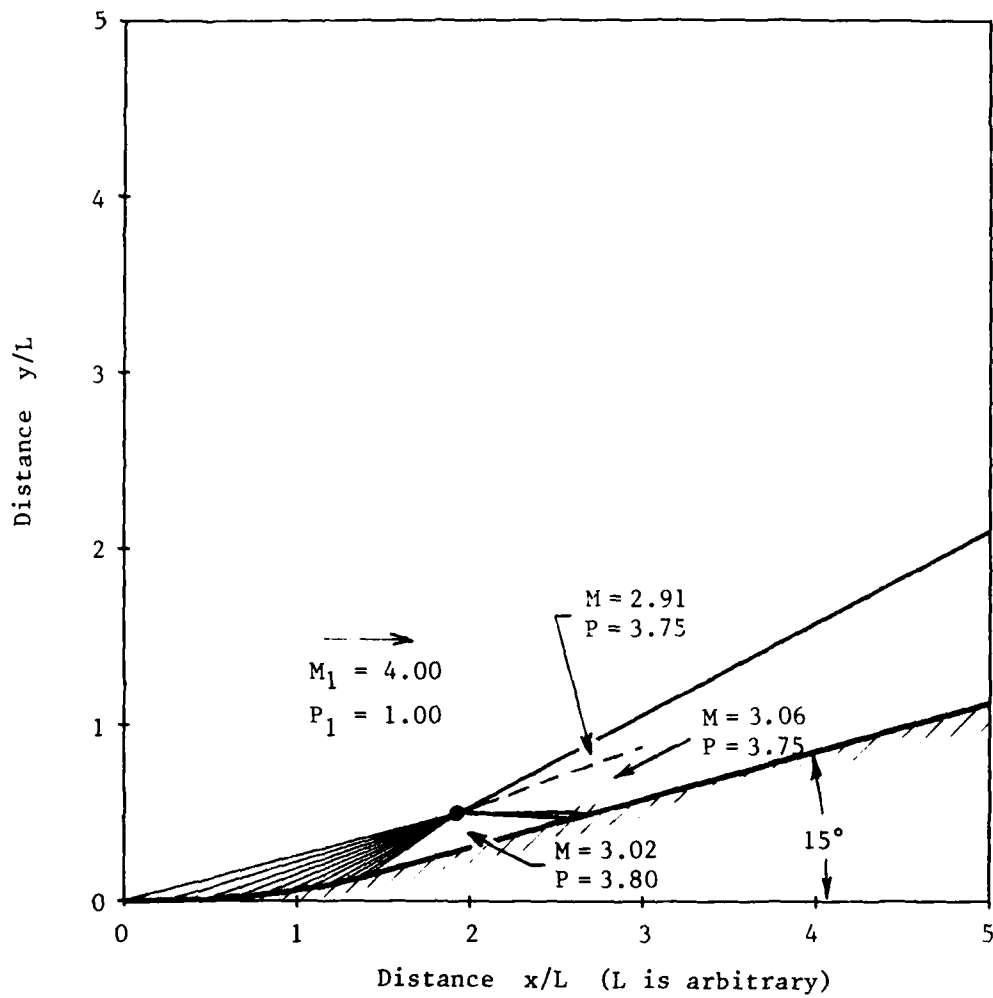


Fig. 11d. Flow over a contoured compressive corner ( $M_1 = 4.00$ ).

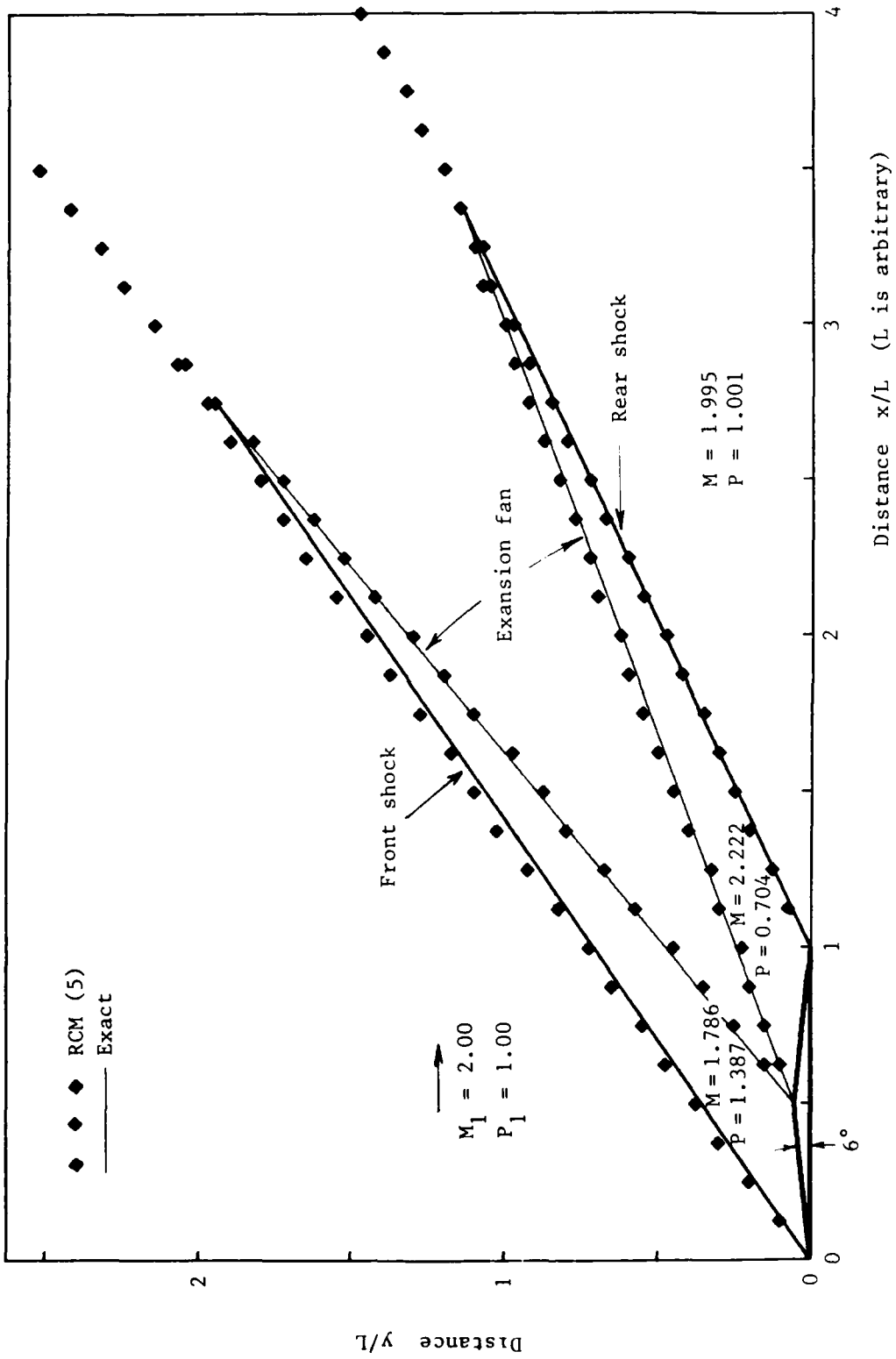


Fig. 12a. Wave diagram of the supersonic flow over a double wedge.

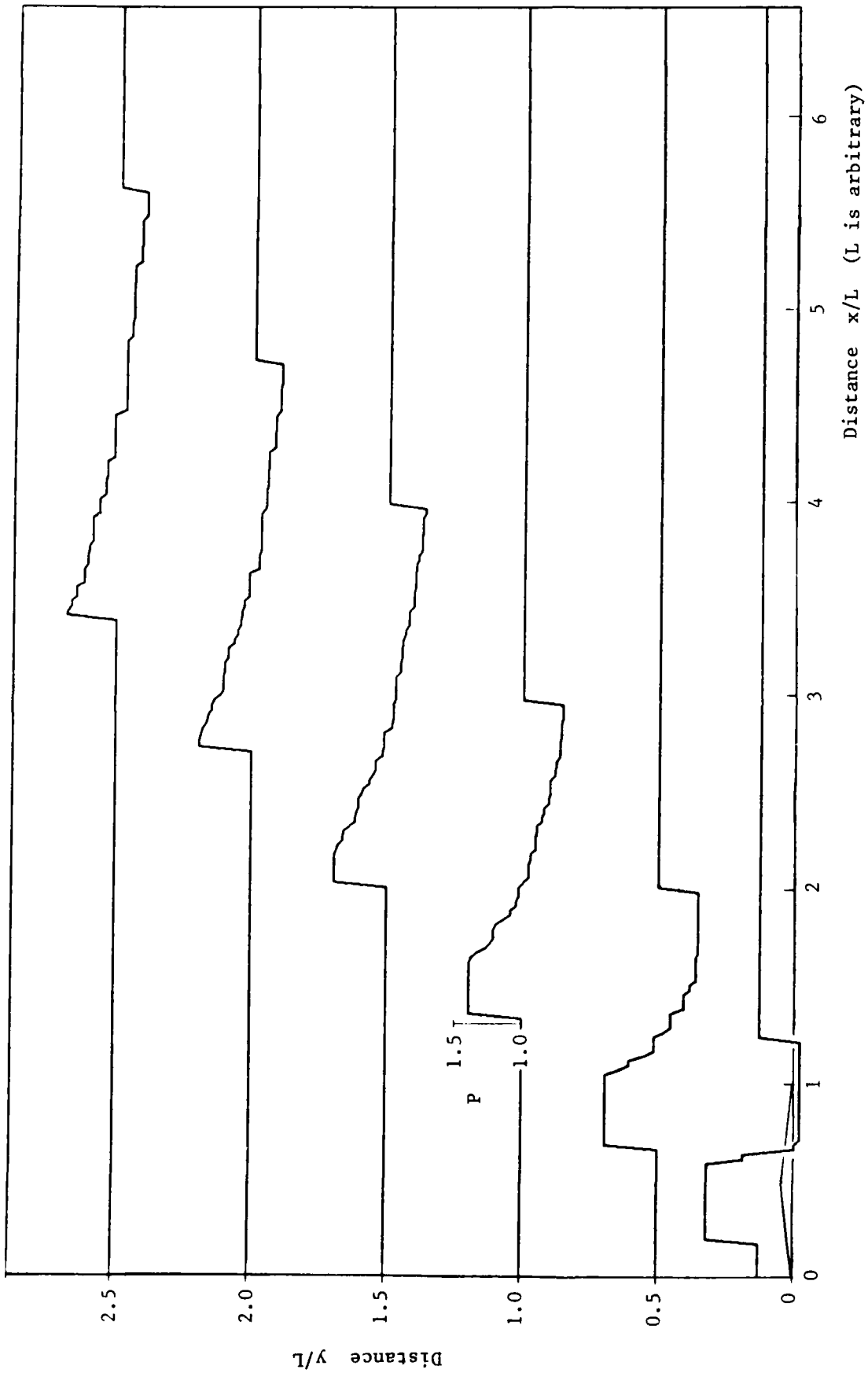


Fig. 12b. Pressure distributions of the supersonic flow over a double wedge.

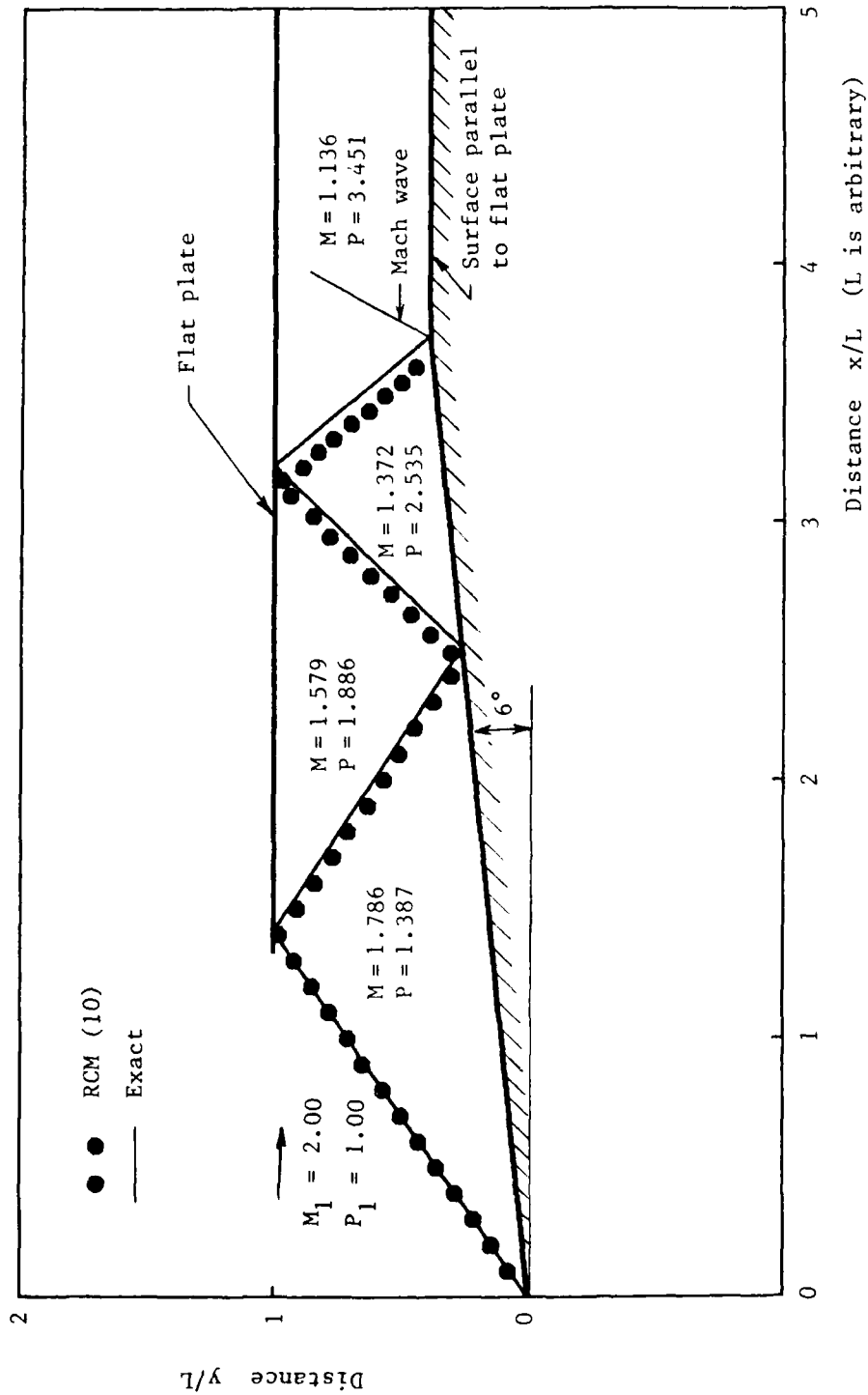


Fig. 13. Flow in a duct inlet made of a flat plate and compressive wedge (6 degrees).

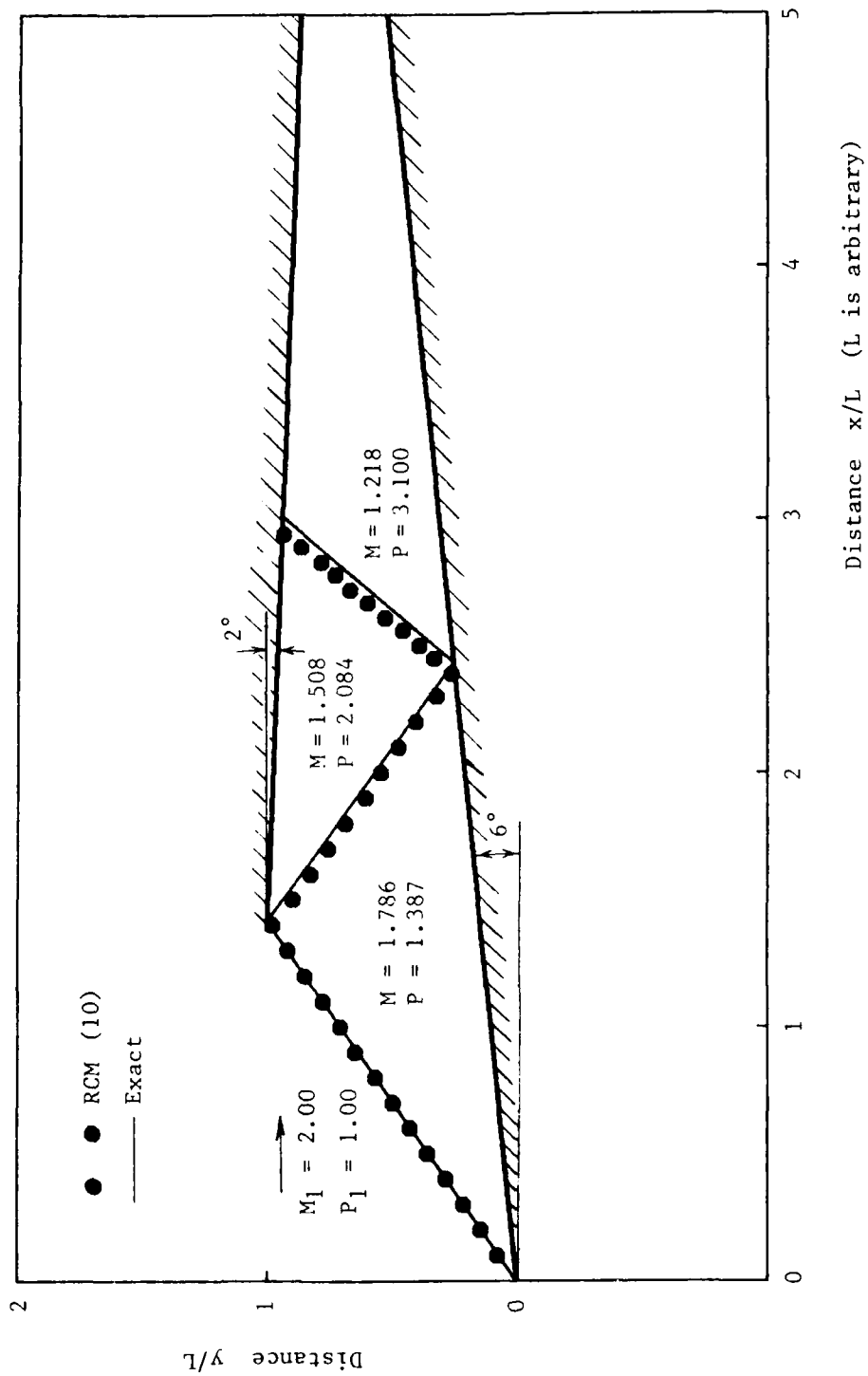


Fig. 14. Flow in a duct inlet made of two compressive wedges (2 and 6 degrees).

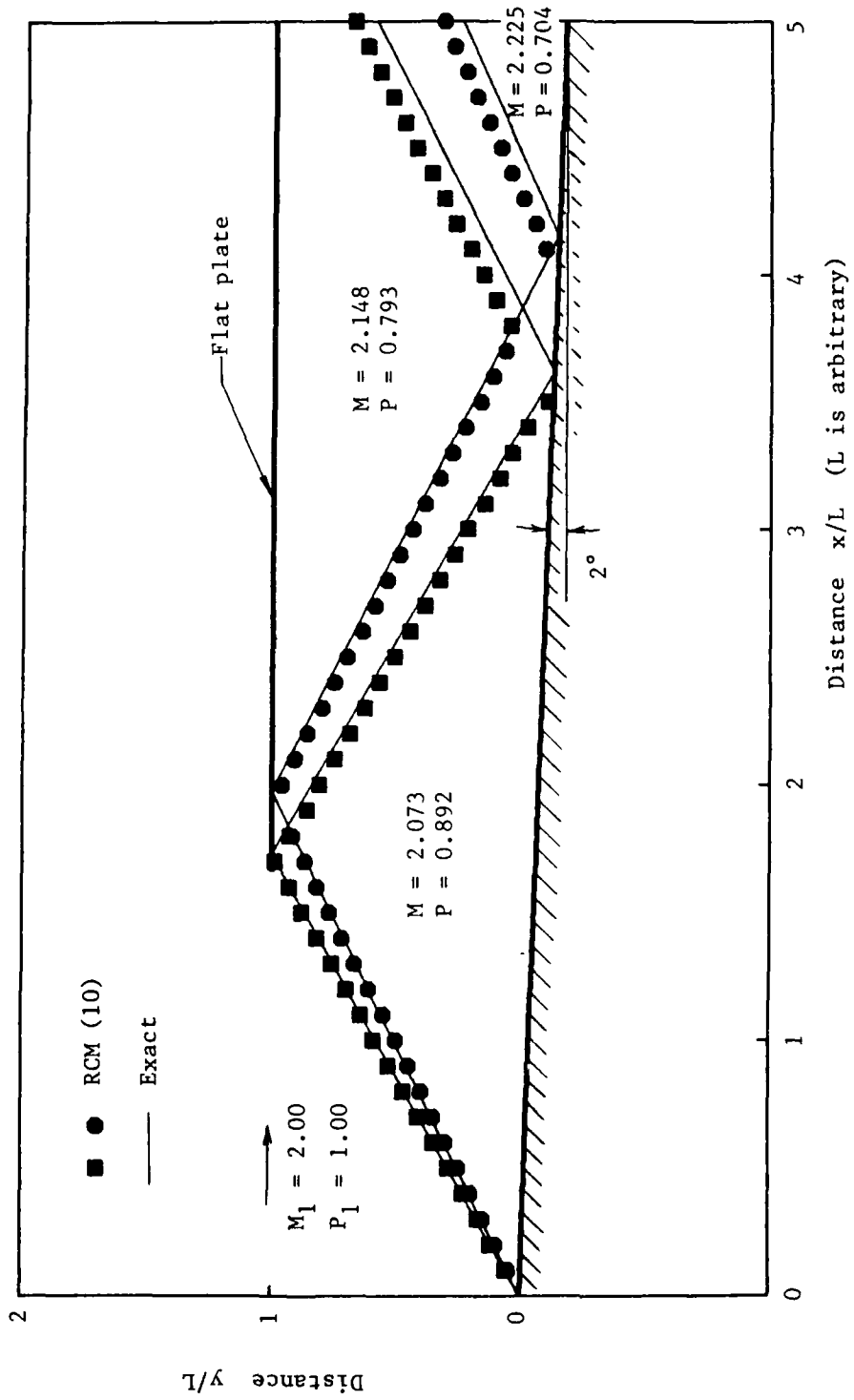


Fig. 15. Flow in a duct inlet made of a flat plate and sharp expansive corner (2 degrees).

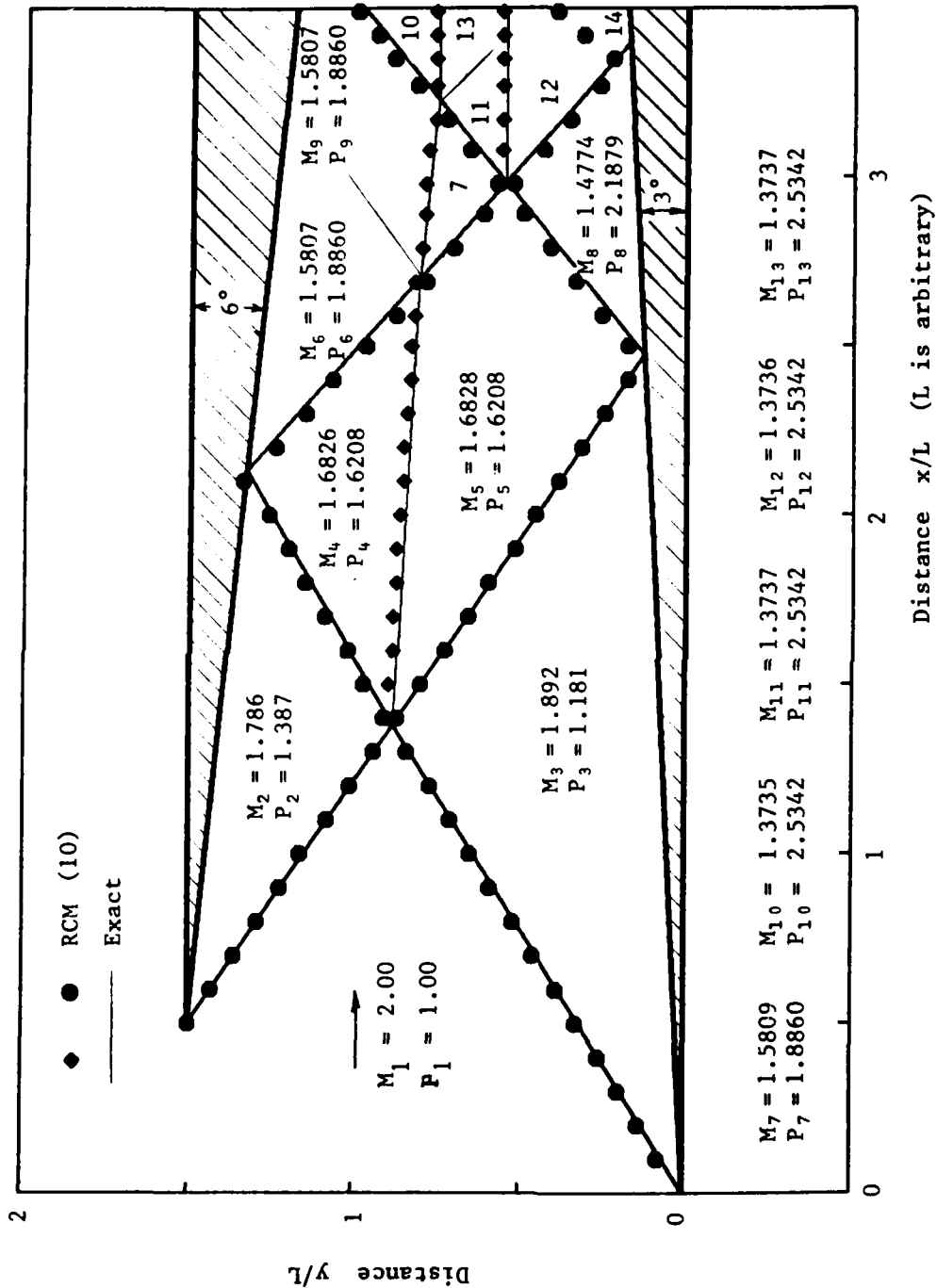


Fig. 16. Flow in a duct inlet made of two compressive wedges (6 and 3 degrees).

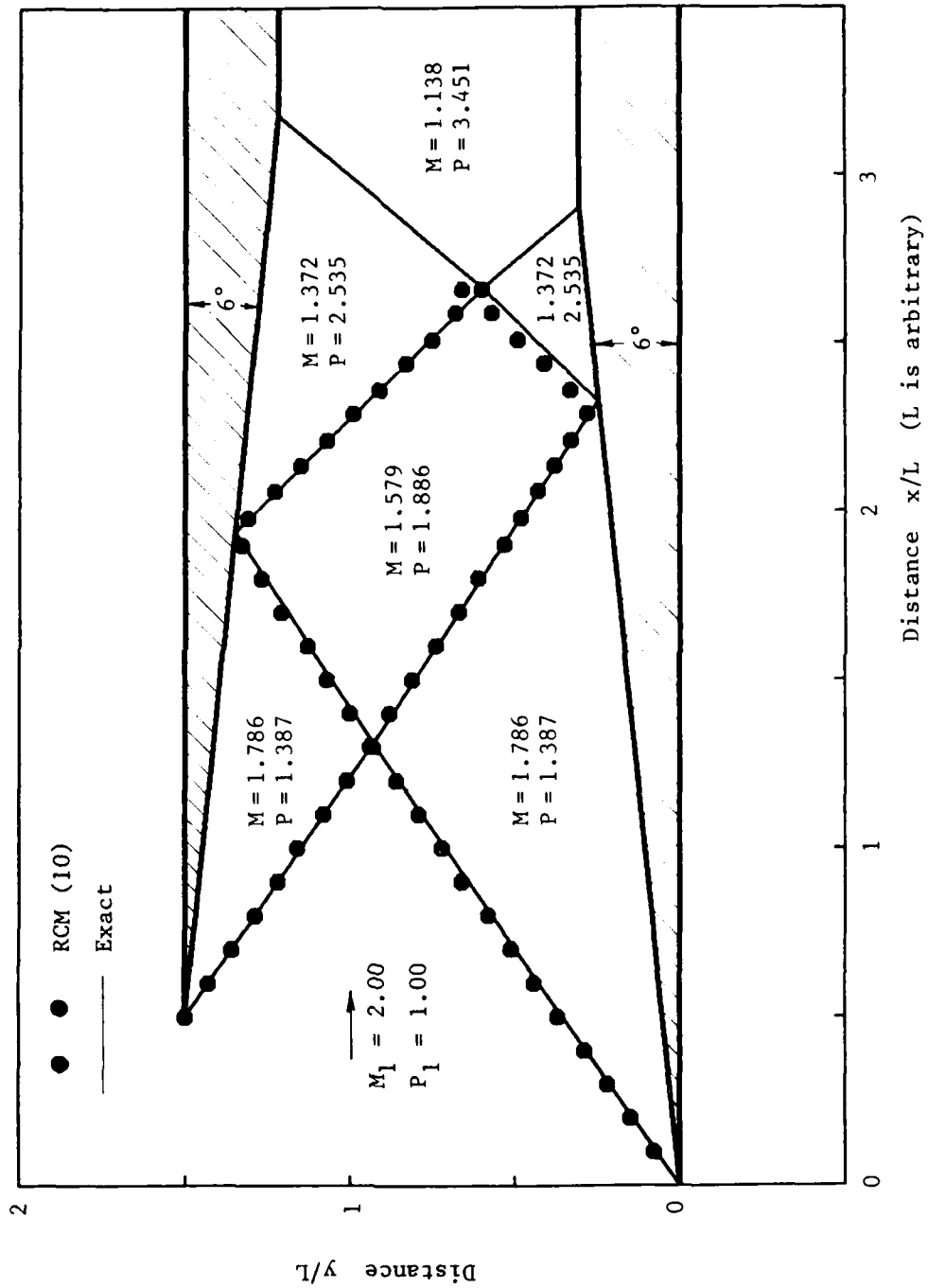


Fig. 17. Flow in a duct inlet made of two compressive wedges (both with 6 degrees).

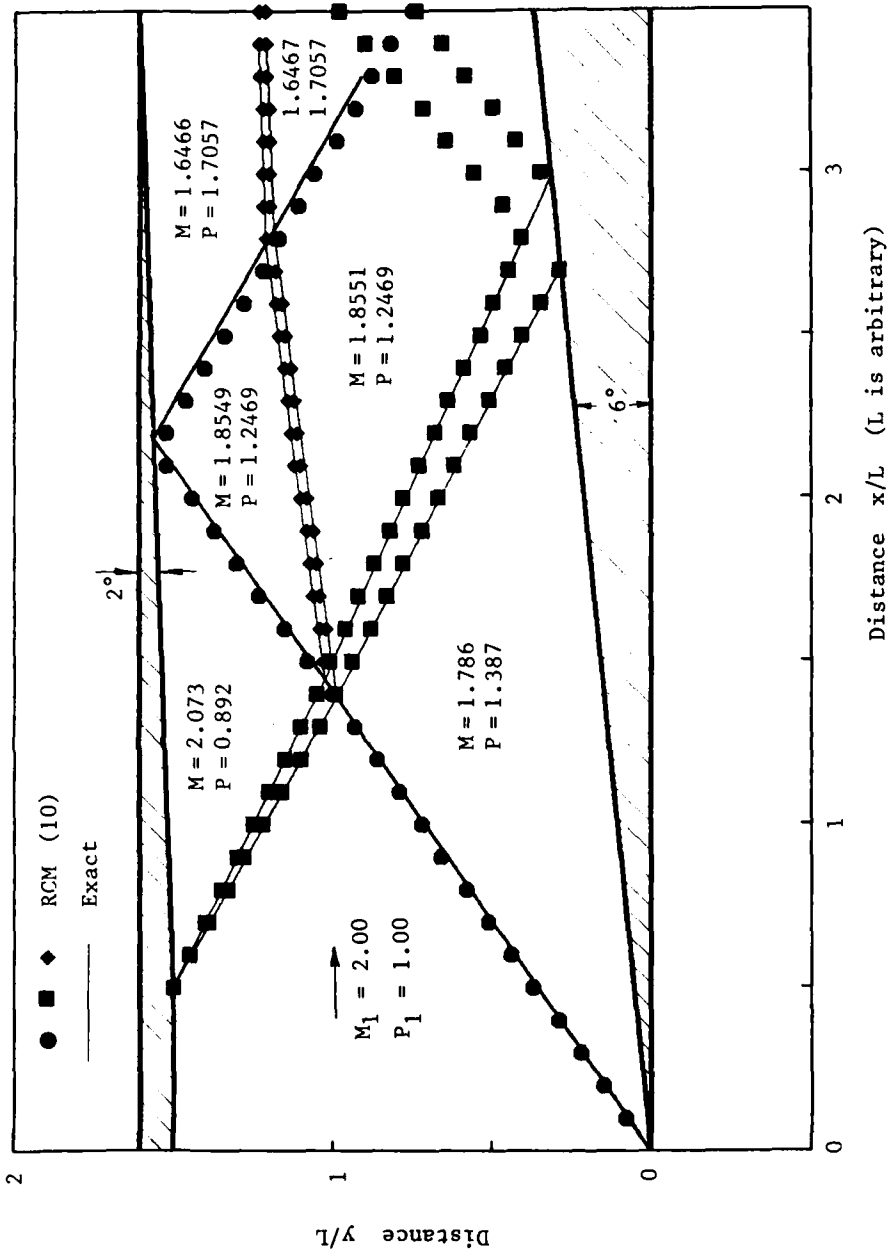


Fig. 18. Flow in a duct inlet made of one expansive wedge (2 degrees) and one compressive wedge (6 degrees).

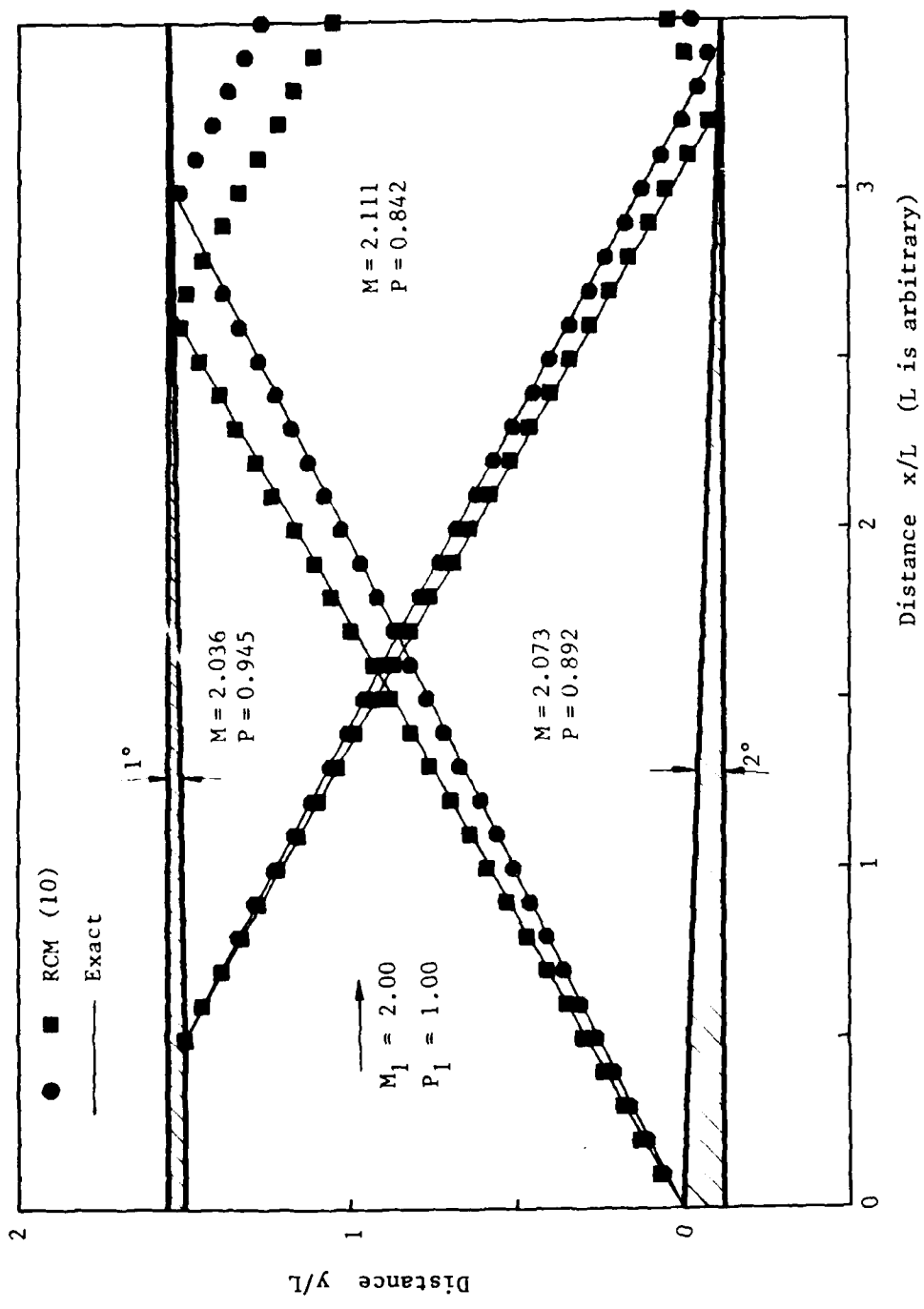


Fig. 19. Flow in a duct inlet made of two expansive wedges (1 and 2 degrees).

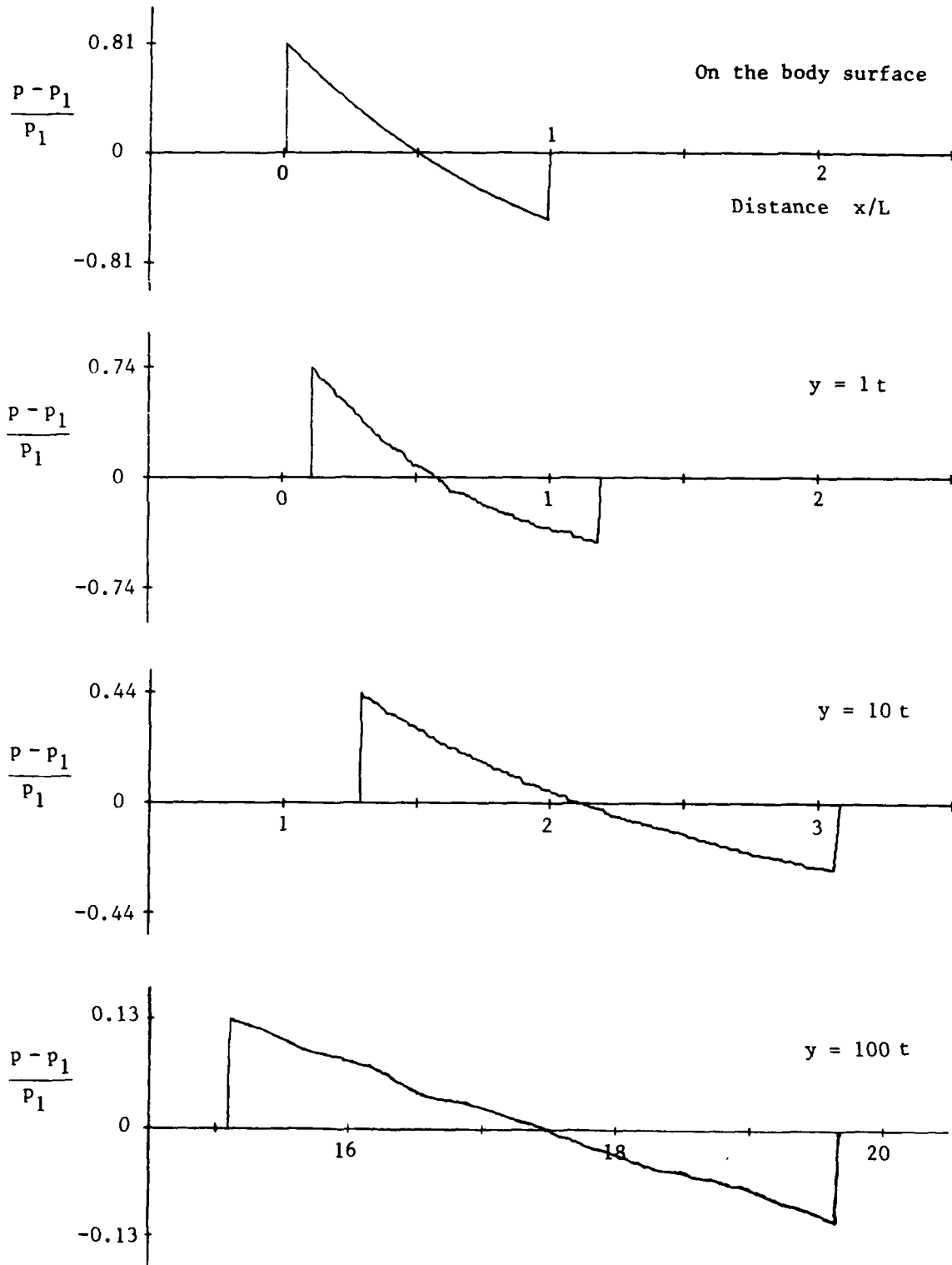


Fig. 20. Overpressure signatures on the surface of, and at 1, 10 and 100 body thicknesses from, a parabolic shaped airfoil ( $t/L = 0.10$ ) in a supersonic flow ( $M_1 = 2.0$ ).

□ ○ RCM (5)

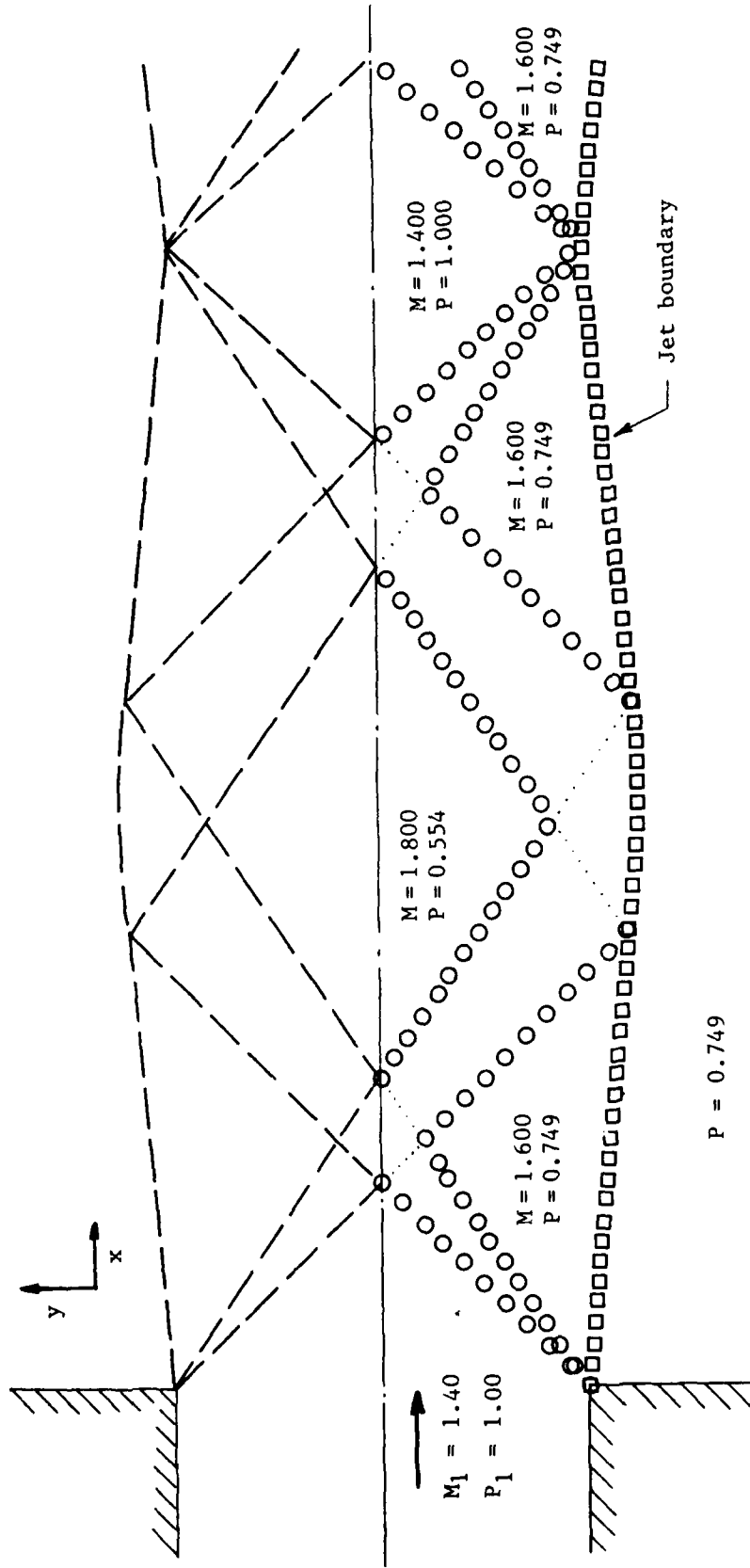


Fig. 21. Numerical computations for a free jet ( $M_1 = 1.40$ ).

○ □ RCM (5)

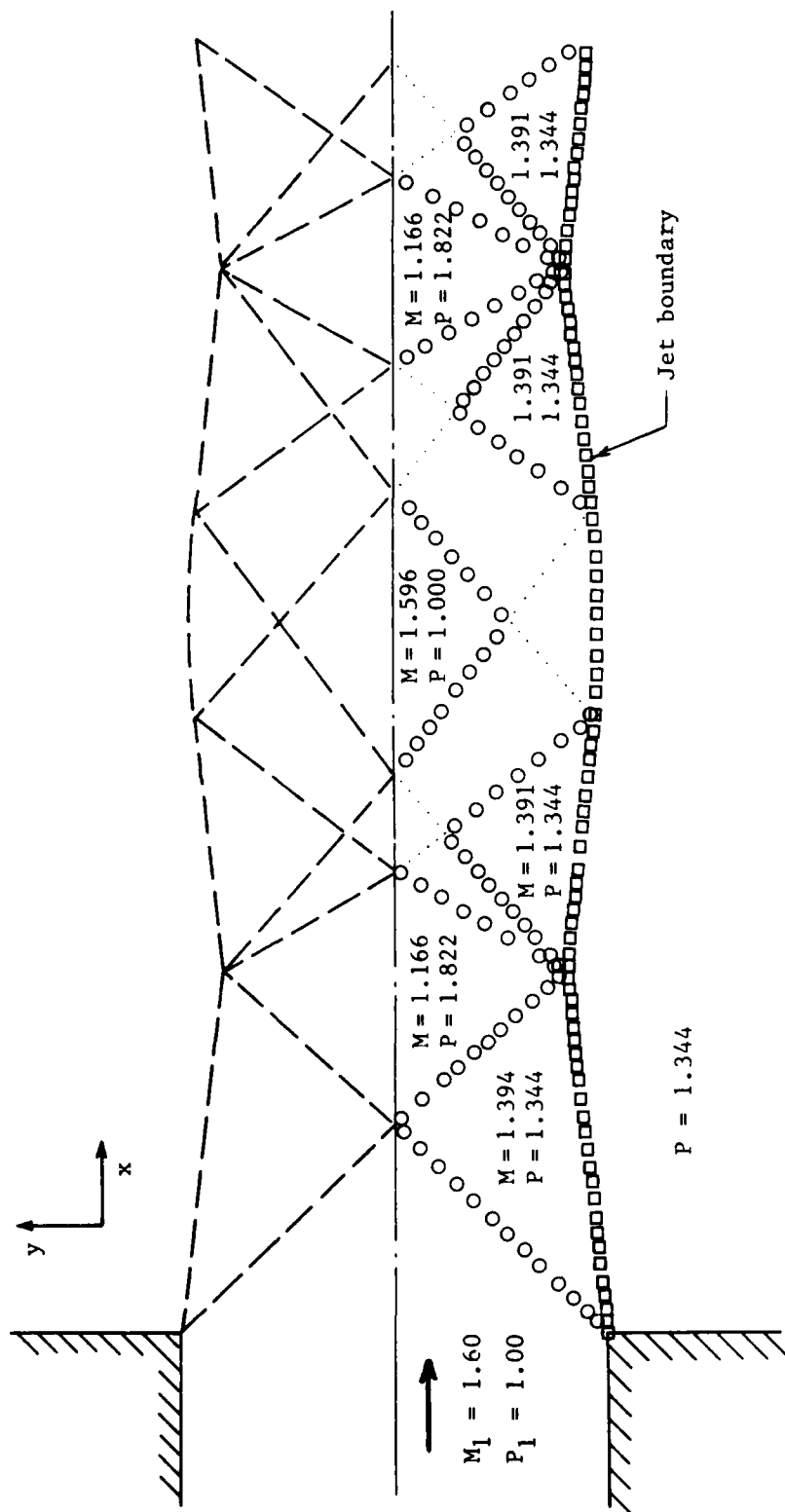


Fig. 22. Numerical computations for a free jet ( $M_1 = 1.60$ ).

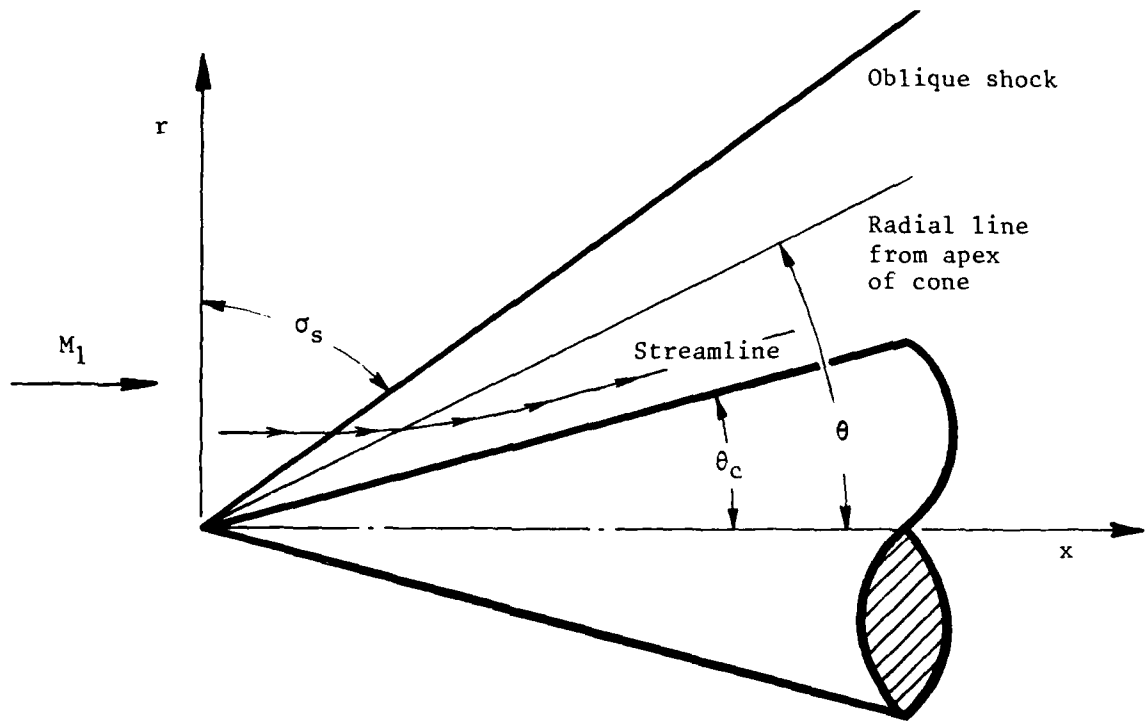


Fig. 23. Illustration of supersonic flow over a cone (aligned with the flow).

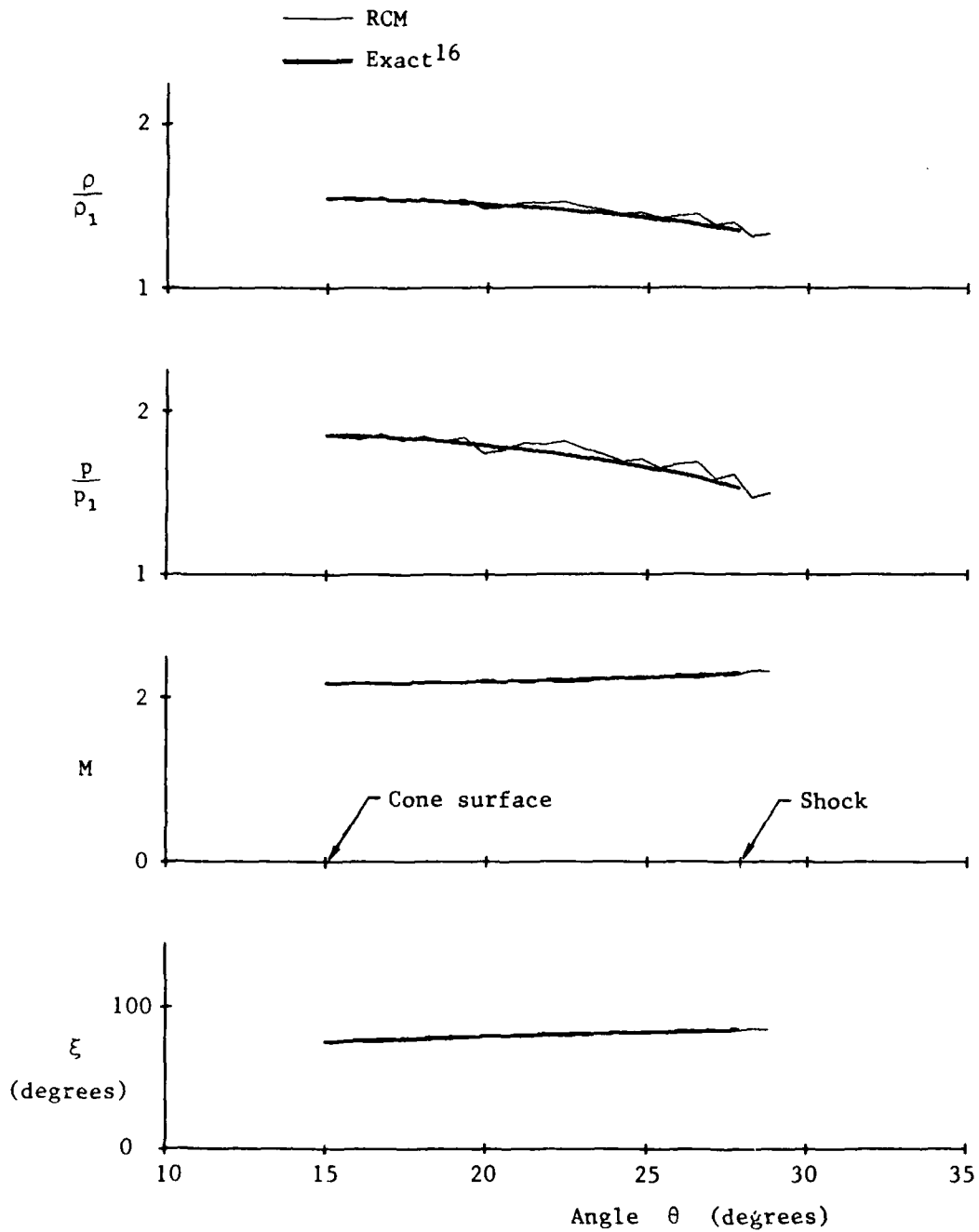


Fig. 24a. Comparison of RCM and exact results for a supersonic flow over a 15-degree cone ( $M_1 = 2.5787$ , 80 grid nodes downstream of the cone apex).

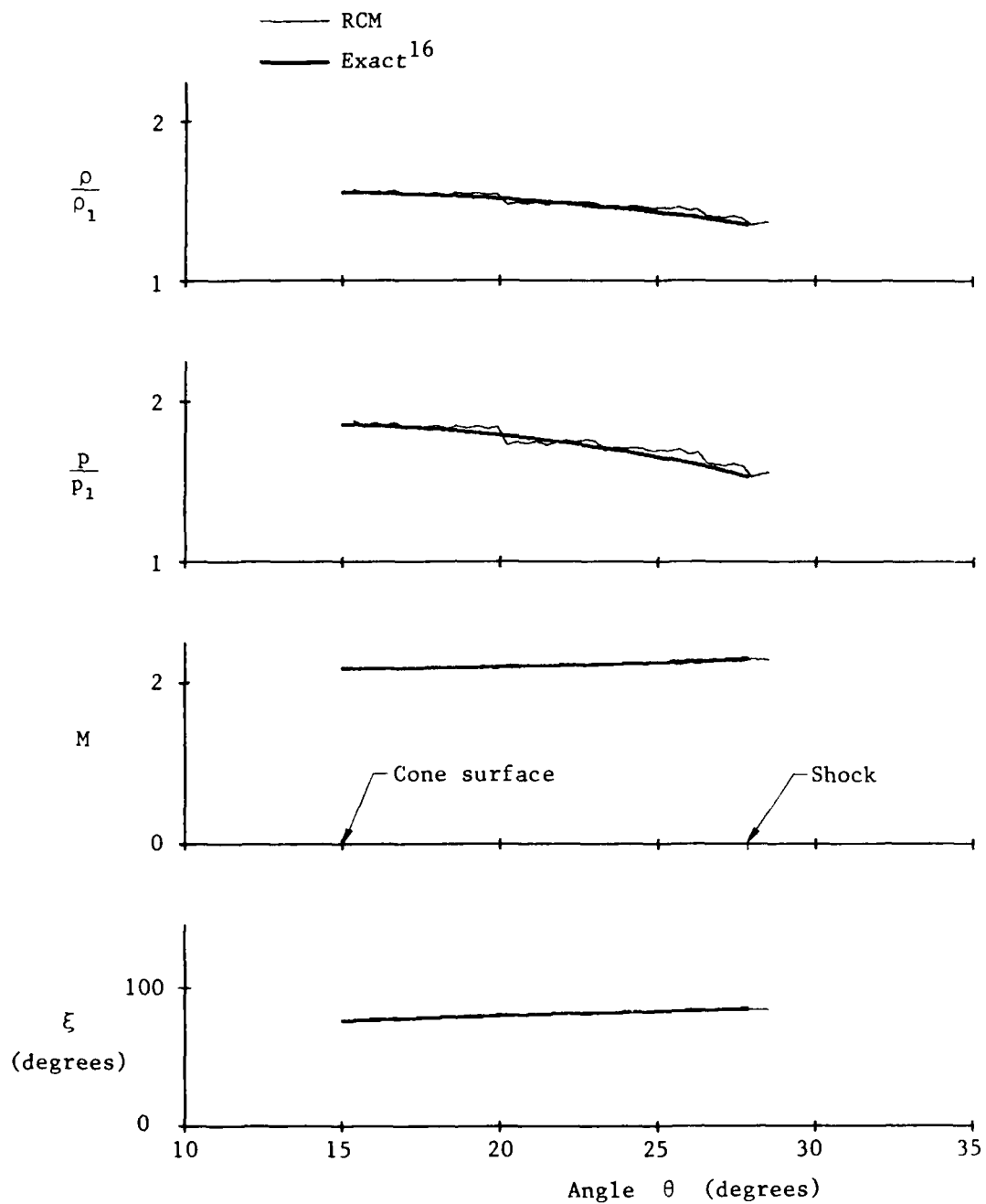


Fig. 24b. Comparison of RCM and exact results for a supersonic flow over a 15-degree cone ( $M_1 = 2.5787$ , 160 grid nodes downstream of the cone apex).

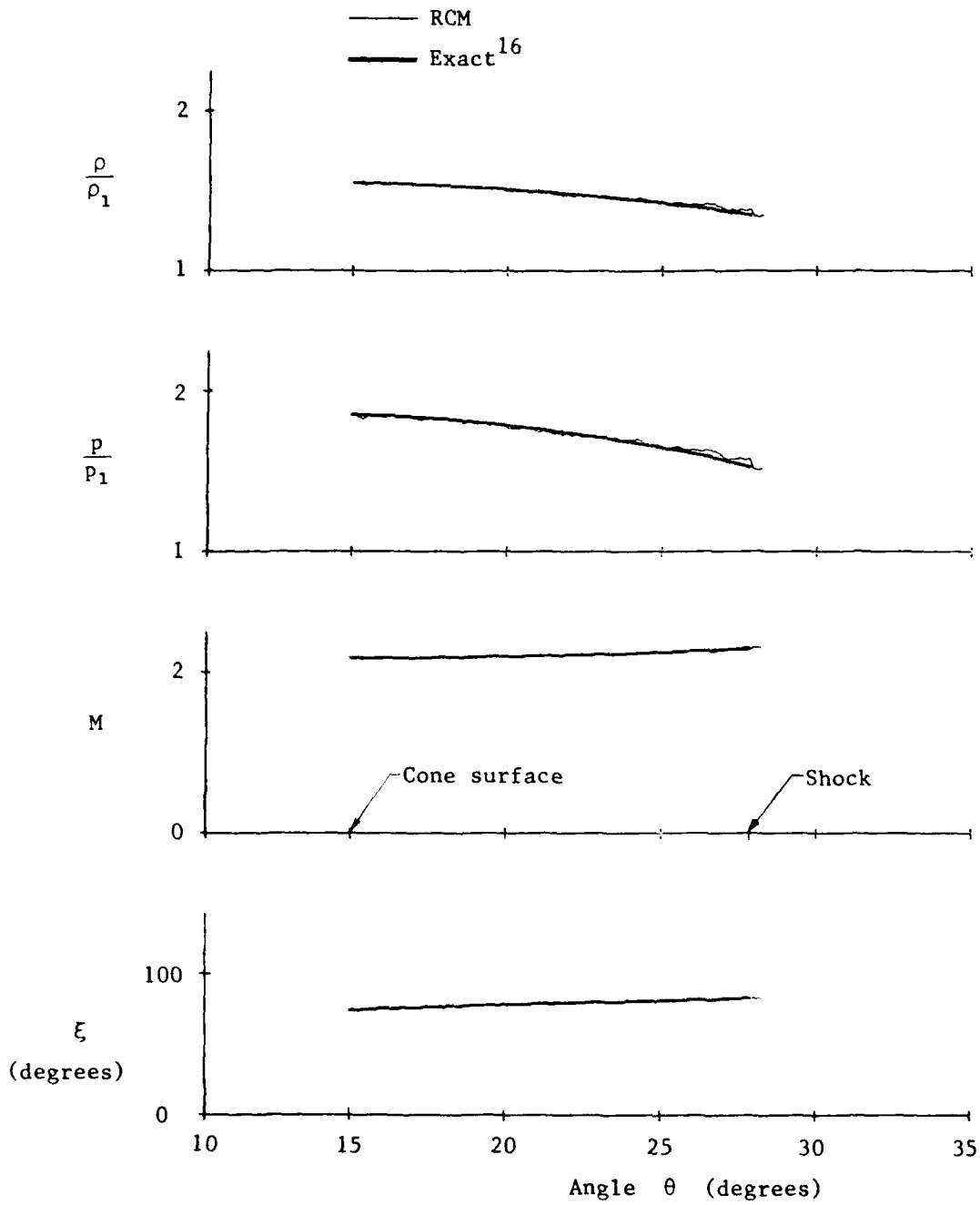


Fig. 24c. Comparison of RCM and exact results for a supersonic flow over a 15-degree cone ( $M_1 = 2.5787$ , 320 grid nodes downstream of the cone apex).

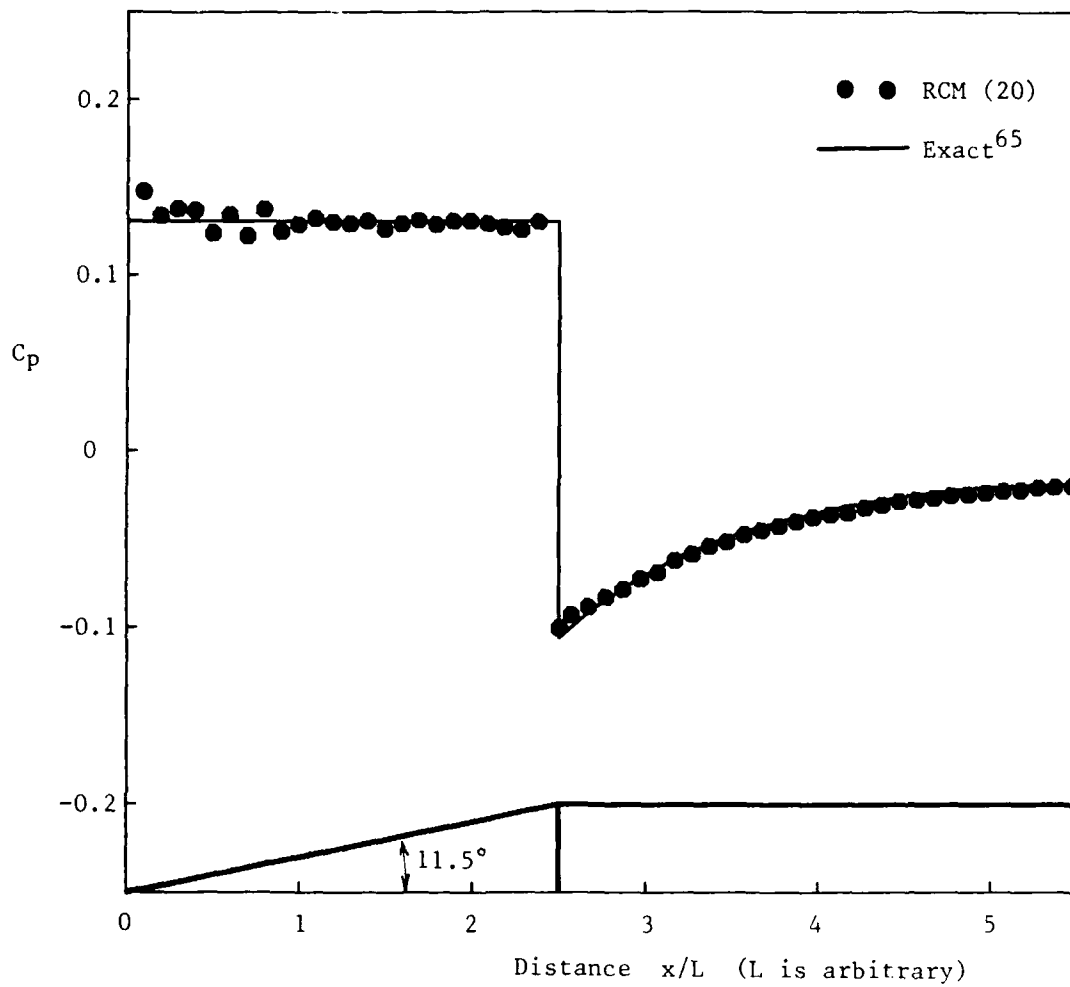


Fig. 25. Comparison of RCM and exact results for the pressure coefficient for the supersonic flow ( $M_1 = 2.0$ ) over a cone-cylinder.

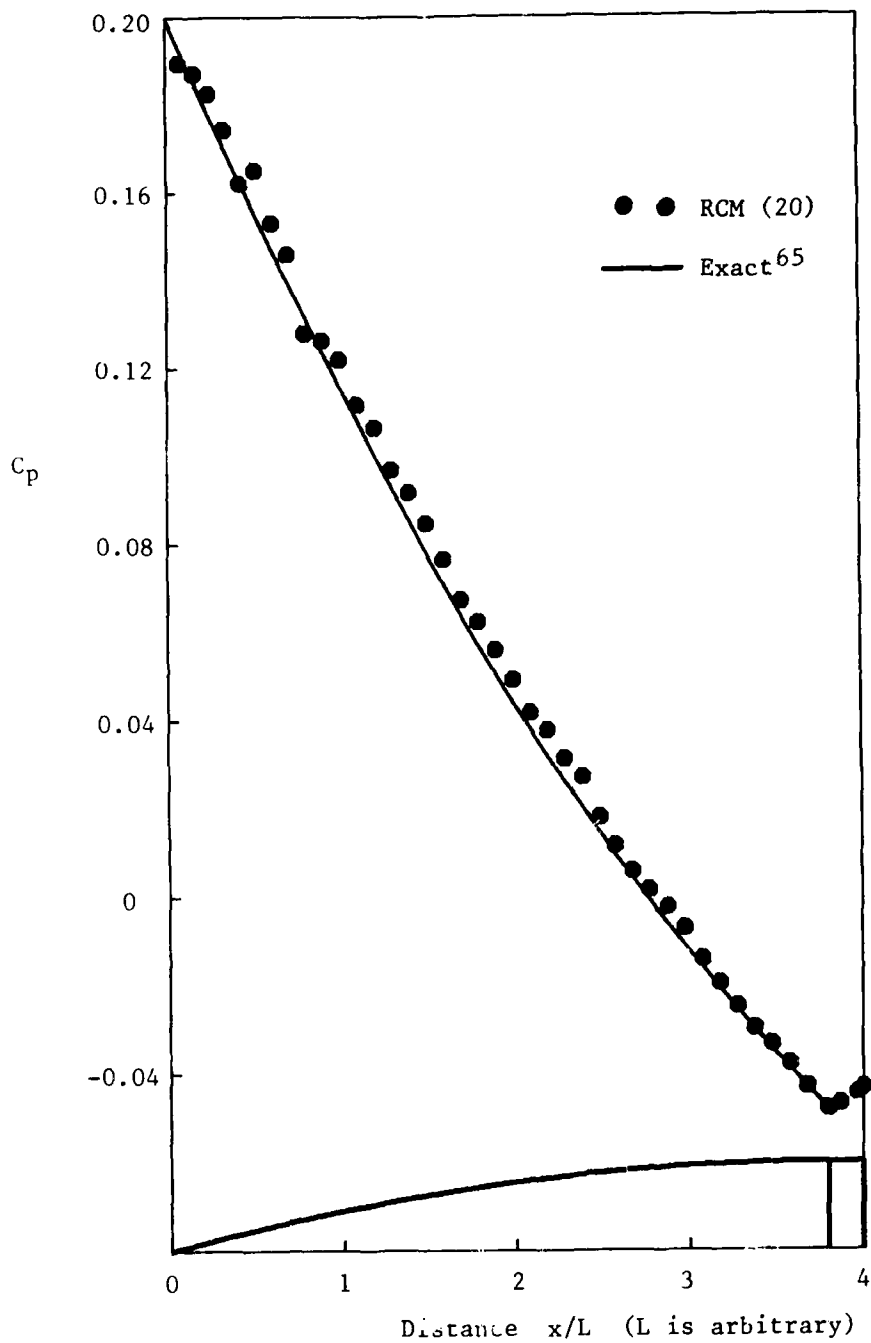


Fig. 26a. Comparison of RCM and exact solutions for the pressure coefficient for the supersonic flow ( $M_1 = 2.0$ ) over a cylindrical body with a parabolic nose.

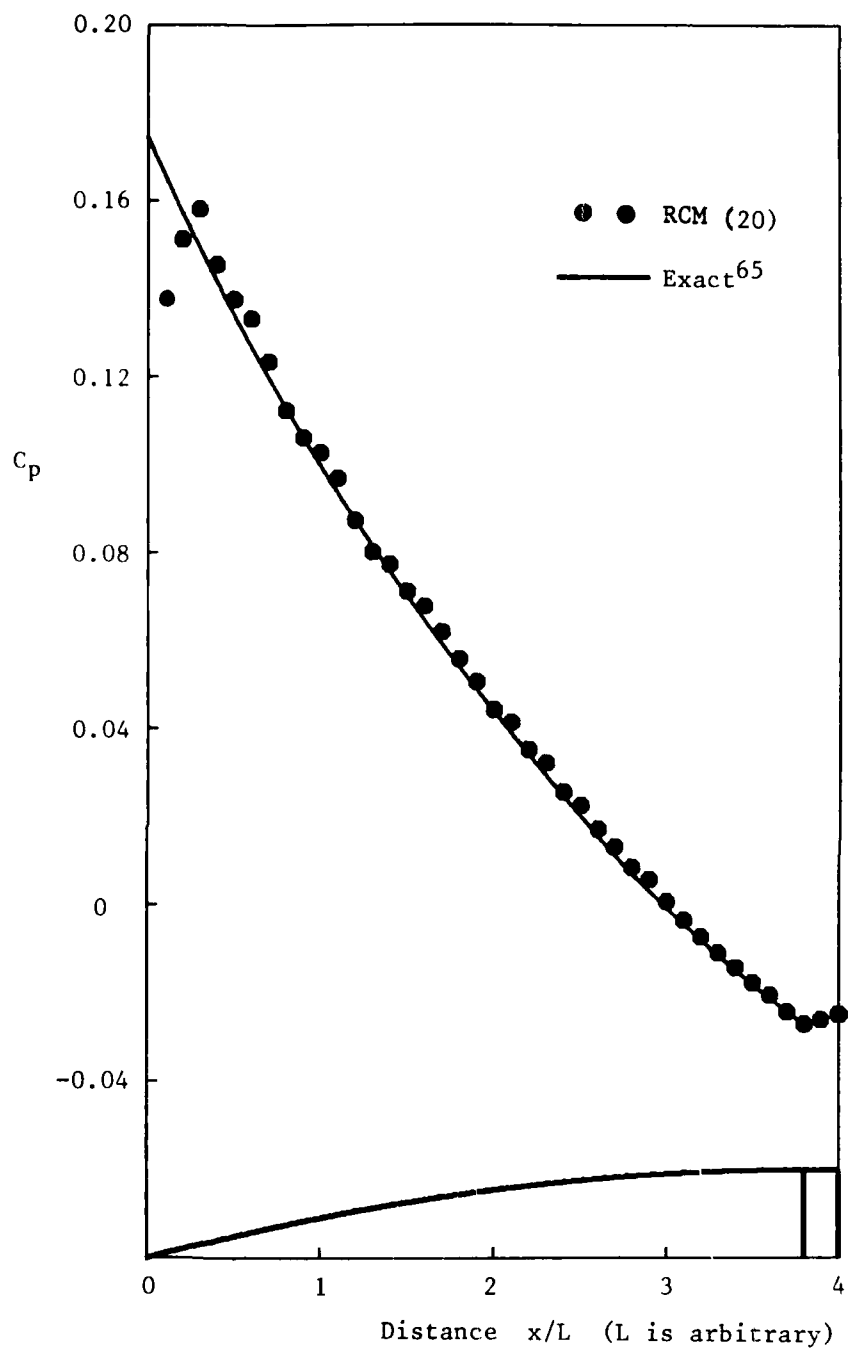


Fig. 26b. Comparison of RCM and exact solutions for the pressure coefficient for the supersonic flow ( $M_1 = 3.0$ ) over a cylindrical body with a parabolic nose.

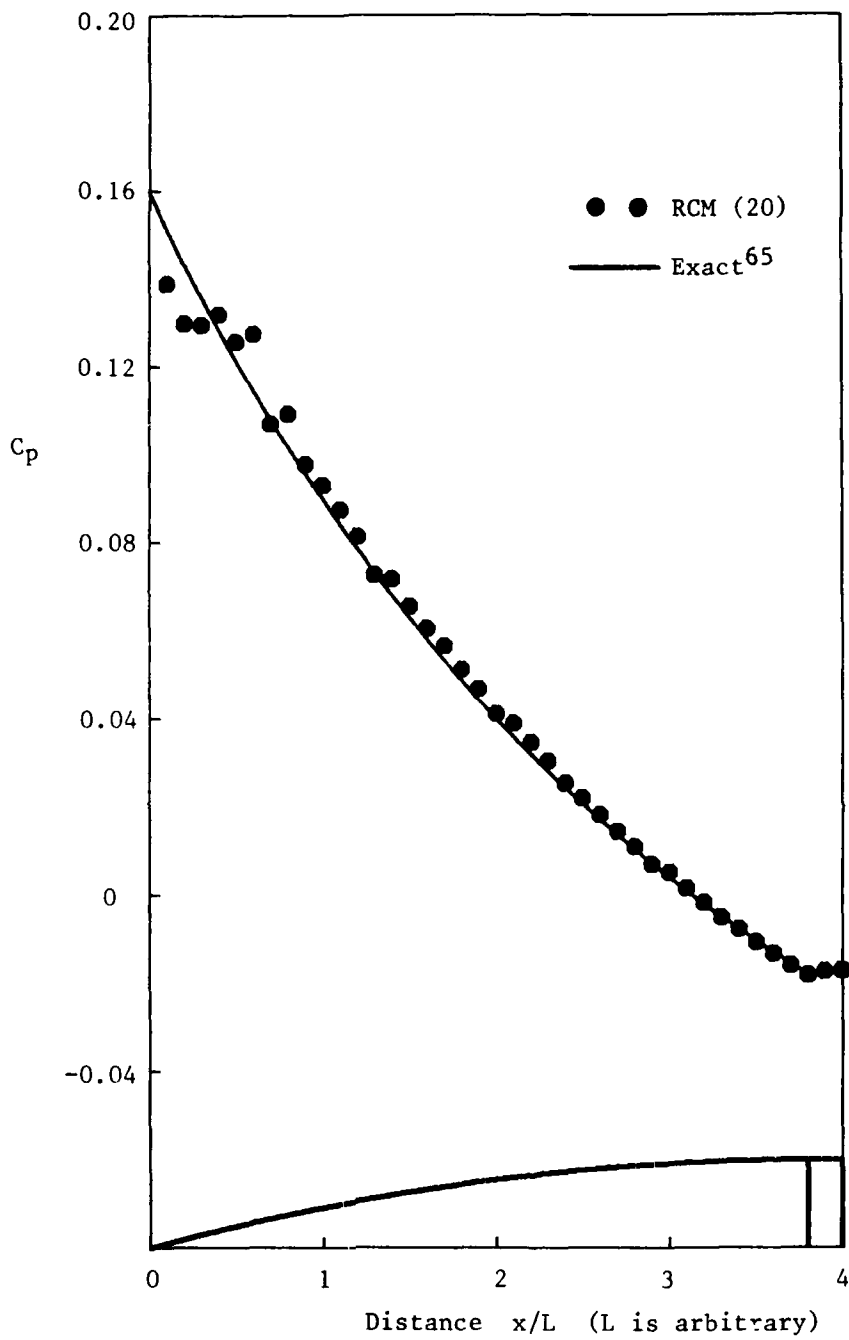


Fig. 26c. Comparison of RCM and exact solutions for the pressure coefficient for the supersonic flow ( $M_1 = 3.92$ ) over a cylindrical body with a parabolic nose.

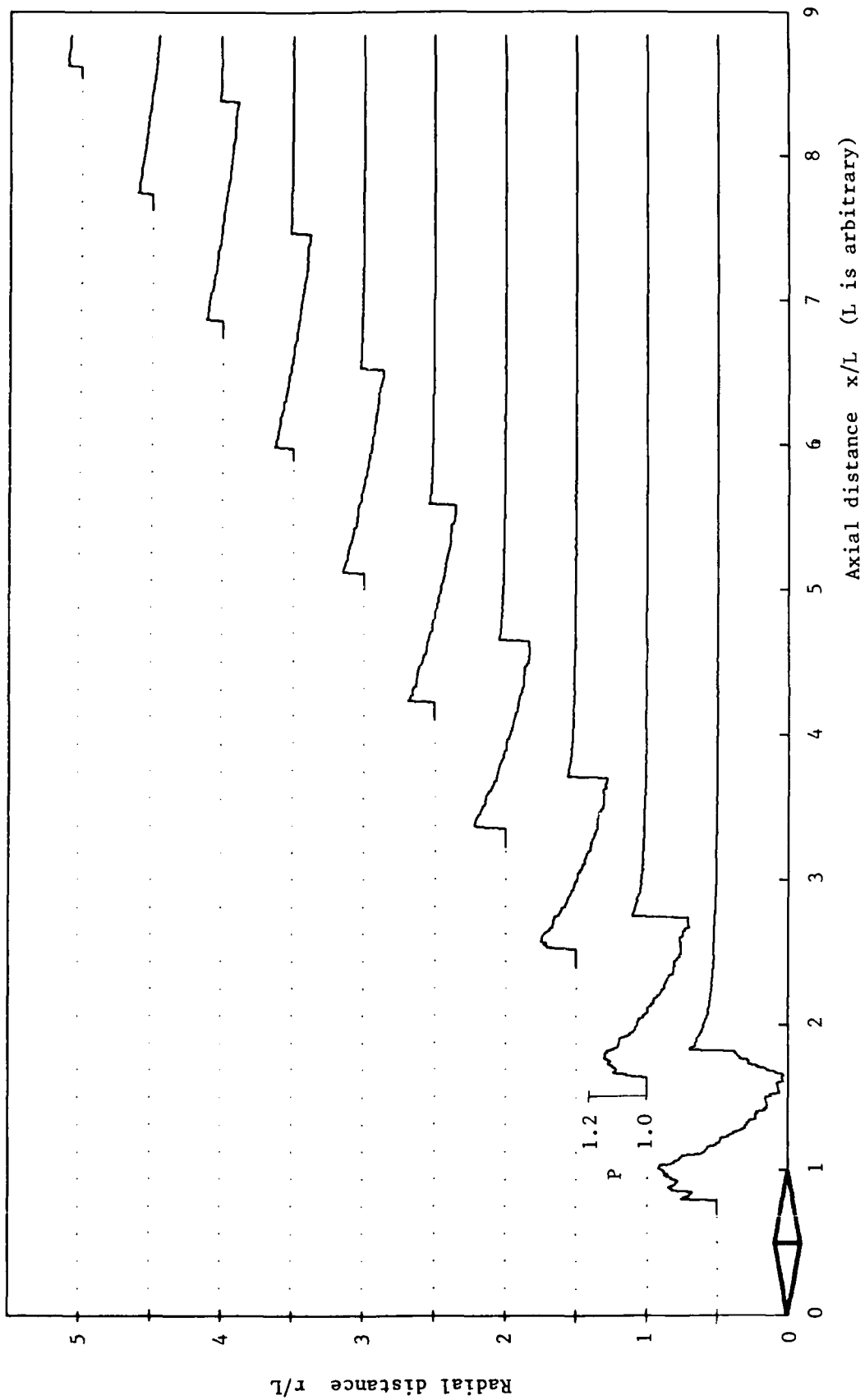


Fig. 27. Pressure profiles for a supersonic flow ( $M_1 = 2.075$ ) over a symmetric double-cone (semivertex angle of 10 degrees). The RCM computations include the lower right region but not the upper left region.

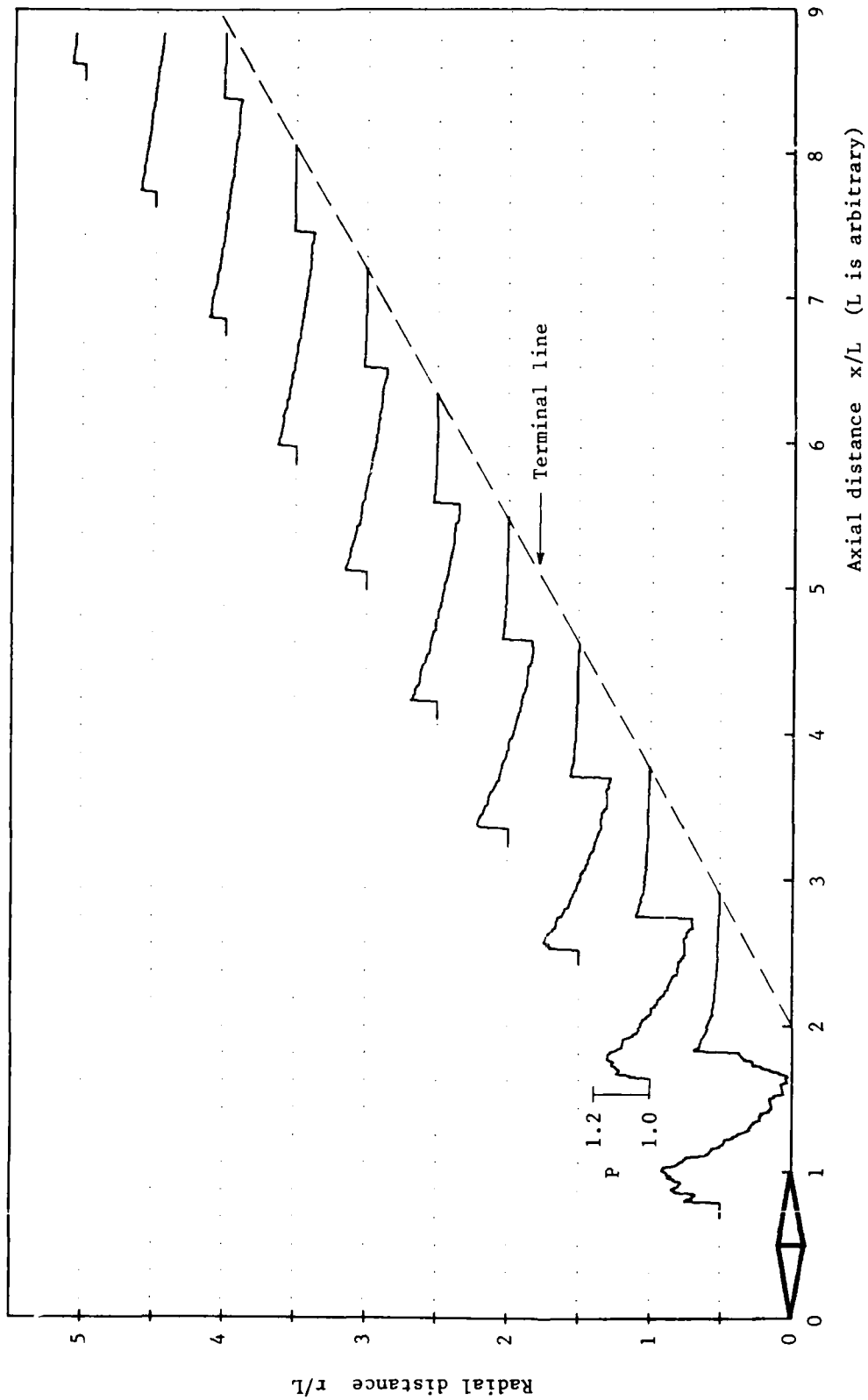


Fig. 28. Pressure profiles for a supersonic flow ( $M_j = 2.075$ ) over a symmetric double-cone (semivertex angle of 10 degrees). The RCM computations do not include the upper left and lower right regions.

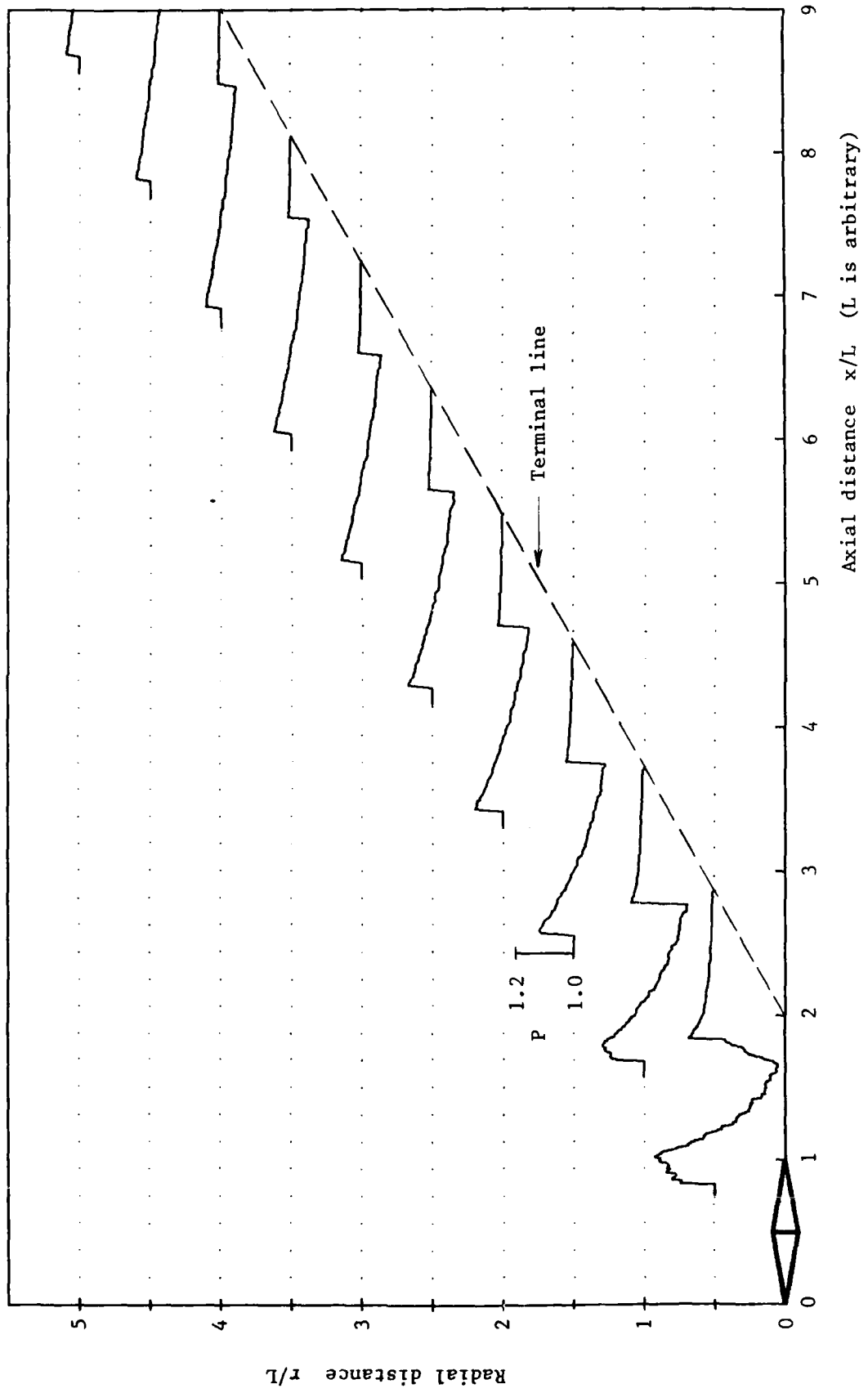


Fig. 29. Pressure profiles for a supersonic flow ( $M_1 = 2.075$ ) over a symmetric double-cone with a semivertex angle of 10 degrees.

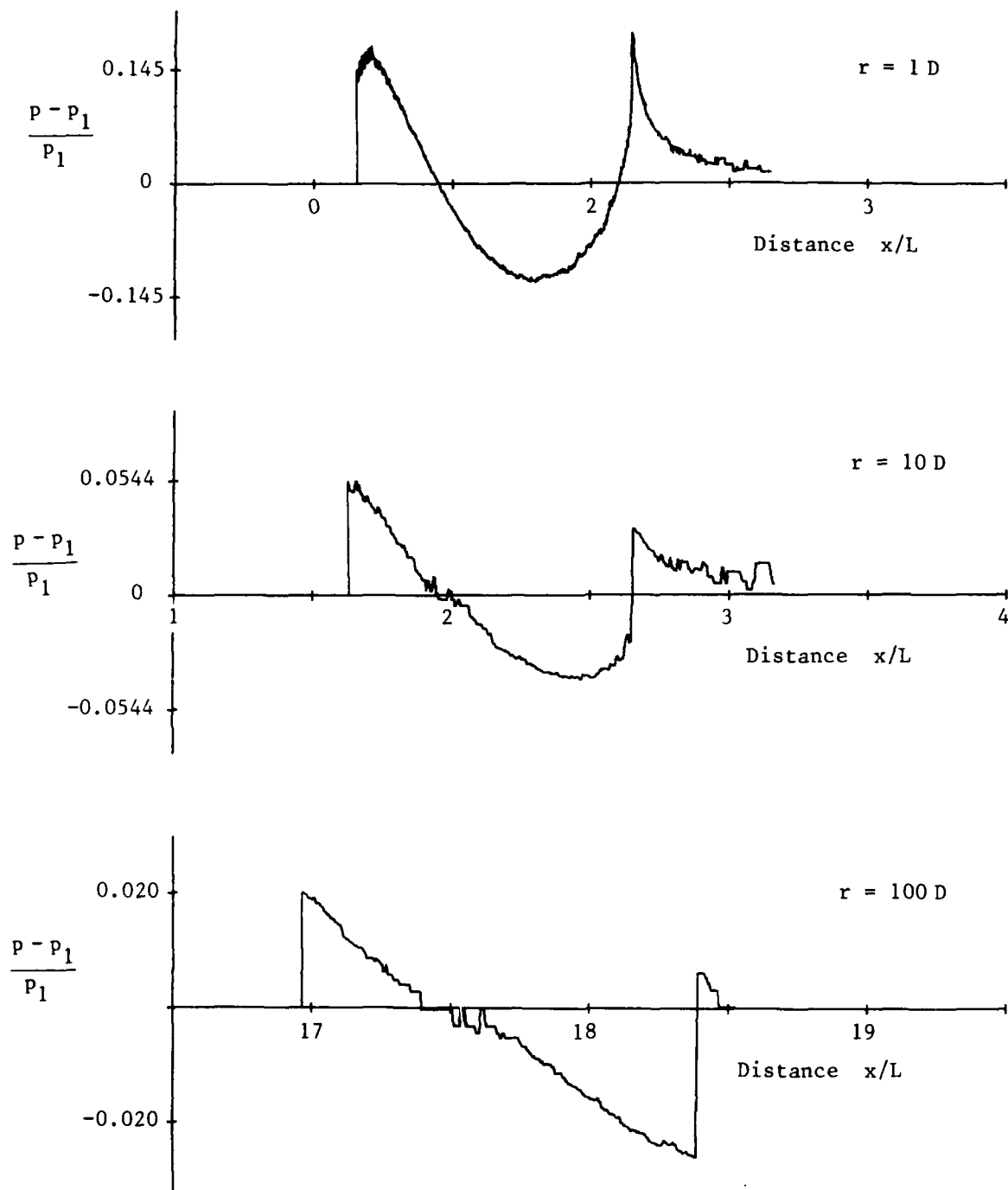


Fig. 30. Overpressure signatures at radii of 1, 10, and 100 diameters from a parabolic-spindle shaped body ( $D/L = 0.10$ ) in a supersonic flow ( $M_1 = 2$ ).

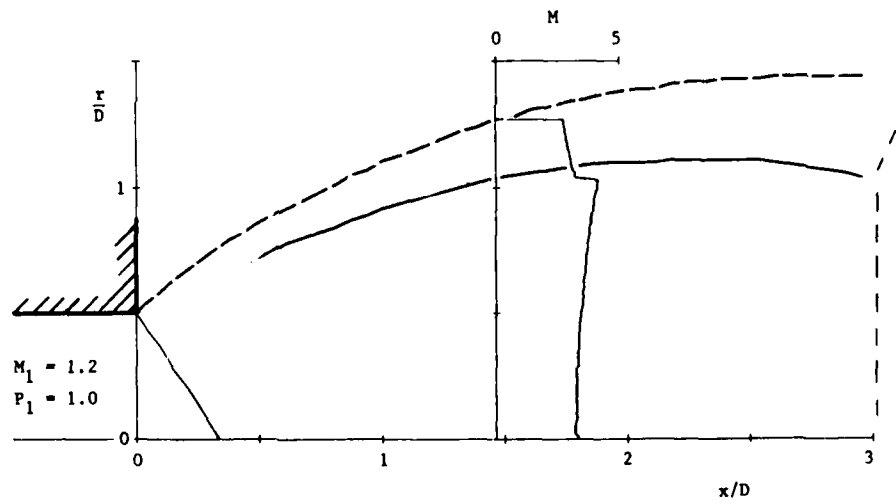
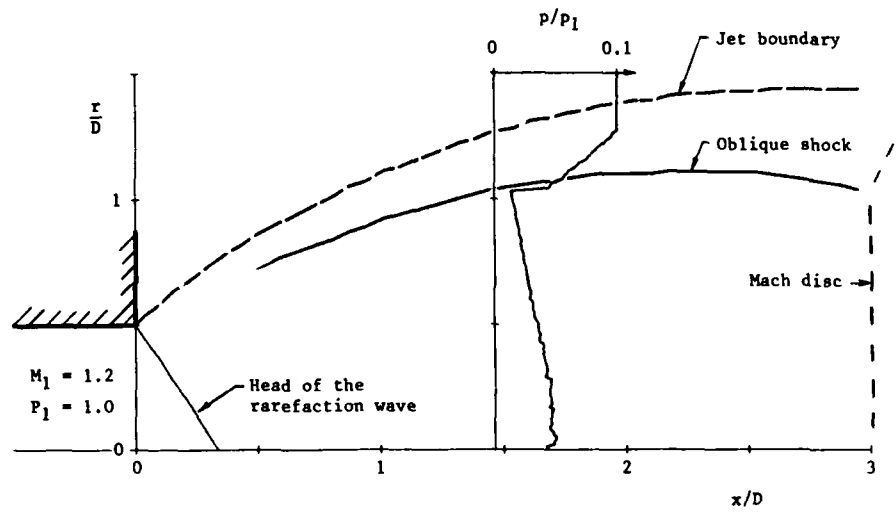


Fig. 31. Numerical results for an axisymmetric supersonic free jet with a backpressure one-tenth that of the exit pressure.

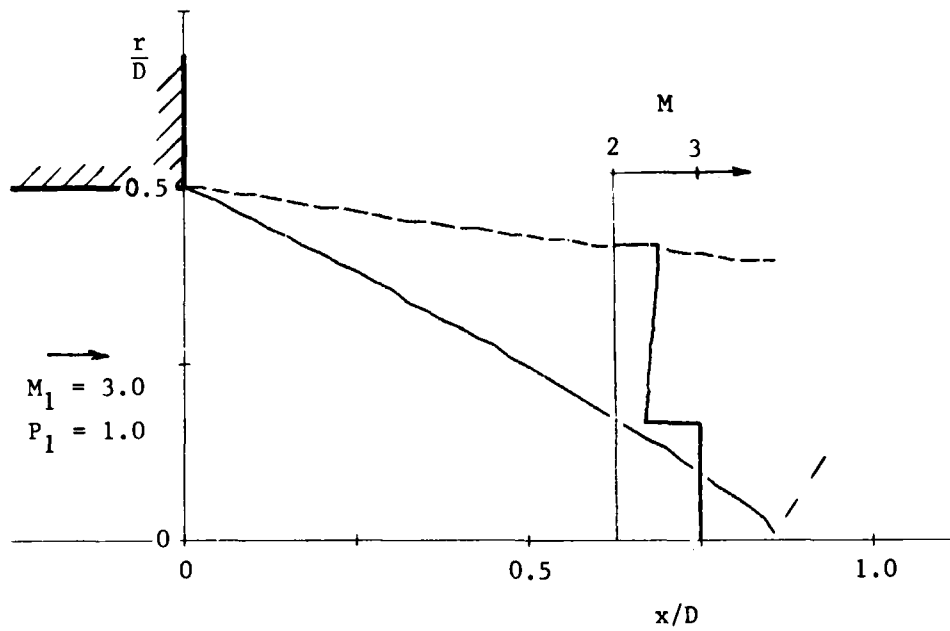
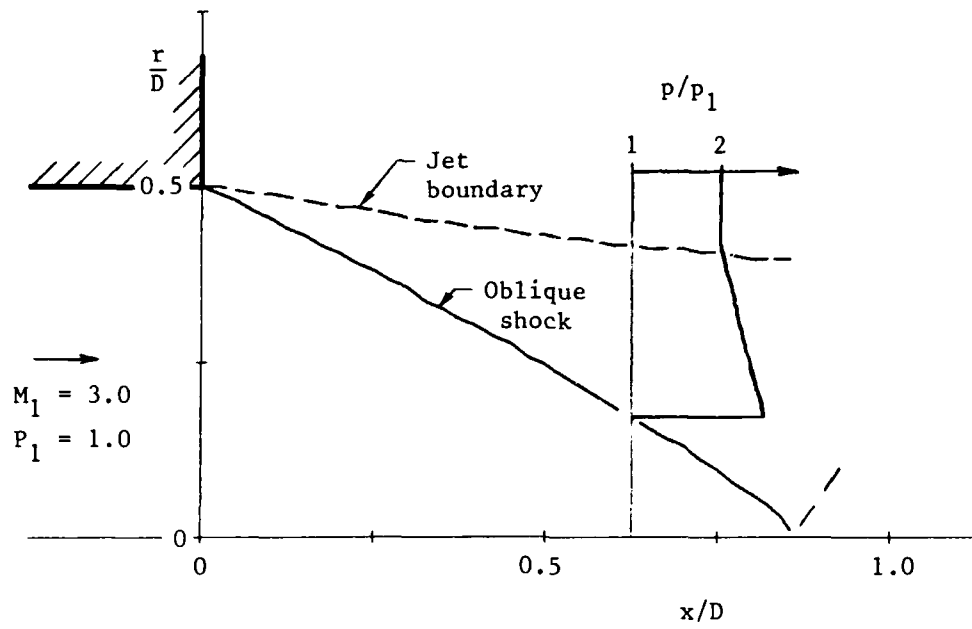


Fig. 32. Numerical results for an axisymmetric supersonic free jet with a backpressure twice that of the initial exit pressure.

## APPENDIX A

### COMPUTER-PROGRAM LISTING

#### FOR SOLVING TWO-DIMENSIONAL STEADY SUPERSONIC FLOW PROBLEMS

In the present numerical investigation, many slightly different computer programs were used to obtain numerical solutions for two-dimensional planar and axisymmetric flow fields of an inviscid, compressible and polytropic gas over and around different shaped bodies, inside duct inlets, and in free jets from slots and orifices. Only one typical version of these computer programs, which is based on the random-choice method is listed here, that which was used for computations of the flow over an axisymmetric body.

The algorithm for the random-choice method solves a basic Riemann problem for two-dimensional steady supersonic flow between adjacent grid points in the radial direction at increments of axial distance that are sufficiently small to satisfy the well-known Courant-Friedrichs-Lewy stability condition. It also includes an operator-splitting technique which can modify the initial Riemann solution for two-dimensional planar flows so that the desired solution for two-dimensional axisymmetric flows can be obtained.

In the computer program, all dependent thermodynamic and dynamic values are nondimensional. They are designated here by using an overhead bar and given as follows:

$$\bar{p} = p/p_0, \quad \bar{\rho} = \rho/\rho_0, \quad \bar{u} = u/(p_0/\rho_0)^{1/2}, \quad \bar{v} = v/(p_0/\rho_0)^{1/2},$$

where the dependent variables  $p$ ,  $\rho$ ,  $u$ , and  $v$  denote the static pressure and density and the radial and axial components of gas velocity, respectively. The variables with the subscript 0 are free-stream or reference flow conditions. The independent distance variables of  $x$  and  $r$  are also given in nondimensional form as follows:

$$\bar{x} = x/L, \quad \bar{r} = r/L,$$

where  $L$  is a certain characteristic reference length, which can be a body length or diameter.

The computer code consists of one main program followed by five subroutines and seven functions. The main purposes of the subroutines and functions are not described here because they are already outlined as commentary at the beginning of each listing.

RANDOM-CHOICE METHOD FOR TWO-DIMENSIONAL  
STEADY SUPERSONIC FLOWS

COMPUTER PROGRAM FOR SOLVING SUPERSONIC FLOWS OF AN  
INVISCID, COMPRESSIBLE, AND POLYTROPIC GAS  
AROUND A BODY OF REVOLUTION

BY ZONG CHENG SHI

MAIN PROGRAM

THIS PROGRAM EMPLOYS THE RANDOM-CHOICE METHOD AND AN  
OPERATOR-SPLITTING TECHNIQUE TO CALCULATE THE TWO-DIMENSIONAL  
STEADY SUPERSONIC FLOW OF AN INVISCID, COMPRESSIBLE AND  
POLYTROPIC GAS AROUND A BODY OF REVOLUTION. THE FREE-STREAM  
FLOW CONDITIONS, MESH NUMBER, AND SO ON ARE SPECIFIED IN THIS  
PROGRAM, AND THE VARIOUS SUBROUTINES NECESSARY TO DETERMINE  
THE FLOW PROPERTIES FROM GRID POINT TO GRID POINT ARE CALLED  
WHEN NECESSARY. THE MORE SUITABLE VAN DER CORPUT RANDOM-NUMBER  
ALGORITHM IS ALSO EMPLOYED HERE.

INPUT VARIABLES

NSTOP = MAXIMUM NUMBER OF STEPS ALONG THE AXIAL COORDINATE  
N = NUMBER OF GRID POINTS  
NP = NUMBER OF THE GRID POINT AT THE BODY SURFACE  
NPRINT = NUMBER OF CYCLES FOR EACH PRINT OUT  
BL = DENSITY OF THE FREE-STREAM FLOW  
PL = PRESSURE OF THE FREE-STREAM FLOW  
AML = MACH NUMBER OF THE FREE-STREAM FLOW  
XIWAO = WEDGE ANGLE OF THE BODY SURFACE  
XO = LOCATION WHERE THE CALCULATION IS STOPPED  
G = RATIO OF SPECIFIC HEATS (7/5 FOR AIR)

OUTPUT VARIABLES

X = THE AXIAL LOCATION WHERE DATA ARE PRINTED OUT  
RHO(5) = DENSITY AT GRID POINT NO. 5  
PRE(5) = PRESSURE AT GRID POINT NO. 5  
AMCH(5) = MACH NUMBER AT GRID POINT NO. 5  
AXI(5) = FLOW ANGLE AT GRID POINT NO. 5  
NS = NUMBER OF THE GRID POINT WHERE THE SHOCK IS LOCATED

A2

COMMON/HDX,RL,PL,AML,XIL,R,P,AM,XI,RR,PR,AMB,IIR,RI,Y  
COMMON/OUT1,RHO(150),PRE(150),AMCH(150),AXI(150)  
COMMON/GE/G,G1,G2,G3,EFS,EPS1

READ(3,18) NSTOP  
READ(3,18) N  
READ(3,18) NP  
READ(3,18) NPRINT  
READ(3,19) RL  
READ(3,19) PL  
READ(3,19) AML  
READ(3,19) XIWAO  
READ(3,19) XO

G=1.4  
G1=(G-1.)/2.  
G2=1./(G-1.)  
G3=(G+1.)/2.  
EFS=1.E-5  
EPS1=1.E-6  
NI=NI+1  
DE=1.49/FLOAT(N)  
X=0.  
NP1=NP+1  
NIN=0

WRITE(2,18) NSTOP  
WRITE(2,18) N  
WRITE(2,18) NP  
WRITE(2,18) NPRINT  
WRITE(2,19) RL  
WRITE(2,19) PL  
WRITE(2,19) AML  
WRITE(2,19) XIWAO  
WRITE(2,19) XO

SET INITIAL CONDITIONS

XIL=1.570796  
CALL BOUND(XIWAO,X)  
DO 9 I=1,NP  
RHO(I)=RR  
PRE(I)=PR  
AMCH(I)=AMB  
AXI(I)=XIR  
9 CONTINUE  
DO 10 I=NP1,NI  
RHO(I)=RL  
PRE(I)=PL  
AMCH(I)=AML  
AXI(I)=XIL  
10 CONTINUE

A3

```

C C COMPUTE THE FIRST HALF STEP
C C DO 40 I=NP1,NR
C C RL=RHO(I)
C C PL=PRE(I)
C C AML=AMCH(I)
C C XIL=AXI(I)
C C IF(I.EQ.NP1) GO TO 43
C C RR=RIN
C C PR=PIM
C C AMR=AMIN
C C XIR=XIN
C C GO TO 44
C C BOUNDARY CONDITION OF FLOW ADJACENT TO THE BODY SURFACE
C C 43 RR=RHO(NP)
C C PR=PRE(NP)
C C AMR=AMCH(NP)
C C XIR=AXI(NP)
C C 44 CALL SZCJY
C C IF(I.NE.NP1) GO TO 45
C C NIN=I
C C IF(RI.GE.Y) NIN=0
C C 45 RIN=RHO(I)
C C EHO(I)=E
C C PIM=PRE(I)
C C PRE(I)=P
C C ANIM=AMCH(I)
C C AMCH(I)=AM
C C XIM=AXI(I)
C C AXI(I)=XI
C C 40 CONTINUE
C C NP1=NP1+NIN
C C NP=NP1-1
C C USE OPERATOR-SPLITTING METHOD
C C CALL JYJZC(DR,EDI,NP,NE,I)
C C SET BOUNDARY CONDITION OF THE BODY SURFACE
C C RL=RHO(NP1)
C C PL=PRE(NP1)
C C AML=AMCH(NP1)
C C XIL=AXI(NP1)
C C CALL BOUND(XIWA0,I)
C C EHO(NP)=ER
C C PRE(NP)=PR
C C AMCH(NP)=AMR
C C AXI(NP)=XIR
C C END OF THE FIRST HALF STEP

```

```

NSTEP=0
ANG=(XIL-XIR)*57.295780
WRITE(2,20) X,NP,ANG,NSTEP
WRITE(2,21) RHO(NP),PRE(NP),AMCH(NP),AXI(NP)
BEGIN STEPS IN X DIRECTION
NS=NP
NR=NP+2
DO 100 NSTEP=1,NSTOP
C C DETERMINE MAXIMUM SLOPE OF MACH LINES FOR CFL CONDITION
C C SLP=1.
C C DO 11 I=NP,NR
C C ANU=ASIN(1./AMCH(I))
C C SLP1=ABS(TAN AXI(I)-ANU)
C C IF(SLP1.LT.SLP) SLP=SLP1
C C SLP1=ABS(TAN(AXI(I)+ANU))
C C IF(SLP1.LT.SLP) SLP=SLP1
C C 11 CONTINUE
C C SET THE INTERVAL OF X IN THE FIRST HALF STEP
C C DI=2.0*PI*DR EDI=DI/2.0
C C EDI=0.5*DR*SLP
C C XI=X+EDI
C C IF(X.GE.XO) NPRINT=1
C C GENERATE RANDOM NUMBER
C C NCE=2*NSTEP-1
C C NZ=0
C C SI=0.
C C 13 NZ=NZ+1
C C ND=MOD(NCE,2**N2)
C C IF(ND.EQ.0) GO TO 13
C C SI=SI+1./2.**N2
C C NCE=NCE-ND
C C IF(NCE.EQ.0) GO TO 14
C C GO TO 13
C C 14 CONTINUE
C C SI LIES BETWEEN -0.5*DR AND 0.5*DR
C C RI=(SI-0.5)*DR

```





AD-A172 903

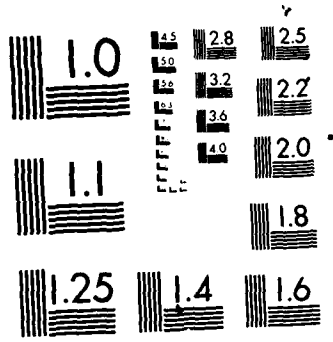
RANDOM-CHOICE-METHOD SOLUTIONS FOR TWO-DIMENSIONAL  
PLANAR AND AXISYMMETRIC (U) TORONTO UNIV DOWNSIDE  
(ONTARIO) INST FOR AEROSPACE STUDIES Z C SHI ET AL  
JAN 86 UTIAS-297 AFOSR-IR-86-0902 F/G 20/4

2/2

UNCLASSIFIED

NL





MICROCOPY RESOLUTION TEST CHART  
NATIONAL BUREAU OF STANDARDS-1963-A

```

C 130 LEFT SIDE OF RIGHT RAREFACTION FAN
P-PSTAR
AM-AMSTAR
XI-XISTAR
RETURN
C
C LEFT SIDE OF THE SLIP LINE
C
C 200 IF(PSTAR.LE.PL) GO TO 220
COMPUTE LEFT SHOCK WAVE ANGLE
XIS-XIL-CSI(PSTAR/PL,AML)
Z-BDX*TAN(1.570796-XIS)
IF(RI.GT.Z) GO TO 210
RIGHT SIDE OF LEFT SHOCK WAVE
P-PSTAR
R-RSTARL
AM-AMSTAR
XI-XISTAR
RETURN
C LEFT SIDE OF LEFT SHOCK WAVE
210 R-RL
P-PL
AM-AML
XI-XIL
RETURN
C COMPUTE THE ANGLE OF THE TAIL OF LEFT
RAREFACTION WAVE
220 XIT-XISTAR-ASIN(1./AMSTAR)
Z-BDX*TAN(1.570796-XIT)
IF(RI.GT.Z) GO TO 230
RIGHT OF LEFT RAREFACTION FAN
R-RSTARL
P-PSTAR
AM-AMSTAR
XI-XISTAR
RETURN
C COMPUTE THE ANGLE OF THE HEAD OF LEFT
RAREFACTION WAVE
230 XIB-XIL-ASIN(1./AML)
Z-BDX*TAN(1.570796-XIB)
IF(RI.GE.Z) GO TO 240
IN LEFT RAREFACTION FAN
AMI-0.5*(AML+AMSTAR)
IF(AMSTAR-AML.LE.EPS1) GO TO 42
CALL SSDZJK(AMI,EPS,EPS1,3,1.)
42 AM-AMI
XI-1.570796-ATAN(RI/BDX)*ASIN(1./AM)
R-RL*(1.+G1*AML*AML)/(1.+G1*AM*AM)**G2
P-PL*(R/RL)**G
RETURN
C LEFT SIDE OF LEFT RAREFACTION FAN
240 R-RL

```

```

P-PL
AM-AML
XI-XIL
RETURN
END

```

SUBROUTINE BOUND(AA, XI)

SUBROUTINE TO CALCULATE THE FLOW PROPERTIES AT THE BODY SURFACE THAT ARE THE BOUNDARY CONDITIONS

```

COMMON/BDX,RL,PL,AML,XIL,E,P,AM,XI,ER,PR,AMR,XIR,RI,I
DETA=XIL-XIWA(AA, XI)
R-RL
P-PL
AM-AML
XIR=XIL-2.*DETA
RETURN
END

```

SUBROUTINE SSDZJK(KT, E1, E2, L, A)

SUBROUTINE BY USING THE PARABOLIC CURVE INTERPOLATION METHOD TO FIND THE ROOT OF PRESSURE AT EITHER SIDE OF A SLIP LINE OR THE ROOT OF MACH NUMBER AT THE SAMPLING POINT INSIDE A RAREFACTION FAN

```

M1-10
N=0
IF(KT.LE.A) GO TO 01
X0=0.95*KT
X1=1.05*KT
X2=KT
H=-0.05*KT

```









UTIAS Report No. 297

University of Toronto, Institute for Aerospace Studies (UTIAS)  
4925 Dufferin Street, Downsview, Ontario, Canada, M3H 5T6

RANDOM-CHOICE-METHOD SOLUTIONS FOR TWO-DIMENSIONAL PLANAR AND AXISYMMETRIC STEADY SUPERSONIC FLOWS

Shi, Z. C., Gottlieb, J. J.

1. Random choice method
2. Steady supersonic flows
3. Supersonic inlet flows
4. Free-jet flows

II. Shi, Z. C., Gottlieb, J. J.

A random-choice method (RCH) is developed for obtaining fairly practical and efficient numerical solutions for two-dimensional planar and axisymmetric steady supersonic flows, such as those for sharp-edged planar airfoils, supersonic inlets of aircraft engines, pointed bodies of revolution, supersonic nozzles, and free jets. This method is based on the solution of a Riemann problem, which is the elemental solution of the hyperbolic equations of two-dimensional steady supersonic flows. The Riemann problem consists of two waves separated by a slip stream, and each wave can be either an oblique shock wave or a Prandtl-Meyer expansion wave. Advanced techniques are given for solving the Riemann problem iteratively, handling the boundary conditions along body and free-jet surfaces, and computing only certain parts of flow fields of interest. Many interesting and practical numerical solutions are presented for different types of planar and axisymmetric flows, to demonstrate the applicability, capability, and limitations of the RCH. Numerical results are shown to be in excellent agreement with both known analytical solutions and results from the method of characteristics.

Available copies of this report are limited. Return this card to UTIAS, if you require a copy.



UTIAS Report No. 297

University of Toronto, Institute for Aerospace Studies (UTIAS)  
4925 Dufferin Street, Downsview, Ontario, Canada, M3H 5T6

RANDOM-CHOICE-METHOD SOLUTIONS FOR TWO-DIMENSIONAL PLANAR AND AXISYMMETRIC STEADY SUPERSONIC FLOWS

Shi, Z. C., Gottlieb, J. J.

1. Random choice method
2. Steady supersonic flows
3. Supersonic inlet flows
4. Free-jet flows

II. Shi, Z. C., Gottlieb, J. J.

A random-choice method (RCH) is developed for obtaining fairly practical and efficient numerical solutions for two-dimensional planar and axisymmetric steady supersonic flows, such as those for sharp-edged planar airfoils, supersonic inlets of aircraft engines, pointed bodies of revolution, supersonic nozzles, and free jets. This method is based on the solution of a Riemann problem, which is the elemental solution of the hyperbolic equations of two-dimensional steady supersonic flows. The Riemann problem consists of two waves separated by a slip stream, and each wave can be either an oblique shock wave or a Prandtl-Meyer expansion wave. Advanced techniques are given for solving the Riemann problem iteratively, handling the boundary conditions along body and free-jet surfaces, and computing only certain parts of flow fields of interest. Many interesting and practical numerical solutions are presented for different types of planar and axisymmetric flows, to demonstrate the applicability, capability, and limitations of the RCH. Numerical results are shown to be in excellent agreement with both known analytical solutions and results from the method of characteristics.

Available copies of this report are limited. Return this card to UTIAS, if you require a copy.



UTIAS Report No. 297

University of Toronto, Institute for Aerospace Studies (UTIAS)  
4925 Dufferin Street, Downsview, Ontario, Canada, M3H 5T6

RANDOM-CHOICE-METHOD SOLUTIONS FOR TWO-DIMENSIONAL PLANAR AND AXISYMMETRIC STEADY SUPERSONIC FLOWS

Shi, Z. C., Gottlieb, J. J.

1. Random choice method
2. Steady supersonic flows
3. Supersonic inlet flows
4. Free-jet flows

II. Shi, Z. C., Gottlieb, J. J.

A random-choice method (RCH) is developed for obtaining fairly practical and efficient numerical solutions for two-dimensional planar and axisymmetric steady supersonic flows, such as those for sharp-edged planar airfoils, supersonic inlets of aircraft engines, pointed bodies of revolution, supersonic nozzles, and free jets. This method is based on the solution of a Riemann problem, which is the elemental solution of the hyperbolic equations of two-dimensional steady supersonic flows. The Riemann problem consists of two waves separated by a slip stream, and each wave can be either an oblique shock wave or a Prandtl-Meyer expansion wave. Advanced techniques are given for solving the Riemann problem iteratively, handling the boundary conditions along body and free-jet surfaces, and computing only certain parts of flow fields of interest. Many interesting and practical numerical solutions are presented for different types of planar and axisymmetric flows, to demonstrate the applicability, capability, and limitations of the RCH. Numerical results are shown to be in excellent agreement with both known analytical solutions and results from the method of characteristics.

Available copies of this report are limited. Return this card to UTIAS, if you require a copy.



UTIAS Report No. 297

University of Toronto, Institute for Aerospace Studies (UTIAS)  
4925 Dufferin Street, Downsview, Ontario, Canada, M3H 5T6

RANDOM-CHOICE-METHOD SOLUTIONS FOR TWO-DIMENSIONAL PLANAR AND AXISYMMETRIC STEADY SUPERSONIC FLOWS

Shi, Z. C., Gottlieb, J. J.

1. Random choice method
2. Steady supersonic flows
3. Supersonic inlet flows
4. Free-jet flows

II. Shi, Z. C., Gottlieb, J. J.

A random-choice method (RCH) is developed for obtaining fairly practical and efficient numerical solutions for two-dimensional planar and axisymmetric steady supersonic flows, such as those for sharp-edged planar airfoils, supersonic inlets of aircraft engines, pointed bodies of revolution, supersonic nozzles, and free jets. This method is based on the solution of a Riemann problem, which is the elemental solution of the hyperbolic equations of two-dimensional steady supersonic flows. The Riemann problem consists of two waves separated by a slip stream, and each wave can be either an oblique shock wave or a Prandtl-Meyer expansion wave. Advanced techniques are given for solving the Riemann problem iteratively, handling the boundary conditions along body and free-jet surfaces, and computing only certain parts of flow fields of interest. Many interesting and practical numerical solutions are presented for different types of planar and axisymmetric flows, to demonstrate the applicability, capability, and limitations of the RCH. Numerical results are shown to be in excellent agreement with both known analytical solutions and results from the method of characteristics.

Available copies of this report are limited. Return this card to UTIAS, if you require a copy.